Politecnico di Milano
School of Industrial and Information Engineering
Master of Science in Space Engineering
Dipartimento di Scienze e Tecnologie Aerospaziali

Analysis of post-buckled variable-stiffness panels using Ritz method and Koiter's approach

Advisor: Prof. Riccardo Vescovini
Co-advisor: Prof. Lorenzo Dozio
Co-advisor: Dr. ir. Eelco Jansen

Master Thesis by:

Enrico Spigarolo ID: 878278

Academic Year 2017-2018

To the teacher that during my senior year in high school, after I failed the Astronomy test, told me: "I don't think you are cut for scientific studies."

Acknowledgements

I would like to express my sincere gratitude to professor Vescovini for all the support he gave me while working on this thesis: without his guide (and his patience) I would probably still be lost between energy functional and curvilinear fibers.
I would also like to thank the rest of my thesis committee: professor Dozio who, with his lessons, encouraged me to go deeper into this topic, and professor Jansen for his precious help and for welcoming me among his colleagues at the Institut für Statik und Dynamik at Leibniz University.

This thesis is a big arrival point for me, as it means that I survived Milano and Politecnico. I am sure that the time I spent here would have been much more boring without the people I shared this experience with. Thank you, friends I met the first days of class, friends I made during the endless hours of study and friends I know for totally unrelated reasons. Also, thank you to the amazing people who shared a beer with me in Hannover.

Nevertheless, the most funny stories that happened in these years took place in the flat I shared with some crazy people: thank you to the "old", the "less old" and the present flatmates. In particular, thank you to Enrico, who shared with me six years of very bad jokes.

Furthermore, I would like to thank the person that, in all these years, helped me to keep my mind between the clouds: thank you, Anita.

Finally, I want to express gratitude to all my family: to my mum, Mirella, who will never stop believing in me; to my sister, Cristina, for being the beautiful person that she is; to my dad, Stefano, who, as the experienced engineer that he is, tried to dissuade me from applying to engineering; to my grandma, Sabina, for all the lasagne.

Abstract

In the past years, increasing attention has been devoted toward the analysis of variable stiffness panels (VSP). Due to improved design flexibility, VSP offer drastic potentialities to achieve better buckling and strength performance with respect to classical straight-fiber configurations. Appealing advantages of variable stiffness panels are found also with respect to their response in the post-buckling field, which is of particular interest for lightweight aerospace applications. Within this context, simplified design tools are valuable means for supporting the preliminary design phase and gathering insight into their structural response. The present work illustrates the comparison of different semi-analytical strategies for analysing the buckling and post-buckling response of variable-stiffness plates and shells. In the first part of the work, a Ritz-based strategy is illustrated based on a variational formulation using a von Kármán-Donnell type shell theory, where the unknowns are expressed in terms of Airy force function and out-of-plane deflections. Governing equations are derived after approximating the unknown fields by means of orthogonal polynomials. The second part of the activity illustrates the application of a basic version of Koiter's perturbation approach for the initial post-buckling analysis, which also uses von Kármán-Donnell type theory. Special care is given to the formulation of the second order problem in the perturbation analysis. The quality of the predictions achieved using the two approaches is assessed by comparison against finite element calculations.

Sommario

Negli ultimi anni, un'attenzione sempre maggiore è stata dedicata all'ambito dei pannelli a rigidezza variabile (VSP). Questo tipo di elemento strutturale, infatti, grazie alla versalità che lo contraddistingue, garantisce migliori prestazioni in termini di carico critico e resistenza rispetto ai classici laminati a fibra rettilinea. Un altro aspetto interessante è legato al comportamento dei VSP in campo post-critico, soprattutto per quanto riguarda i pannelli sottili adottati nell'ambito aerospaziale. Lo studio di strumenti che consentano una rapida analisi di queste strutture nelle fasi preliminari di progetto diventa, perciò, di estremo interesse. Nel presente lavoro vengono comparati diversi modelli semi-analitici per l'analisi lineare e non-lineare di piastre e gusci a rigidezza variabile. Nella prima parte viene illustrata una strategia basata sul metodo di Ritz. Le equazioni sono derivate da una formulazione variazionale, ottenuta sulla base della teoria di von Kármán-Donnell per i gusci. Le incognite sono espresse per mezzo della funzione di Airy e dello spostamento fuori dal piano. La seconda parte del lavoro si concentra, invece, sull'applicazione di una versione base del metodo perturbativo alla Koiter, per lo studio del comportamento post-critico nell'intorno del punto di biforcazione. Quest'ultima formulazione è basata anch'essa sulla teoria di von Kármán-Donnell. Particolare attenzione è data alla formulazione del problema di secondo ordine. La qualità delle previsioni, ottenute con i due metodi, è poi verificata sulla base di confronti con analisi a elementi finiti.

Contents

List of Figures

List of Tables

Chapter 1

Introduction

Since the beginning of the flight era in 1905, a significant effort has been spent to design and manufacture structures that are, at the same time, light and strong. In this context, thin plates and shells made of composite materials are widely used in typical aerospace constructions, such as aircraft constructions (Figure 1.1a) and rockets (Figure 1.1b).
It is well known that the usage of composite materials, such as carbon fiber reinforced polymers, may be exploited to achieve structures with lower mass-to-strength and mass-to-stiffness ratios with respect to their metallic counterpart. Laminated panels are obtained by the stacking of multiple plies, each oriented at a different angle: this feature is particularly appealing from a design standpoint, as a large flexibility is made possible due to the large combinations of orientation angles to compose the stack.
In classical laminated panels, the fibers within a ply are generally straight and parallel to each other, resulting in overall macroscopic constant material properties throughout the panel domain. This means that the homogenized properties of the laminate are, in general, characterised by a fully anisotropic constitutive law, accounting for several elastic-coupling effects that are absent in the case of isotropic panels.
Additional tailoring opportunities can be achieved if the restriction of straight fiber is removed, and the fibers are allowed to follow arbitrary paths. This idea introduces the concept of variable-stiffness panels (VSP).

Variable-stiffness panels have been theoretically formulated at the beginning of the ninetiens: the underlying idea is to exploit the fibers properties in order to obtain a structure in which the stiffness is made to vary across the laminate.

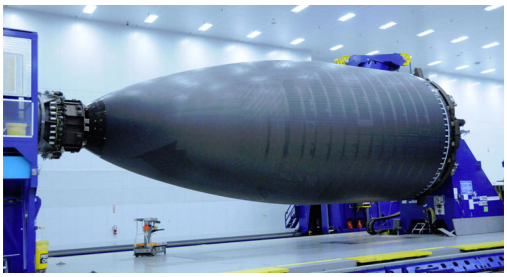

(a) Boeing 787 fuselage

(b) Falcon 9 interstages

Figure 1.1: Examples of composite materials in aerospace applications.

This concept has been initially proposed by Leissa and Martin [1]: in their pioneering work, the authors provided insights on the benefits that can be expected by a design based on variable-stiffness configurations. Later studies by Hyer and Charette [2] and Gürdal and Olmedo [3] also confirmed that these kind of structural elements, if properly designed, can achieve better performances than classical laminates. Among the significant advantages –and with focus on the buckling behaviour– it is worth highlighting that:

- Higher buckling loads can be expected with respect to classical straight fibers panels.
- The drop of stiffness after buckling can be mitigated.

In the context of composite panels there are a couple of ways to obtain a structure with non-constant stiffness properties: varying the volume fraction of fibers (Leissa and Martin [1], Senocak et al. [4], Setooddeh et al. [5]) or dropping/adding plies to the laminate (Curry and Turnes [6], Pauluch et al. [7]).
The present work deals with the case of non-constant fiber orientations. In other words, fibers are forced to follow a non-straight reference path (Figure 1.2), that can be different from ply to ply. This feature allows the designer to exploit additional

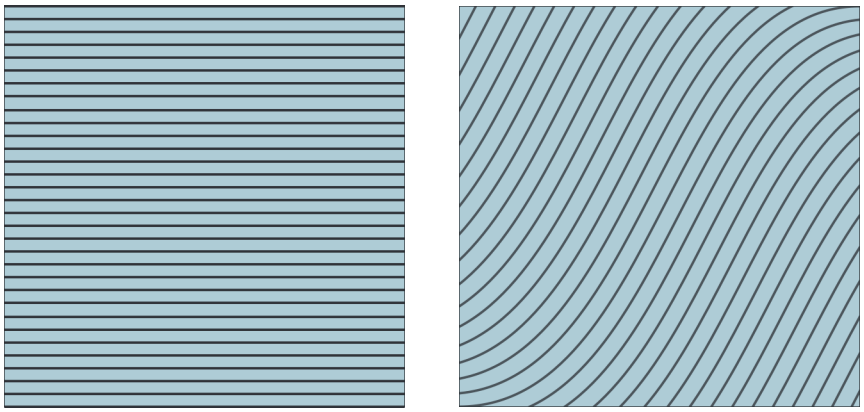

(a) (b)

Figure 1.2: Fiber path in a fiber-reinforced composite: (a) straight, (b) curvilinear.

degrees of freedom with respect to classical straight fiber laminates: by doing so, the material properties can be optimized according to the project requirements. Moreover, employing curvilinear fibers does not results in discontinuous geometric properties, as in the case of the dropped plies concept.

This result cannot be achieved with classical lamination techniques such as the tape layup machine or the manual manufacturing: as a matter of fact these techniques do not have the capability of spatially vary the fiber orientation within a single lamina [9]. Very precise results are obtained with the aid of computer controlled machines, such as a Tow Placement Machine (or Automated Placement Machine), that are able to unroll and deposit fibers with a spatially varying orientation. This machine is essentially a robotic arm that can move on multiple axis (usually seven) and that delivers the fibers on a mould surface through a reel, mounted on the head of the arm [8]. A schematic representation of such a machine is shown in Figure 1.3.

The idea of laminates with non-constant fiber orientation angles was originally introduced by Hyer and Lee [2]: they investigated the possibility of improving the buckling resistance of a composite plate with a central circular hole. Gürdal and Olmedo [3] modelled the elastic response of a variable stiffness panel, providing closed-form solutions for the evaluation of the pre-buckling solution for a number of relevant cases, introducing the notation that is still commonly used for defining the stacking sequence of variable-stiffness laminates. The work was further extended by Gürdal and co-workers [10] to analyse the linear buckling response, while accounting for practical manufacturing constraints [9].

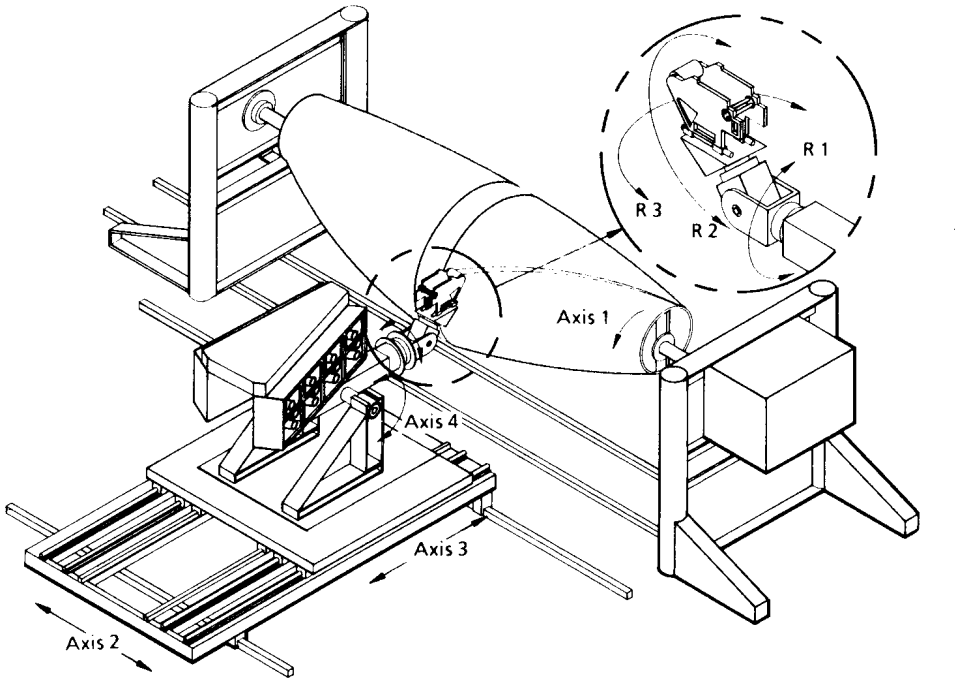

Figure 1.3: A schematic representation of a Tow Placement Machine (taken form [8]).

Years of theoretical and experimental investigations allowed to develop analysis method, understanding the underlying mechanisms and identifying possible advantages and difficulties associated with a variable-stiffness design [11][12]. However, this field cannot be claimed to be mature yet, and novel analytical, numerical and experimental techniques need to be developed in order to reach a higher technology readiness.
For instance, new modelling tools are needed for analysing the buckling and post-buckling response, to fully exploit the opportunities offered by variable-stiffness panels since the early phases of the design project. With this regard, finite element strategies have been widely adopted by many authors [9][5][13][14][15]. On the other hand, the finite element method is generally too costly to make it possible the introduction of non-linear studies since the very first phases of a structural design. New fast yet reliable tools are thus necessary for fully assessing the advantages and the potentialities due to variable-stiffness.

In the years, Ritz-based formulations were developed both for assessing the buckling and post-buckling behaviour of laminated panels, with straight and non-straights fibers. Buckling formulations are briefly reviewed first, while non-linear post-

buckling formulations are discusses next.

The requirement of perform a large number of analyses without too much computational effort lead the scientific research toward *ad hoc* semi-analytical approaches. In their early works, both Leissa and Martin [1] and DiNardo and Lagace [16] adopted the Ritz method in the context of the thin plate theory. It is well known that the Ritz method allows for a reduction of the continuous system to a discrete one. This is achieved by approximating the unknowns of the problem with series expansions: the advantage with respect to the finite element method is that, by a proper choice of the trial functions, the size of the problem can be limited.
The Ritz method has been applied by Alhajahmad et al. [13] in the context of a displacement-based formulation for analysing the optimal fiber distribution for the pressure-pillowing problem. A similar Ritz-based formulation was proposed by Wu et al. [17] to study the linear buckling behaviour of variable-stiffness plates: the governing equations were sought by minimizing the membrane complementary energy, properly written in terms of the Airy stress function. With this solution, the problem is further simplified: the unknowns of the problem are only two (the stress function and the out-of-plane displacement) instead of three, as in the case of a displacement-based formulation.

Other semi-analytical models have been proposed by Waldhart et al. [9], that employed a specific software package to solve the classical equilibrium differential equations; Raju et al. [18] adopted the the Differential Quadrature Method (DQM), which was used, combined with the Ritz method, by Haldar et al. [19] to compute snap-through loads of variable-stiffness shells.
These methods have been proven to be efficient in modelling the linearised buckling behaviour of variable-stiffness panels.

When considering the post-buckled analysis, close-form solutions have been derived in the years [20][21][22], as well as semi-analytical formulations.
Based on the von Kàrmàn non-linear strain-displacement relation, approximate solutions have been obtained for the post-buckling analysis of isotropic plates. Marguerre [23] minimized the total potential energy expressing the problem with the Airy stress function, and Levy [24] employed Fourier expansions to approximate the out-of-plane displacement and the stress function: these relations were then substituted into the non-linear equilibirum equations. The Galerkin method was subsequently used by Prabhakara and Chia [25] to investigate the post-buckling

response of orthotropic laminated plates.
The Ritz method has also been employed in the context of non-linear analyses: for instance, Bisagni and Vescovini [26] developed an analytical formulation based on an energy principle and the method of Ritz for the post-buckling analysis of stiffened composite panels. The same authors also proposed [27] an approach, based on the works of Giavotto [28], to perform the post-buckling analysis by means of a unitary energy functional. The latter was written by means of a mixed formulation, thus employing the Airy stress function and the out-of-plane displacement. The non-linear governing equations were then obtained by employing the Ritz method and minimizing the unitary functional. Milazzo and Olivieri [29] developed a Ritz model by modelling the plate's behaviour by means of the first-order shear deformation and von Kàrmàn geometric non-linearities. A similar model was subsequently used to analyse variable-stiffness plates [30], also accounting for thermal-mechanical coupling.

The approach proposed in [27] was also adopted by Wu et al. [31] to investigate the post-buckling behaviour of variable-stiffness panels: the authors demonstrated that enhanced post-buckling performances can be expected by these kind of structures. As a matter of fact, they found that the reduction of stiffness, usually associated with the post-buckled regime, can be contained by properly tailoring the lamination sequence. This aspect was further investigated by White and Weaver [32], who optimised the fibers angles orientation in order to obtain laminates with negligible degradation of axial post-buckling stiffness.

The perturbation method represent a very interesting option for addressing the post-buckling behaviour of variable-stiffness panels.
This method has been proposed by Koiter [33], who developed the perturbation theory to explain why some structures are able to withstand loads above the buckling load and why others behaviour is drastically different from the predicted one. To this aim, the solution is expanded around the critical point and the non-linear problem is reduced to a set of linear algebraic equations. The advantage of this method is that it provides an useful tool to rapidly evaluate the initial post-buckling behaviour. This aspect have been exploited several times in the past, also in the field of aerospace structures (Jansen et al. [34]).

The Koiter method has been often used in the context of imperfection's sensitive

structures: Koth [35] and Arbcoz [36] confirmed that initial geometric imperfections result in a deviation of the buckling load from the theoretical predicted value. Also, Koht and Venkayya [37] studied the effect of the fibers orientation on the initial post-buckling behaviour of composite cylindrical shells. Other insights on this topic have been given by Garcea et al. [38]. The influence of geometrical imperfections have also been considered by Jansen [39], who studied the natural frequencies of cylindrical anisotropic shells.
Following the functional notation initially proposed by Budiansky [40] and by Byskov and Hutchinson [41], several applications of the Koiter method have been proposed: for instance, Arbocz [36] developed a semi-analytical model based on the non-linear Donnell-type equations in the framework of a Ritz-based method. More often, the perturbation approach is used in the context of finite element-based approaches (Rahman and Jansen [42], Olsen and Byskov [43]).

In the recent years, the perturbation method became relevant also for variable-stiffness applications. The first insights on the post-buckling behaviour of variable-stiffness plates were obtained by Rahman et al. [44]: by applying the Koiter's perturbation theory, the authors were able to accurately captures the post-buckling behaviour in the neighbourhood of the bifurcation point. White et al. [45] studied the initial post-buckling behaviour of variable-stiffness curved panels by proposing a method combining the perturbation analyses to the Generalized Quadrature Method; in a subsequent work [32], the authors used this approach to optimize the fibers angles in order to reduce the degradation of the post-buckling stiffness. Another optimization technique based on the perturbation method has been recently proposed by Henrichsen et al. [46], who used a finite element-based model to limit the development of the post-buckled shape. Finally, Madeo et al. [47] developed a finite element model by using the Koiter's theory: the energy variation for the asymptotic expansion was obtained by means of a corotational approach. The authors demonstrated the importance of accounting for multiple buckling modes when recovering the post-buckling path.

In the present thesis work, two semi-analytical tools, based on the Ritz method and the Koiter's theory, will be developed to address the linear and non-linear behaviour of variable-stiffness panels.
It will be shown that the Ritz-based formulation can trace the post-buckling behaviour of this kind of structures with a good degree of accuracy, with focus on

shallow cylindrical shells. Moreover, a generalised Ritz-Koiter approach is proposed, and it will be shown how this solution is able to provide insights on the initial post-buckling behaviour: this strategy is believed to be particularly useful when, in the preliminary design phases, it is necessary to run an high number of tests, particularly in the case of variable-stiffness panels, where a large design space is present.

1.1 Thesis's Outline

This thesis is organized as follows: a brief overview of thin-plate and shallow theory is presented in Chapter 2. Classical Lamination Theory is reviewed and specialised to the case of variable-stiffness panels is also presented.

Chapter 3 is devoted to the presentation of the approaches for the analysis of variable-stiffness panels. The relevant energy functional are derived, and the advantages of employing this approach are discussed.

In Chapter 4, the Ritz method is used to derive the pre-, buckling and post-buckling problems. After a general introduction to the Ritz method, the trial functions to approximate the unknowns of the problems are presented. Subsequently, it will be shown how the relevant governing equations are derived. Finally, the results obtained with the developed model are presented. Comparison against results from literature and finite element analysis are provided and discussed in order to verify the accuracy of the model.

The subject of Chapter 5 is the application of the Koiter's approach to the analysis of variable-stiffness panels. A general introduction on the perturbation method is provided, and subsequently a generalized Koiter-Ritz approach is proposed. Results are reported for an extensive set of variable-stiffness configurations, and comparison against results from literature and finite element analyses are presented.

Chapter 2

Theory of Thin Plates and Shallow Cylindrical Shells

In this Chapter preliminary theoretical aspects are introduced with regard to thin plate and shallow shell theory. Firstly, the kinematic model adopted to describe the behaviour of plates and shells is presented, together with the underlying assumptions. The Classical Lamination Theory is introduced, and it is specialized to the case of variable-stiffness panels. Finally, an overview is provided regarding the main features characterizing the response of thin panels subjected to compressive loads.

2.1 Kinematic Assumptions

A thin panel is a three-dimensional structural element characterized by one dimension that is particularly small with respect to the others. Typically, a panel is denoted as thin if one dimension, the thickness, is less than 1/20 of its length and width [48]. The stress-strain relation is assumed in the form of a plane stress constitutive law, i.e. $\sigma_{iz} = 0$ with $i = x, y, z$. The transverse shear deformability is neglected, as well as the energy contributions associated with the stretching along the thickness direction. The above assumptions well describe the behaviour of thin 2D structures, and offer the main advantage of obtaining relatively simple governing equations. The panels analysed in this thesis are either flat plates or shallow cylindrical shells.

The plates under considerations are rectangular and characterized by length and width denoted with a and b, respectively, and thickness h. A Cartesian coordinate

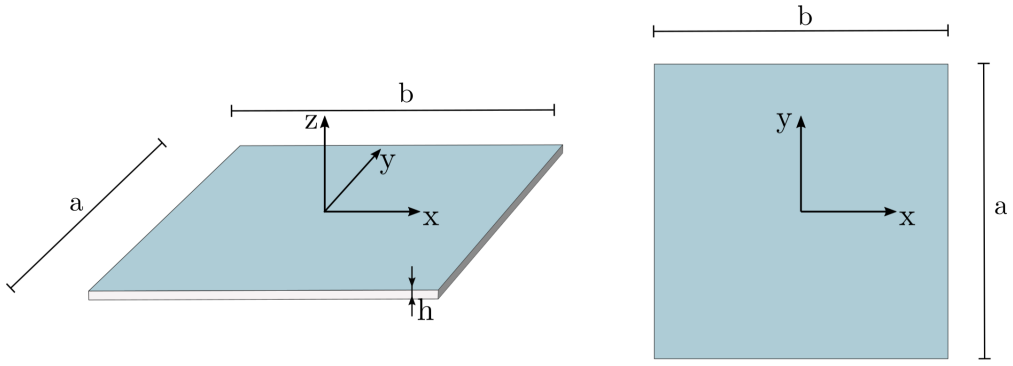

Figure 2.1: Dimensions and reference system of a flat plate.

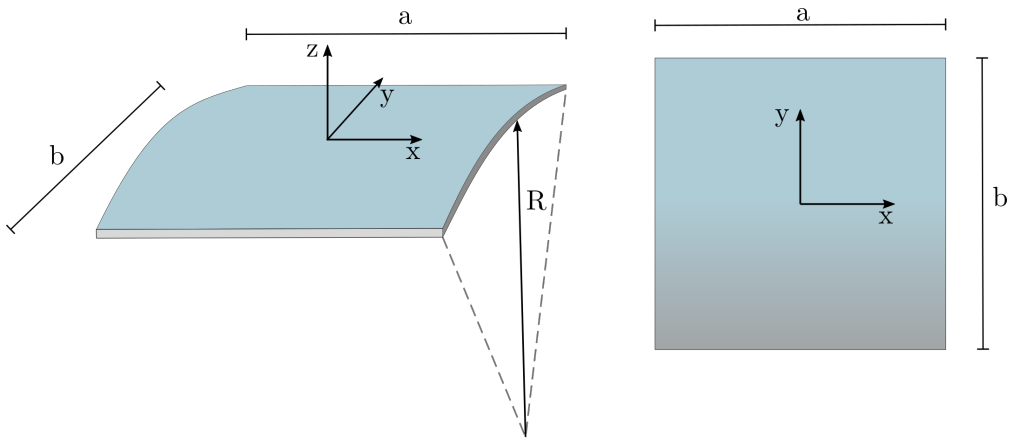

Figure 2.2: Dimensions and reference system of a shallow cylindrical shell.

system is taken as illustrated in Figure 2.1. The x coordinate runs parallel to the length of the plate, the y-direction is directed parallel to the width, while z defines the thickness-wise direction. The displacement components along x and y will be denoted as in-plane displacement, whilst the one along z will be referred to as out-of-plane displacement. Moreover, the plate midplane is taken as reference surface.

The shell panels analysed in this work are characterized by a cylindrical curvature in which the rise with regard to any chord is small [49]. In other words, a shell panel can be seen as a plate characterized by a radius of curvature R, as illustrated in Figure 2.2. It is assumed here that the shell is shallow, meaning that the radius of curvature is much higher with respect to the typical halfwave lengths of the buckled surfaces. It can be worth noting that this assumption is not too restrictive for typical aerospace panels. Furthermore, it offers the advantage of leading to simpler equations to those governing the response of the so-called deep shells, i.e.

shell with smaller radii of curvature.
Shells will be studied by considering a coordinate system similar to the one used for plates, where x denotes the axial direction, y denotes the circumferential one, and z is parallel to the normal to the shell surface. The origin of the system is taken at the centre of the shell. Note that the graphical results for shells (in terms of in-plane stresses or buckling modes) will be displayed in a 2D representation. Therefore, the curvature of the panel will not be visible.

The kinematic model which is assumed for modelling plates and shells refers to the classical model due to Donnell-von Kármán. The underlying assumptions are summarized as:

i The midplane's deflection is small with respect to the thickness pf the panel.

ii Panel sections that are initially plane and normal to the midplane remain plane and normal to the midplane during the deformation process (Kirchhoff hypothesis).

iii In plane displacements are infinitesimal, while the out-of-plane displacement is finite but small.

iv The radius of curvature (if any) is much higher with respect to the typical halfwave length of the buckled configuration.

The first hypothesis means that the theory is developed under small strains and rotations assumptions. For this reason, the displacement of a generic point is expressed by means of the midplane displacement.
The displacement of any point along the x, y and z directions is denoted with $u(x, y, z)$, $v(x, y, z)$ and $w(x, y)$ respectively. The displacement field's components u and v are functions of the three coordinates x, y and z; on the contrary, the out-of-plane displacement does not depend on z, thus the deformation ϵ_{zz} associated with the kinematic model is zero. This aspect is sometimes referred to as an inconsistency of the kinematic model [50], and it would lead to a plane strain behaviour, which is in contrast to the plane stress assumptions discussed before. Nevertheless, the approach is energetically consistent, as the energy contribution due to the thickness is, in any case, equal to zero.

The components of the stress tensor are represented, using a matrix-notation, as

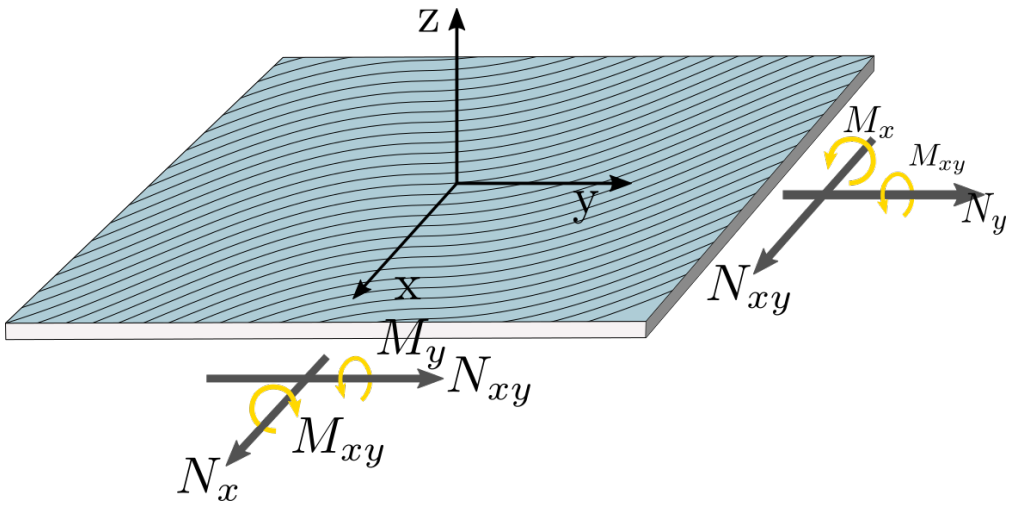

Figure 2.3

[51]

$$\sigma = \begin{bmatrix} \sigma_{xx} & \tau_{yx} & \tau_{zx} \\ \tau_{xy} & \sigma_{yy} & \tau_{zy} \\ \tau_{xz} & \tau_{yz} & \sigma_{zz} \end{bmatrix} \tag{2.1}$$

Consistently with the kinematic assumptions, the generalized forces are defined as:

$$\begin{aligned} N_x &= \int_{-\frac{h}{2}}^{+\frac{h}{2}} \sigma_{xx} dz \qquad N_y = \int_{-\frac{h}{2}}^{+\frac{h}{2}} \sigma_{yy} dz \qquad N_{xy} = \int_{-\frac{h}{2}}^{+\frac{h}{2}} \tau_{xy} dz \\ M_x &= \int_{-\frac{h}{2}}^{+\frac{h}{2}} \sigma_{xx} z dz \quad M_y = \int_{-\frac{h}{2}}^{+\frac{h}{2}} \sigma_{yy} z dz \quad M_{xy} = \int_{-\frac{h}{2}}^{+\frac{h}{2}} \tau_{xy} z dz \end{aligned} \tag{2.2}$$

The quantities N_{ik} and M_{ik} define forces and moment per unit length, respectively. The sign convention adopted is represented in Figure 2.3.

The generalized strain components of the kinematic model can be introduced by recalling the expression of the Green strain tensor, which is given by:

$$\epsilon_{ij} = \frac{1}{2}(u_{/j} + v_{/i} + w_{/i} w_{/j}) - w r_{ij} - z w_{/ij} \tag{2.3}$$

where r_{ij} is the curvature tensor for the case of cylindrical curvature. Eq. 2.3 can be written as:

$$\boldsymbol{\epsilon} = \left\{ \begin{array}{c} \epsilon_{xx} \\ \epsilon_{yy} \\ \gamma_{xy} \end{array} \right\} = \left\{ \begin{array}{c} \epsilon^0_{xx} \\ \epsilon^0_{yy} \\ \gamma^0_{xy} \end{array} \right\} + z \left\{ \begin{array}{c} k_x \\ k_y \\ k_{xy} \end{array} \right\} = \left\{ \begin{array}{c} u_{0/x} + \dfrac{w^2_{0/x}}{2} \\ v_{0/y} + \dfrac{w_0}{R} + \dfrac{w^2_{0/y}}{2} \\ u_{0/x} + v_{0/y} + w_{0/x} w_{0/y} \end{array} \right\} + z \left\{ \begin{array}{c} -w_{0/xx} \\ -w_{0/yy} \\ -2w_{0/xy} \end{array} \right\} \tag{2.4}$$

that in compact form is

$$\boldsymbol{\epsilon} = \boldsymbol{\epsilon}^0 + z\boldsymbol{k} \tag{2.5}$$

where $\boldsymbol{\epsilon}^0$ are the membrane strain and $\mathbf{k}$ are the flexural strain, or curvatures.
In the case of plates the membrane strains can be obtained by taking $R \to \infty$, so:

$$\boldsymbol{\epsilon}^0 = \left\{ \begin{array}{c} u_{0/x} + \dfrac{w^2_{0/x}}{2} \\ v_{0/y} + \dfrac{w^2_{0/y}}{2} \\ u_{0/x} + v_{0/y} + w_{0/x} w_{0/y} \end{array} \right\} \tag{2.6}$$

Regarding the constitutive equations, it is assumed that the panels are made of an elastic material with a linear behaviour. Starting from the general case of a 3D continuum, the constitutive law (Hooke's law) reads:

$$\boldsymbol{\sigma} = \mathbb{C}\boldsymbol{\epsilon} \tag{2.7}$$

or, in terms of components:

$$\sigma_{ij} = \mathbb{C}_{ijkl}\epsilon_{kl} \tag{2.8}$$

where $\mathbb{C}$ is the elasticity fourth-order tensor.
By introducing the Kelvin-Voigt notation, it is possible to collect stress and strain components into vectors, whilst the constitutive law components are organized into a matrix. Note that this approach is usually introduced for facilitating the manipulation of the expressions, but the tensorial nature of strain, stresses and constitutive law should still be preserved.

The strain and stress components are reorganized as:

$$\boldsymbol{\sigma} = \begin{Bmatrix} \sigma_{xx} \\ \sigma_{yy} \\ \sigma_{zz} \\ \gamma_{yz} \\ \gamma_{xz} \\ \gamma_{xy} \end{Bmatrix}, \boldsymbol{\epsilon} \begin{Bmatrix} \epsilon_{xx} \\ \epsilon_{yy} \\ \epsilon_{zz} \\ \tau_{yz} \\ \tau_{xz} \\ \tau_{xy} \end{Bmatrix} \tag{2.9}$$

The elastic stiffness tensor become a 6×6 matrix

$$\mathbb{C} = \boldsymbol{C} = \begin{bmatrix} C_{11} & C_{12} & C_{13} & C_{14} & C_{15} & C_{16} \\ C_{12} & C_{22} & C_{23} & C_{24} & C_{25} & C_{26} \\ C_{13} & C_{23} & C_{33} & C_{34} & C_{35} & C_{36} \\ C_{14} & C_{24} & C_{34} & C_{44} & C_{45} & C_{46} \\ C_{15} & C_{25} & C_{35} & C_{45} & C_{55} & C_{56} \\ C_{16} & C_{26} & C_{36} & C_{46} & C_{56} & C_{66} \end{bmatrix} \tag{2.10}$$

The number of independent components of the stiffness matrix is 21, and they are referred to as elastic constants. The constitutive law is written in matrix form as

$$\boldsymbol{\sigma} = \boldsymbol{C}\boldsymbol{\epsilon} \tag{2.11}$$

This equation can be inverted as

$$\boldsymbol{\epsilon} = \boldsymbol{C}^{-1}\boldsymbol{\sigma} = \boldsymbol{S}\boldsymbol{\sigma} \tag{2.12}$$

where $\boldsymbol{S}$ is the compliance matrix

$$\boldsymbol{S} = \begin{bmatrix} S_{11} & S_{12} & S_{13} & S_{14} & S_{15} & S_{16} \\ S_{12} & S_{22} & S_{23} & S_{24} & S_{25} & S_{26} \\ S_{13} & S_{23} & S_{33} & S_{34} & S_{35} & S_{36} \\ S_{14} & S_{24} & S_{34} & S_{44} & S_{45} & S_{46} \\ S_{15} & S_{25} & S_{35} & S_{45} & S_{55} & S_{56} \\ S_{16} & S_{26} & S_{36} & S_{46} & S_{56} & S_{66} \end{bmatrix} \tag{2.13}$$

The expression of Eqs. 2.10 and 2.13 refer to the case of a generically anisotropic material. Considering now the case of orthotropic material, it is possible to further

reduce the number of independent constants to 9. The assumption of orthotropy is generally a proper modelling choice for plies of composite materials, where three mutually orthogonal planes of material symmetry exist. In this way the expression of the stiffness and compliance matrix modifies as:

$$\boldsymbol{C} = \begin{bmatrix} C_{11} & C_{12} & C_{13} & 0 & 0 & 0 \\ C_{12} & C_{22} & C_{23} & 0 & 0 & 0 \\ C_{13} & C_{23} & C_{33} & 0 & 0 & 0 \\ 0 & 0 & 0 & C_{44} & 0 & 0 \\ 0 & 0 & 0 & 0 & C_{55} & 0 \\ 0 & 0 & 0 & 0 & 0 & C_{66} \end{bmatrix} \tag{2.14}$$

and

$$\boldsymbol{S} = \begin{bmatrix} S_{11} & S_{12} & S_{13} & 0 & 0 & 0 \\ S_{12} & S_{22} & S_{23} & 0 & 0 & 0 \\ S_{13} & S_{23} & S_{33} & 0 & 0 & 0 \\ 0 & 0 & 0 & S_{44} & 0 & 0 \\ 0 & 0 & 0 & 0 & S_{55} & 0 \\ 0 & 0 & 0 & 0 & 0 & S_{66} \end{bmatrix} \tag{2.15}$$

The components of the compliance matrix can be expressed by means of the so called engineering constants, i.e. the Young's modulus (E_x, E_y, E_z), the shear modulus (G_{xy}, G_{xz}, G_{yz}) and the Poisson's ratios (ν_{xy}, ν_{xz}, ν_{yz}) as:

$$\begin{aligned} S_{11} &= \frac{1}{E_x} \quad S_{12} = \frac{-\nu_{xy}}{E_x} \quad S_{13} = \frac{-\nu_{xz}}{E_x} \\ S_{22} &= \frac{1}{E_y} \quad S_{23} = \frac{-\nu_{yz}}{E_y} \quad S_{33} = \frac{1}{E_z} \\ S_{44} &= \frac{1}{G_{yz}} \quad S_{55} = \frac{1}{G_{xz}} \quad S_{66} = \frac{1}{G_{xy}} \end{aligned} \tag{2.16}$$

The notation can be further simplified by exploiting the following relations

$$E_x\nu_{yx} = E_y\nu_{xy}, \qquad E_y\nu_{zy} = E_z\nu_{yz}, \qquad E_z\nu_{xz} = E_x\nu_{zx} \tag{2.17}$$

Finally, it is possible to assume a plane stress state. For this special case, the elastic constitutive law in Eq. 2.11 is

$$\begin{Bmatrix} \sigma_{xx} \\ \sigma_{yy} \\ \tau_{xy} \end{Bmatrix} = \begin{bmatrix} Q_{11} & Q_{12} & 0 \\ Q_{12} & Q_{22} & 0 \\ 0 & 0 & Q_{66} \end{bmatrix} \begin{Bmatrix} \epsilon_{xx} \\ \epsilon_{yy} \\ \gamma_{xy} \end{Bmatrix} \tag{2.18}$$

with

$$\begin{aligned} Q_{11} &= \frac{E_x}{(1-\nu_{xy}\nu_{yx})} \quad Q_{12} = \frac{\nu_{xy}E_y}{(1-\nu_{xy}\nu_{yx})} \\ Q_{22} &= \frac{E_y}{(1-\nu_{xy}\nu_{yx})} \qquad Q_{66} = G_{xy} \end{aligned} \tag{2.19}$$

Using a compact notation, the stress strain relation is written as:

$$\boldsymbol{\sigma} = \boldsymbol{Q}\boldsymbol{\epsilon} \tag{2.20}$$

where $\boldsymbol{Q}$ is defined according to Eq. 2.18, while $\boldsymbol{\sigma}$ and $\boldsymbol{\epsilon}$ are the vectors collecting the stress and the strain components associated with the plane stress assumptions. This relation will be exploited in the next Section in order to describe the behaviour in terms of generalized forces and strains of a laminate panel.

2.2 Classical Lamination Theory

Composite panels are structural elements obtained by the stacking of plies, each oriented at a different angle.

Each ply is made of two separate phases, namely the fibers and the matrix, and can be generally modelled with an orthotropic constitutive law as outlined in the previous section. Long fibers are usually employed in the aerospace field and are commonly characterized by a high length-to-diameter ratio and a near-crystal-sized diameter. Carbon or glass based fibres are able to withstand several thousands of MPa, being at the same time extremely light.

However, fibers alone are not able to efficiently operate in a structural sense, since they can only transmit uniaxial tensile loads. Therefore, they are immersed into a binder material that is able to stick together all the fibers, with the drawback that such binder (called matrix) has usually low stiffness and strength properties.

The matrix is supposed to provide the shape and the dimensional stability to the structure and allows the transmission of the load in different directions beside the

uniaxial one. Matrices are usually made of epoxy or polymers materials. The fibers and the matrix combine together to form a ply.
The result is a material that has strength and stiffness properties that are a compromise between fibers and the matrix ones: it is possible to tune the volume content of fibers and matrix in order to obtain different material characteristics.
Fibers are usually parallel to each other and oriented in the same direction within a ply. Therefore it is possible to assemble plies oriented in different direction to form a laminate.

To describe how plies are assembled together, a *lamination sequence*, or *lay-up*, is defined. If θ_k is the orientation of the k-th ply, the lamination sequence of a N-plies laminate is written as

$$[\theta_1/\theta_2/\cdots/\theta_k/\cdots/\theta_N] \tag{2.21}$$

The lamination sequence can be specified and optimized in order to achieve the design requirements and the combinations are almost unlimited.
However, laminates that are most commonly adopted for engineering applications are characterized by specific sequences, aimed at avoiding undesired elastic couplings. Among the various categories, three of them are here summarized:

- **Symmetric Laminates**: the layers are symmetric with respect to the mid-plane ($\forall\,\theta$ at z_k, $\exists\,\theta$ at $-z_k$)

$$[\theta_1/\cdots/\theta_i/\theta_N/\theta_N/\theta_k/\cdots/\theta_1] = [\theta_1/\cdots/\theta_k/\theta_N]_S \tag{2.22}$$

- **Anti-symmetric Laminates**: the layers below the midplane are inverted with respect to the ones above ($\forall\,\theta$ at z_k, $\exists\,-\theta$ at $-z_k$)

$$[\theta_1/\cdots/\theta_k/\theta_N/-\theta_N/-\theta_k/\cdots/-\theta_1] \tag{2.23}$$

- **Balanced Laminates**: every layer has a specular layer which is not necessarily at the opposite z-coordinate ($\forall\,\theta$ at z_k, $\exists\,-\theta$)

In many engineering applications, symmetric laminates are preferred over the non-symmetric ones. Even though this assumption has the effect of reducing the tailoring possibilities, it offers the advantage of avoiding the coupling between in-plane and out-of-plane response. This latter is often undesirable, especially due to the complicating effects on the manufacturing process. For this reason, only

symmetric laminates have been considered in the present work.

In order to obtain the constitutive relation between generalized stresses (forces and moments per unit length) and generalized deformations (membrane strains and curvatures), the Classical Lamination Theory (CLT) is introduced.
To compute the properties of the laminate, a local reference system is defined for each ply rotating the x and y axes of the global reference system counterclockwise through an angle θ_k around the z-axis.
Given the different orientation of the plies composing the stack, it is necessary to express the constitutive law of each ply in the global reference system. To this aim, the constitutive law of Eq. 2.18 can be rotated as:

$$\overline{\boldsymbol{Q}}_k = \boldsymbol{T}_k^{-1}\boldsymbol{Q}_k\boldsymbol{T}_k^{-T} = \begin{bmatrix} \overline{Q}_{11} & \overline{Q}_{12} & \overline{Q}_{16} \\ \overline{Q}_{12} & \overline{Q}_{22} & \overline{Q}_{26} \\ \overline{Q}_{16} & \overline{Q}_{26} & \overline{Q}_{66} \end{bmatrix} \tag{2.24}$$

where $\boldsymbol{T}_k$ is a rotation matrix defined as:

$$\boldsymbol{T}_k = \begin{bmatrix} \cos^2(\theta) & \sin^2(\theta) & 2\sin(\theta)\cos(\theta) \\ \sin^2(\theta) & \cos^2(\theta) & -2\sin(\theta)\cos(\theta) \\ -\sin(\theta)\cos(\theta) & \sin(\theta)\cos(\theta) & \cos^2(\theta) - \sin^2(\theta) \end{bmatrix} \tag{2.25}$$

where θ is the orientation angle of a ply. The rotated constitutive law for the k-th ply is:

$$\boldsymbol{\sigma}_k = \overline{\boldsymbol{Q}}_k\boldsymbol{\epsilon} \tag{2.26}$$

Alternatively the components of $\overline{\boldsymbol{Q}}_k$ can be written as [48]:

$$\begin{aligned} \overline{Q}_{11} &= U_1 + U_2\cos(2\theta) + U_3\cos(4\theta) \\ \overline{Q}_{12} &= U_4 - U_3\cos(4\theta) \\ \overline{Q}_{22} &= U_1 - U_2\cos(2\theta) + U_3\cos(4\theta) \\ \overline{Q}_{16} &= \frac{1}{2}U_2\sin(2\theta) + U_3\sin(4\theta) \\ \overline{Q}_{26} &= \frac{1}{2}U_2\sin(2\theta) - U_3\sin(4\theta) \\ \overline{Q}_{22} &= U_5 - U_3\cos(4\theta) \end{aligned} \tag{2.27}$$

where the constants U are:

$$\begin{aligned} U_1 &= \frac{3Q_{11} + 3Q_{22} + 2Q_{12} + 4Q_{66}}{8} \\ U_2 &= \frac{Q_{11} - Q_{22}}{2} \\ U_3 &= \frac{Q_{11} + Q_{22} - 2Q_{12} - 4Q_{66}}{8} \\ U_4 &= \frac{Q_{11} + Q_{22} + 6Q_{12} - 4Q_{66}}{8} \\ U_5 &= \frac{Q_{11} + Q_{22} - 2Q_{12} + 4Q_{66}}{8} \end{aligned} \tag{2.28}$$

Using Eq. 2.2 the force resultants are written for a composite panel with N-layers of thickness h_k as:

$$\begin{Bmatrix} N_x \\ N_y \\ N_{xy} \end{Bmatrix} = \int_{-\frac{h}{2}}^{+\frac{h}{2}} \begin{Bmatrix} \sigma_{xx} \\ \sigma_{yy} \\ \tau_{xy} \end{Bmatrix} dz = \sum_{k=1}^{N} \int_{h_k} \begin{Bmatrix} \sigma_{xx} \\ \sigma_{yy} \\ \tau_{xy} \end{Bmatrix}_k dz \tag{2.29}$$

inserting Eq. 2.26 into Eq. 2.29 gives:

$$\begin{Bmatrix} N_x \\ N_y \\ N_{xy} \end{Bmatrix} = \sum_{k=1}^{N} \int_{h_k} \overline{\boldsymbol{Q}}_k \boldsymbol{\epsilon} dz = \sum_{k=1}^{N} \int_{h_k} \begin{bmatrix} \overline{Q}_{11} & \overline{Q}_{12} & \overline{Q}_{16} \\ \overline{Q}_{12} & \overline{Q}_{22} & \overline{Q}_{26} \\ \overline{Q}_{16} & \overline{Q}_{26} & \overline{Q}_{66} \end{bmatrix}_k (\boldsymbol{\epsilon}^0 + z\boldsymbol{k}) dz \tag{2.30}$$

and by separating the membrane and the flexural parts is is obtained

$$\begin{Bmatrix} N_x \\ N_y \\ N_{xy} \end{Bmatrix} = \sum_{k=1}^{N} \int_{h_k} \begin{bmatrix} \overline{Q}_{11} & \overline{Q}_{12} & \overline{Q}_{16} \\ \overline{Q}_{12} & \overline{Q}_{22} & \overline{Q}_{26} \\ \overline{Q}_{16} & \overline{Q}_{26} & \overline{Q}_{66} \end{bmatrix}_k \boldsymbol{\epsilon}^0 dz + \sum_{k=1}^{N} \int_{h_k} \begin{bmatrix} \overline{Q}_{11} & \overline{Q}_{12} & \overline{Q}_{16} \\ \overline{Q}_{12} & \overline{Q}_{22} & \overline{Q}_{26} \\ \overline{Q}_{16} & \overline{Q}_{26} & \overline{Q}_{66} \end{bmatrix}_k z\boldsymbol{k}) dz \tag{2.31}$$

The expression of Eq. 2.31 can be finally written as:

$$\begin{Bmatrix} N_x \\ N_y \\ N_{xy} \end{Bmatrix} = \begin{bmatrix} A_{11} & A_{12} & A_{16} \\ A_{12} & A_{22} & A_{26} \\ A_{16} & A_{26} & A_{66} \end{bmatrix} \boldsymbol{\epsilon}^0 + \begin{bmatrix} B_{11} & B_{12} & B_{16} \\ B_{12} & B_{22} & B_{26} \\ B_{16} & B_{26} & B_{66} \end{bmatrix} \boldsymbol{k} = \boldsymbol{A}\boldsymbol{\epsilon}^0 + \boldsymbol{B}\boldsymbol{k} \tag{2.32}$$

where $\boldsymbol{A}$ is the membranal stiffness matrix and $\boldsymbol{B}$ is the extension-bending coupling matrix, whose components are defined as

$$A_{ij} = \sum_{k=1}^{N} \int_{h_k} (\overline{\boldsymbol{Q}}_{ij})_k dz = \sum_{k=1}^{N} (\overline{\boldsymbol{Q}}_{ij})_k (z_k - z_{k-1}) \tag{2.33}$$

$$B_{ij} = \sum_{k=1}^{N} \int_{h_k} (\overline{\boldsymbol{Q}}_{ij})_k z_k dz = \sum_{k=1}^{N} (\overline{\boldsymbol{Q}}_{ij})_k \frac{(z_k^2 - z_{k-1}^2)}{2} \tag{2.34}$$

The same procedure can be used to obtain a relation between moments per unit length and the generalized strain components:

$$\begin{Bmatrix} M_y \\ M_x \\ M_{xy} \end{Bmatrix} = \int_{-\frac{h}{2}}^{+\frac{h}{2}} \begin{Bmatrix} \sigma_{xx} \\ \sigma_{yy} \\ \tau_{xy} \end{Bmatrix} dz = \sum_{k=1}^{N} \int_{h_k} \begin{Bmatrix} \sigma_{xx} \\ \sigma_{yy} \\ \tau_{xy} \end{Bmatrix}_k dz \tag{2.35}$$

inserting Eq. 2.26

$$\begin{Bmatrix} M_y \\ M_x \\ M_{xy} \end{Bmatrix} = \sum_{k=1}^{N} \int_{h_k} \overline{\boldsymbol{Q}}_k \boldsymbol{\epsilon} dz = \sum_{k=1}^{N} \int_{h_k} \begin{bmatrix} \overline{Q}_{11} & \overline{Q}_{12} & \overline{Q}_{16} \\ \overline{Q}_{12} & \overline{Q}_{22} & \overline{Q}_{26} \\ \overline{Q}_{16} & \overline{Q}_{26} & \overline{Q}_{66} \end{bmatrix}_k z_k (\boldsymbol{\epsilon}^0 + z\boldsymbol{k}) dz \tag{2.36}$$

separating the membrane and the flexural parts

$$\begin{Bmatrix} M_y \\ M_x \\ M_{xy} \end{Bmatrix} = \sum_{k=1}^{N} \int_{h_k} \begin{bmatrix} \overline{Q}_{11} & \overline{Q}_{12} & \overline{Q}_{16} \\ \overline{Q}_{12} & \overline{Q}_{22} & \overline{Q}_{26} \\ \overline{Q}_{16} & \overline{Q}_{26} & \overline{Q}_{66} \end{bmatrix}_k z\boldsymbol{\epsilon}^0 dz + \sum_{k=1}^{N} \int_{h_k} \begin{bmatrix} \overline{Q}_{11} & \overline{Q}_{12} & \overline{Q}_{16} \\ \overline{Q}_{12} & \overline{Q}_{22} & \overline{Q}_{26} \\ \overline{Q}_{16} & \overline{Q}_{26} & \overline{Q}_{66} \end{bmatrix}_k z^2\boldsymbol{k}) dz \tag{2.37}$$

and integrating

$$\begin{Bmatrix} M_y \\ M_x \\ M_{xy} \end{Bmatrix} = \begin{bmatrix} B_{11} & B_{12} & B_{16} \\ B_{12} & B_{22} & B_{26} \\ B_{16} & B_{26} & B_{66} \end{bmatrix} \boldsymbol{\epsilon}^0 + \begin{bmatrix} D_{11} & D_{12} & D_{16} \\ D_{12} & D_{22} & D_{26} \\ D_{16} & D_{26} & D_{66} \end{bmatrix} \boldsymbol{k} = \boldsymbol{B}\boldsymbol{\epsilon}^0 + \boldsymbol{D}\boldsymbol{k} \tag{2.38}$$

where $\boldsymbol{D}$ is the bending-stiffness matrix, whose components are defined as

$$D_{ij} = \sum_{k=1}^{N} \int_{h_k} (\overline{\boldsymbol{Q}}_{ij})_k z_k^2 dz = \sum_{k=1}^{N} (\overline{\boldsymbol{Q}}_{ij})_k \frac{(z_k^3 - z_{k-1}^3)}{3} \tag{2.39}$$

The final constitutive law that links the resultant forces and moments to the midplane strains is

$$\begin{Bmatrix} \boldsymbol{N} \\ \boldsymbol{M} \end{Bmatrix} = \begin{bmatrix} \boldsymbol{A} & \boldsymbol{B} \\ \boldsymbol{B} & \boldsymbol{D} \end{bmatrix} \begin{Bmatrix} \boldsymbol{\epsilon}^0 \\ \boldsymbol{k} \end{Bmatrix} \tag{2.40}$$

and the extended form of the so-called $[AB; BD]$ matrix is

$$[AB; BD] = \begin{bmatrix} A_{11} & A_{12} & A_{16} & B_{11} & B_{12} & B_{16} \\ A_{12} & A_{22} & A_{26} & B_{12} & B_{22} & B_{26} \\ A_{16} & A_{26} & A_{66} & B_{16} & B_{26} & B_{66} \\ B_{11} & B_{12} & B_{16} & D_{11} & D_{12} & D_{16} \\ B_{12} & B_{22} & B_{26} & D_{12} & D_{22} & D_{26} \\ B_{16} & B_{26} & B_{66} & D_{16} & D_{26} & D_{66} \end{bmatrix} \tag{2.41}$$

The $[AB; BD]$ matrix assumes different forms for each of the laminate categories presented at the beginning of this Section. For instance, in the case of a symmetric laminate

$$[AB; BD] = \begin{bmatrix} A_{11} & A_{12} & A_{16} & 0 & 0 & 0 \\ A_{12} & A_{22} & A_{26} & 0 & 0 & 0 \\ A_{16} & A_{26} & A_{66} & 0 & 0 & 0 \\ 0 & 0 & 0 & D_{11} & D_{12} & D_{16} \\ 0 & 0 & 0 & D_{12} & D_{22} & D_{26} \\ 0 & 0 & 0 & D_{16} & D_{26} & D_{66} \end{bmatrix} \tag{2.42}$$

and for anti-symmetric laminates

$$[AB; BD] = \begin{bmatrix} A_{11} & A_{12} & 0 & 0 & 0 & B_{16} \\ A_{12} & A_{22} & 0 & 0 & 0 & B_{26} \\ 0 & 0 & A_{66} & B_{16} & B_{26} & 0 \\ 0 & 0 & B_{16} & D_{11} & D_{12} & D_{16} \\ 0 & 0 & B_{26} & D_{12} & D_{22} & D_{26} \\ B_{16} & B_{26} & 0 & D_{16} & D_{26} & D_{66} \end{bmatrix} \tag{2.43}$$

An alternative form of the constitutive law is generally useful, especially in those cases where the formulation is developed by introducing the stress function. The membrane strains $\boldsymbol{\epsilon}^0$ will be expressed as a function of the resultant forces in a

semi-inverted form of Eq. 2.40, as:

$$\begin{Bmatrix} \boldsymbol{\epsilon^0} \\ \boldsymbol{M} \end{Bmatrix} = \begin{bmatrix} \boldsymbol{a} & \boldsymbol{b} \\ -\boldsymbol{b}^T & \boldsymbol{D^*} \end{bmatrix} \begin{Bmatrix} \boldsymbol{N} \\ \boldsymbol{k} \end{Bmatrix} \tag{2.44}$$

where

$$\boldsymbol{a} = \boldsymbol{A}^{-1}, \quad \boldsymbol{b} = -\boldsymbol{A}^{-1}\boldsymbol{B}, \quad \boldsymbol{D^*} = \boldsymbol{D} - \boldsymbol{B}\boldsymbol{A}^{-1}\boldsymbol{B} \tag{2.45}$$

In general $\boldsymbol{a}$ and $\boldsymbol{D^*}$ are symmetric, while $\boldsymbol{b}$ is not. Moreover, for a symmetric laminate

$$\boldsymbol{b} = 0, \quad \boldsymbol{D^*} = \boldsymbol{D} \tag{2.46}$$

2.2.1 Application to Variable-Stiffness Laminates

Variable-stiffness panels are structural elements characterized by stiffness properties which are function of the in-plane position.
The effect of this assumption is that, in turn, the laminate constitutive law is function of the position. In the most general case, it is:

$$[AB; BD] = \begin{bmatrix} A_{11}(x,y) & A_{12}(x,y) & A_{16}(x,y) & B_{11}(x,y) & B_{12}(x,y) & B_{16}(x,y) \\ A_{12}(x,y) & A_{22}(x,y) & A_{26}(x,y) & B_{12}(x,y) & B_{22}(x,y) & B_{26}(x,y) \\ A_{16}(x,y) & A_{26}(x,y) & A_{66}(x,y) & B_{16}(x,y) & B_{26}(x,y) & B_{66}(x,y) \\ B_{11}(x,y) & B_{12}(x,y) & B_{16}(x,y) & D_{11}(x,y) & D_{12}(x,y) & D_{16}(x,y) \\ B_{12}(x,y) & B_{22}(x,y) & B_{26}(x,y) & D_{12}(x,y) & D_{22}(x,y) & D_{26}(x,y) \\ B_{16}(x,y) & B_{26}(x,y) & B_{66}(x,y) & D_{16}(x,y) & D_{26}(x,y) & D_{66}(x,y) \end{bmatrix} \tag{2.47}$$

Accordingly, the semi-inverse relation in Eq. 2.44 is

$$\begin{Bmatrix} \boldsymbol{\epsilon}^0 \\ \boldsymbol{M} \end{Bmatrix} = \begin{bmatrix} \boldsymbol{a}(x,y) & \boldsymbol{b}(x,y) \\ -\boldsymbol{b}^T(x,y) & \boldsymbol{D^*}(x,y) \end{bmatrix} \begin{Bmatrix} \boldsymbol{N} \\ \boldsymbol{k} \end{Bmatrix} \tag{2.48}$$

Despite the generality of the expressions of Eq. 2.47, which can account for any dependence of the elastic coefficients from x and y, it is worth noting that the variation of the orientation angle is not completely arbitrary. Indeed, this variation is subjected to technological restrictions, which are not, however, the subject of the present investigation.
During the design process it is necessary to define a reference path for the fibers which will characterize the panel and influence its behaviour.

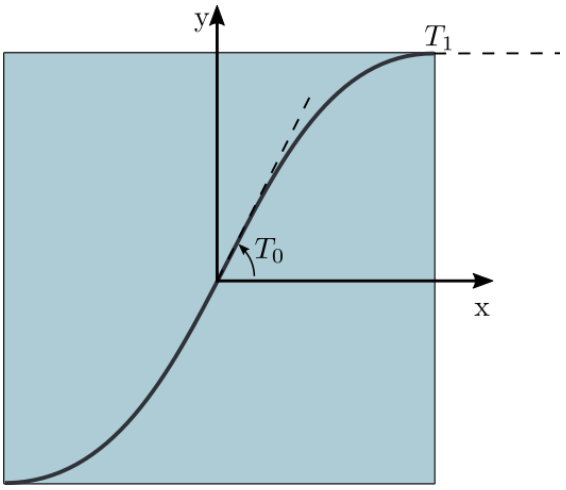

Figure 2.4: Reference path: linear variation along the x-axis.

An early study by Gürdal and Olmedo [3] introduced a standard for the notation of the lamination sequence of variable-stiffness laminates. During the years, however, different ways of prescribing fibers' orientation have been used.
Generalizing, two main categories can be identified: panels with linear fibers path and panels with non-linear fibers path. The formulation presented in this work is general enough to allow the analysis of both these kind of fibers paths. For simplicity, but without loss of generality, most of the results will be presented for linear fiber orientation.

Linear Variation The most simple way of implementing the variable stiffness concept is to allow fibers to linearly vary orientation along one direction. By considering a reference system whose origin is taken in the centre of the panel, as reported in Figure 2.4, the orientation of the fiber is described by:

$$\theta(x) = \frac{2(T_0 - T_1)}{a}|x| + T_0 \tag{2.49}$$

where T_0 is the fiber orientation in the centre of the panel (at $x = 0$) and T_1 is the fiber orientation at the panel's ends (at $x = \pm\frac{a}{2}$). A graphical representation is reported in Figure 2.4. Similarly, for a linear variation of the fibers angles in the y-direction

$$\theta(y) = \frac{2(T_0 - T_1)}{b}|y| + T_0 \tag{2.50}$$

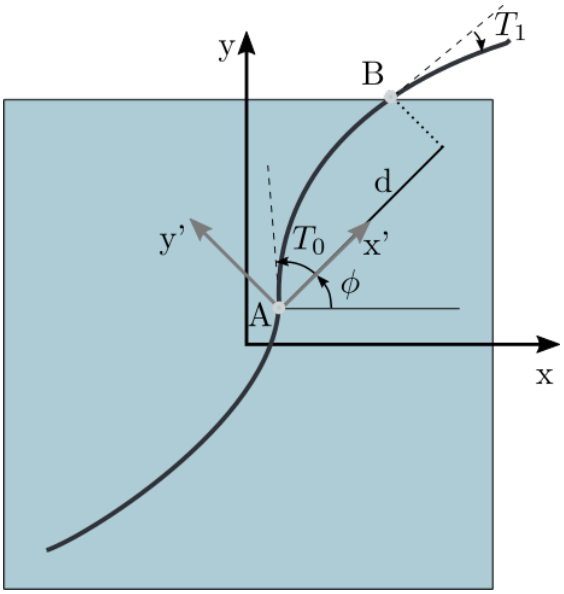

Figure 2.5: Reference path: linear variation along the x'-axis. The orientation angle is a function of x and y.

It can be noted that θ is a function of one coordinate only. Using the linear variation concept is also possible to specify a reference path where the variation is linear with respect to a generally oriented reference line. This allows to specify more lamination sequences, enlarging the design space.
To this aim, the reference path in (x, y) is rotated by an angle ϕ to another reference system (x',y'). The orientation is defined between two points A and B at a general distance d (see Figure 2.5). Hence, the reference path is described as:

$$\theta(x, y) = \theta(x') = \phi + (T_1 - T_0)\frac{x'}{d} + T_0 \tag{2.51}$$

As seen, the description is still linear with respect to the coordinate x' but the fiber's angle is a function of both x and y. Usually the distance d is taken as half of the panel dimension, so that the point A coincide with the panel center and B lies on the panel's edges.
In general, the reference path - the same for all the fibers within a single ply - is characterized by three parameters: ϕ, T_0 and T_1. In this case, the fiber path associated with the generic ply is indicated as:

$$[\phi \langle T_0, T_1 \rangle] \tag{2.52}$$

For example, the lamina in Figure 2.4 is characterized by a fiber that is oriented at $T_0 = 45°$ in the center and $T_1 = 0°$ at the plate's ends. According to the notation introduced, the ply is denoted as $[0\,\langle 45, 0\rangle]$.
Using this notation, it is possible to specify a lamination sequence for laminates with spatially varying stiffness properties. For instance, in the case of a laminate with two plies, characterized by $[0\,\langle 45, 0\rangle]$ and $[0\,\langle -45, 0\rangle]$, the lamination sequence is

$$[0\,\langle 45, 0\rangle\,/0\,\langle -45, 0\rangle]$$

. The following conventions are often used in literature, and they will be also employed in the thesis:

- A $\pm$ sign in front of $\langle T_0, T_1\rangle$ means that there are two adjacent plies with equal and opposite variation of fibers angle e.g. $[\pm\,\langle 45, 15\rangle] = [\langle 45, 15\rangle\,/\,\langle -45, -15\rangle]$
- A $\pm$ sign in front of ϕ means that there are two adjacent plies with equal and opposite ply reference system e.g. $[\pm 50\,\langle 45, 15\rangle] = [+50\,\langle 45, 15\rangle\,/-50\,\langle 45, 15\rangle]$
- Following the usual convention for laminates, an S subscript means that the laminate is symmetric, e.g. $[\pm 50\,\langle 45, 15\rangle]_S = [+50\,\langle 45, 15\rangle\,/ -50\,\langle 45, 15\rangle\,/ -50\,\langle 45, 15\rangle\,/ +50\,\langle 45, 15\rangle]$

Non-linear Variation In literature, some authors proposed more complex descriptions of the fibers path. In this case, the behaviour is not necessarily linear, but non-linear variations are considered. In the most general case the orientation is completely arbitrary and several mathematical expressions are available for describing the fiber path. For instance, Setoodeh et al. [5] considered a highly non-linear distribution, which was the result of a design optimization. A representation of their results is reported in Figure 2.6.

The first attempts to describe a non-linear variation of fibers' orientation have been made in the context of lamination parameters (Abdalla [52], Setoodeh et al. [5], IJsselmuiden et al. [53]) which were used as the main design variables. In this way the optimization process is performed without knowing the lamination sequence, which is recovered in the post-processing phase.
Alternatively, non-linear laws have been used to describe the fiber angle θ. Setoodeh et al. [5] proposed an orientation description based on Lobatto polynomials while Wu et al. [17] implemented a path description based on Lagrangian polynomials.

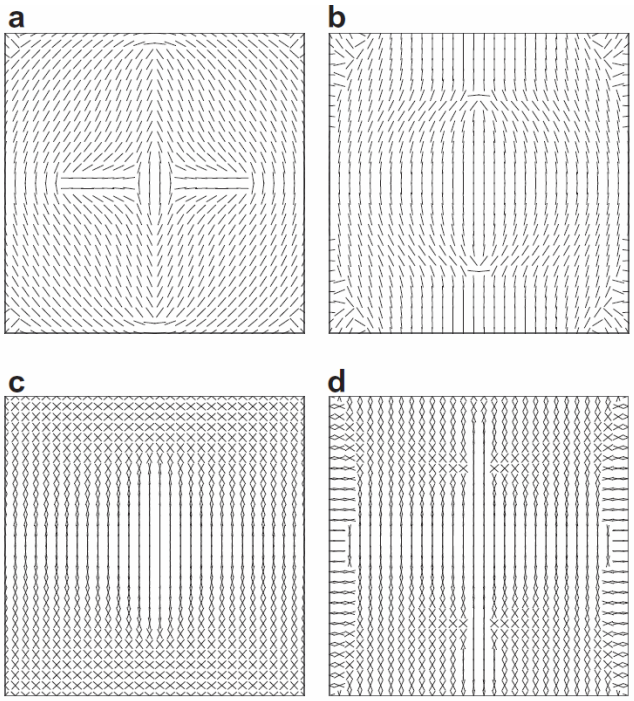

Figure 2.6: Examples of non-linear distribution of fibers obtained by Setoodeh et al. after an optimization process. (taken from [5])

As opposed to formulations based on the use of lamination parameters, these descriptions allows the designer to specify directly the fibers angles at specific points; a post-processing phase to recover the stacking sequence is thus not needed. In the case of Lagrangian polynomials, the fibers path is [17]:

$$\theta(x,y) = \sum_{m=0}^{M-1}\sum_{n=0}^{N-1} T_{mn} \cdot \prod_{m\neq i}\left(\frac{x-x_i}{x_m-x_i}\right) \cdot \prod_{n\neq j}\left(\frac{y-y_j}{y_n-y_i}\right) \tag{2.53}$$

where the coefficients T_{mn} of the polynomials are directly the fiber angle in the points (x_m, y_m). Using a grid of M×N points it is possible to have full control on fibers orientation. The direct link with the orientation angles makes this approach very intuitive and, for this reason, is adopted also in the present work.

Implementation Aspects Within the framework of the present implementation, the variation of the ply angles is accounted for a function that takes as input the panel properties, the material properties (in terms of engineering parameters), the reference path description, the lamination sequence and the position (x_i, y_j) at

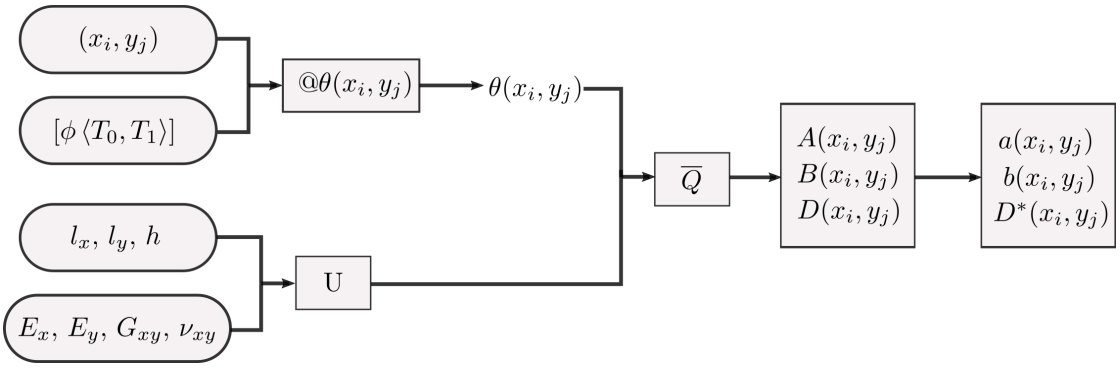

Figure 2.7: Flow chart implemented to include the variable-stiffness feature in the code.

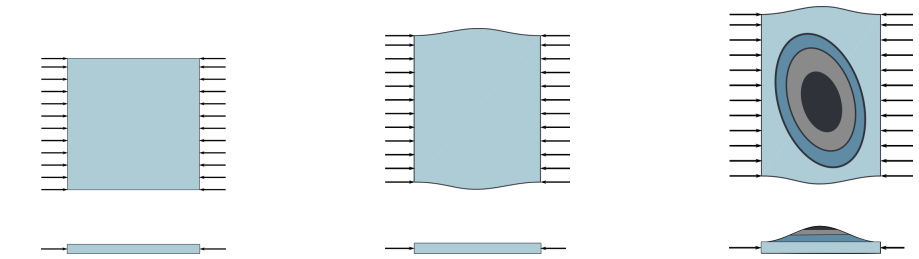

(a) Undeformed Panel (b) In-plane deformation (c) Out-of-plane deformation

Figure 2.8: Pre-buckling and buckling behaviour of a compressed plate.

which the stiffness properties needs to be evaluated. The angle $\theta(x_i, y_j)$ is evaluated and inserted in Eq. 2.27 to obtain the matrix $\overline{\boldsymbol{Q}}_i(x, y)$. The matrices $\boldsymbol{a}(x_i, y_j)$, $\boldsymbol{b}(x_i, y_j)$ and $\boldsymbol{D^*}(x_i, y_j)$ are then computed as described in Eq. 2.45 and returned. The script flow is represented in Figure 2.7.

2.3 Behaviour of Compressed Panels

Typical aircraft-like conditions are such that structural panels are subjected to compressive and shearing loads. This kind of loads may promote instability phenomena, which are thus of crucial importance when analysing and designing aerospace structures.

A qualitatively description of the buckling behaviour of a thin panel is illustrated in Figure 2.8. The plate, assumed for simplicity perfectly flat, is initially compressed by means of a prescribed load per unit length N. As the load increases, the plate undergoes a deformation which is characterized by null out-of-plane deflections. The behaviour involves thus a purely membrane response, and no energy is stored in the form of bending energy. This initial state of deformation is denoted as

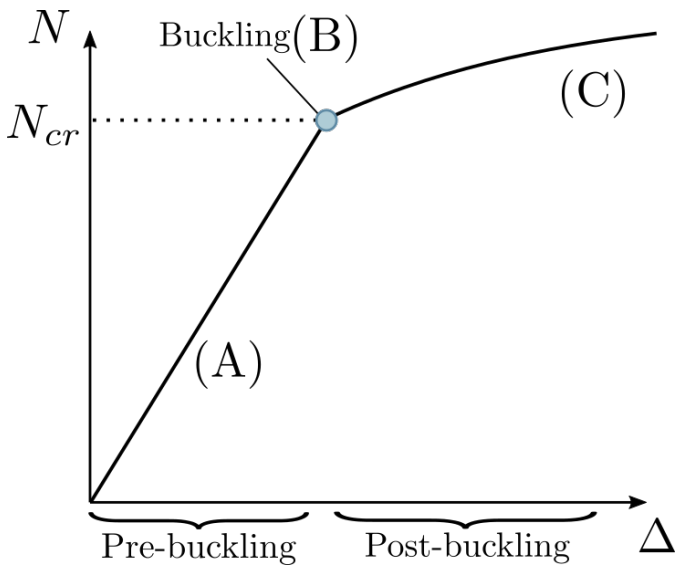

Figure 2.9: Load-displacement curve of a compressed imperfection-free panel.

pre-buckling state.
After reaching a critical load level N_{cr}, the plate buckles, meaning that part of the membrane energy is transferred into bending one. The out-of-plane deflection becomes different from zero, and the deformed configuration becomes characterized by the typical buckles illustrated in Figure 2.8b.
The critical load is also denoted as *buckling load*, and defines the transition between the portion of the equilibirum path where the solution is unique, to the portion where multiple solutions are possible.
As the load is increased beyond the buckling load, the plate enters the so-called *post-buckling* state. The response is no longer linear and is characterized by an inherent non-linear coupling between in-plane and out-of-plane behaviour. The load is carried by means of an internal load re-distribution, and a drop of stiffness is experienced by the structures just after buckling happens.

The behaviour of a compressed structure can be represented with the load-displacement curve, as reported in Figure 2.9, where N is the imposed load and Δ is the average edge displacement of the plate. In Figure 2.9 it can be noted that the initial part of the response is characterized by a linear behaviour. When the critical point is reached (point B), the response suddenly changes, and above the critical load the slope of the curve is no longer linear (C).

For a perfect structure, the transition between pre-buckling and post-buckling

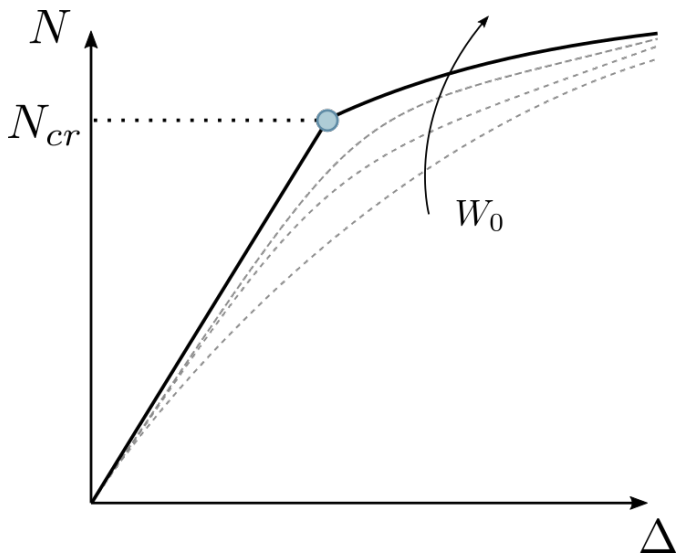

Figure 2.10: Load-displacement curve of a compressed imperfect panel.

conditions is identified by a precise point in the load-displacement curve. This points corresponds to the buckling load, and is also denoted as *bifurcation point*. In the presence of initial imperfections - slightly deviations from the nominal configuration -, the response modifies as illustrated in Figure 2.10: the transition between pre- and post-buckling field is not associated with one single point but, on the contrary, a smoother variation can be noted. In terms of force-displacement curve, this means that the curve is C^0 for a perfect plate, while a higher degree of regularity, characterized by a continuous first derivative, is noted for the imperfect plate. Moreover, the higher the imperfection magnitude w_0, the smoother the transition.

In the case of a cylindrical shell, the post-buckling behaviour is, in general, very different: the equilibrium state might jump to another equilibrium state which isfar away from the previous one, resulting in a *snap-through* behaviour. For instance, the snap-through behaviour is represented in the force-displacement curve in Figure 2.11. In the Figure it is also reported the limit-load N_s, that is a relative maximum of the force-displacement curve.
Shells are said to be imperfective sensitive: this means that a drastic reduction of the limit load is observed as the magnitude of the imperfections is increased. Furthermore, depending on the shape and the magnitude of the initial imperfection, the real behaviour might be very different from the predicted one. The imperfection sensitivity of shells has been one of the main reasons that motivated a huge amount

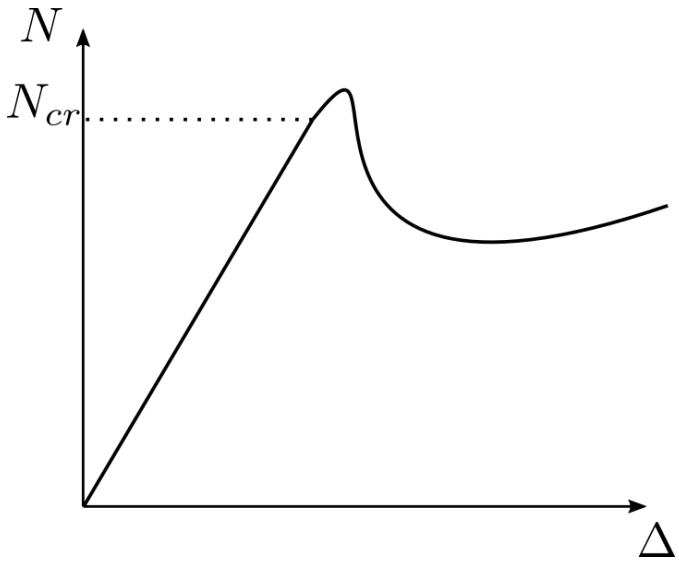

Figure 2.11: Load-displacement curve of a compressed imperfect plate.

of research efforts starting from the last century, and still ongoing in recent research projects (DESICOS, NASA SBKF). It is worth noting that geometric imperfections play a crucial role on the reduction of the limit load. However, imperfections of other nature - material properties, orientation angles, boundary conditions - play also an important role in knocking down the buckling load of shells. For this reason, special purpose tools are generally needed to precisely investigate the response of shells.

Chapter 3

Variational Principles

In this Chapter the pre-, buckling and post-buckling problems are formulated for plates and shallow shells by means of a variational approach.
With this regard, the pre-buckling problem is derived from the complementary energy, and the post-buckling one is obtained by employing a unitary functional, which is also used to derive the linearised buckling problem. The latter is formulated by means of the adjacent equilibrium criteria.
Firstly, the approach followed to obtain the linearised buckling problem and the post-buckling problem is presented.
Subsequently, the energy functional that will be used in the following chapters will be derived.

3.1 Equilibirum and Compatibility Equations

The equilibirum equations for the case of thin plates and shallow shells are [48]:

$$\begin{aligned} N_{x/x} + N_{xy/y} &= 0 \\ N_{xy/x} + N_{y/y} &= 0 \\ M_{x/xx} + 2M_{xy/xy} + M_{y/yy} + N_x w_{/xx} + 2N_{xy} w_{/xy} + N_y w_{/yy} + \frac{1}{R} N_y &= 0 \end{aligned} \tag{3.1}$$

which are the non-linear equilibrium equations for a laminated panel subjected to in-plane loads, according to the kinematic model. The equations, in the form of Eq. 3.1, do not depend on the constitutive law, so they are of general validity and

can be applied for isotropic, composite, as well as variable stiffness panels.
The equilibirum equations, to be solved, should be accompanied by proper boundary conditions, specifying the displacement (essential conditions) and/or the generalised forces (natural conditions) along the boundaries.
While Eq. 3.1 provides the conditions for guaranteeing the equilibrium, the solution of the elastic problem demands also that compatibility conditions are satisfied. The strain-displacement relation of Eq. 2.4 can be derived twice as:

$$\begin{aligned}
\epsilon_{xx/yy} &= u_{0/xyy} - z w_{0/xxyy} + w_{0/xyy} w_{0/x} + w_{0/xy}^2 \\
\epsilon_{yy/xx} &= v_{0/yxx} - z w_{0/yyxx} + \frac{w_{0/xx}}{R} + w_{0/yxx} w_{0/y} + w_{0/xy}^2 \\
\gamma_{xy/xy} &= u_{0/xyy} + v_{0/xxy} + w_{0/xx} w_{0/yy} + w_{0/xxy} w_{0/y} + w_{0/xy}^2 + w_{0/xyy} w_{0/x} - 2 z w_{0/xxyy}
\end{aligned} \tag{3.2}$$

The three equations in 3.2 satisfy the following equation:

$$\epsilon_{xx/yy} + \epsilon_{yy/xx} = \gamma_{xy/xy} + \frac{w_{0/xx}}{R} + w_{0/xy}^2 - w_{0/xx} w_{0/yy} \tag{3.3}$$

which is the non-linear compatibility equation.

If the solution is sought in terms of displacements, the constitutive law can be inserted in Eq. 3.1. With this regard, the equilibirum conditions for a variable-stiffness panel can be retrieved after substitution of Eq. 2.40 into 3.1.
Even though purely displacement-based approaches have been proposed in the past ([9], [3]), this strategy suffers from a major drawback: the resulting set of equations are fully coupled in three unknowns and special techniques must be employed in order to solve the system. Moreover, these equations involve the derivative of the stiffness terms $A(x, y)$, $B(x, y)$ and $D(x, y)$, that, in the special case of variable-stiffness panels, are not constant over the surface and are functions of the panel coordinates.

Other strategies have been proposed in the recent past: of particular interest is the approach adopted in [17] and [13], where a mixed formulation was adopted, together with a variational formulation within the context of a Ritz-like method.
The number of unknowns can be reduced if a mixed formulation is employed. Indeed, mixed formulations for buckling and post-buckling analysis are generally formulated in terms of the out-of-plane displacement w and the Airy stress function ϕ. The latter offers two advantages: it reduces the system order and automatically

satisfy the in-plane equilibirum. On the other hand, the compatibility has to be satisfied by means of discrete equations.
With a Ritz-type approach the unknowns of the problem are approximated by expanding the unknown functions as the linear combination of trial functions, i.e. global functions defined ex-ante. The energy terms are minimized with respect to the coefficients of the series: with this strategy the derivatives of the stiffness terms are avoided and the formulation is simplified. However, special care must be taken when handling the energy integrals: due to the variable-stiffness terms, an exact integration cannot be performed and thus a numerical scheme must be employed.

The approach mentioned above has been pursued in this work: the governing equations for the pre-buckling problem are obtained by means of the principle of stationary complementary energy; the buckling problem is derived by applying the adjacent equilibrium criteria, and results in an eigenvalue problem. The post-buckling formulation is based on the approach proposed by Bisagni and Vescovini [27], and a unitary variation functional is used to derive the equilibrium and the compatibility equations. The post-buckling analysis results in a set of non-linear equations, that must be solved numerically.

The expressions of the energy functional are now presented and, in the next Chapter, they are used to derive the governing, discrete equations.

3.2 Pre-buckling Formulation

In this section the energy functional used to obtain the pre-buckling problem is provided.

From an energy point of view, the condition of equilibrium is achieved by making the first variation of the complementary energy stationary. This condition is expressed by the principle of stationary complementary potential energy. If Π_c is the total complementary energy, a Taylor's expansion around the equilibrium point is

$$\Pi_c + \Delta\Pi_c = \Pi_c + \delta\Pi_c + \frac{1}{2!}\delta^2\Pi_c + \frac{1}{3!}\delta^3\Pi_c + \cdots \tag{3.4}$$

The principle of stationary complementary energy reads [51] "*among all the stress fields which satisfy the equilibrium conditions and the prescribed mechanical boundary conditions, the actual one is that which renders the total complementary energy stationary*", and can be expressed by the condition

$$\delta\Pi_c = 0 \tag{3.5}$$

The total complementary energy will be written in terms of the Airy stress function ϕ, which is defined as:

$$N_x = \frac{\partial^2\phi}{\partial y^2} \quad N_y = \frac{\partial^2\phi}{\partial x^2} \quad N_{xy} = -\frac{\partial^2\phi}{\partial x \partial y} \tag{3.6}$$

The Airy stress function identically satisfies the in-plane equilibrium equations and thus it is necessary to solve only the compatibility equation.

For an elastic body of volume V and surface S under prescribed loads $\overline{N}_x$, $\overline{N}_y$, $\overline{N}_{xy}$ over the boundary S_1 and prescribed displacement $\overline{u}$,$\overline{v}$ over the boundary S_2, the total complementary energy is composed of two parts: the strain complementary energy U_c and the complementary work done by the prescribed displacement Q_c

$$\Pi_c = U_c + Q_c \tag{3.7}$$

The expression of the strain complementary energy is given by the volume integral of the contraction of the stress and strain tensors [54]:

$$U = \frac{1}{2}\int_V (\sigma_{xx}\epsilon_{xx} + \sigma_{yy}\epsilon_{yy} + \tau_{xy}\gamma_{xy}) dV \tag{3.8}$$

where the assumption of plane-stress have been used.
Starting from Eq. 3.8, the strain field can be separated in membrane and curvature contributes

$$U_c = \frac{1}{2}\int_V (\sigma_{xx}(\epsilon^0_{xx} + zk_{xx}) + \sigma_{yy}(\epsilon^0_{yy} + zk_{yy}) + \tau_{xy}(\gamma^0_{xy} + zk_{xy})) dV \tag{3.9}$$

The volume integral is separated into an integral over the thickness and over the surface, and considering a laminate panel with N layers

$$U_c = \frac{1}{2}\int_S \sum_{k=1}^{N} \left\{ \int_{h_k} (\sigma_x(\epsilon_x^0 + zk_{xx}) + \sigma_y(\epsilon_y^0 + zk_{yy}) + \tau_{xy}(\gamma_{xy}^0 + zk_{xy}))dz \right\} dS \tag{3.10}$$

Integrating over the thickness and using the identities in Eq. 2.2

$$U_c = \frac{1}{2}\int_S (N_x\epsilon_{xx}^0 + M_x k_{xx} + N_y\epsilon_{yy}^0 + M_y k_{yy} + N_{xy}\gamma_{xy} + M_{xy}k_{xy})dS \tag{3.11}$$

For plates, a common assumption is to consider the pre-buckling deformation as membrane: this means that there is no coupling between the in-plane stress distribution and the out-of-plane displacement. Moreover, since in the case considered only in-plane loading conditions are assumed, a membrane pre-buckling state also implies that the out-of-plane displacement is null, that is $w = 0$.
For the case of shells, the presence of the curvature determines a coupling between in-plane and out-of-plane behaviour. The coupling contributions are linear, meaning that the response is coupled since the pre-buckling phase. It follows that the out-of-plane displacements are different from zero in the pre-buckling range. However, a commons assumption is to consider w, although not null, negligible.

For the reason mentioned above, only the membrane strain in Eq. 3.11 are kept, while the flexural strain are neglected. The complementary energy in Eq. 3.11 is rewritten as:

$$U_{c,m} = \frac{1}{2}\int_S (N_x\epsilon_x^0 + N_y\epsilon_y^0 + N_{xy}\gamma_{xy}^0)dS \tag{3.12}$$

which is the membrane complementary energy $U_{c,m}$. The constitutive law in the semi-inverse form (Eq. 2.44) for a symmetric laminate ($b_{ij} = 0$) is used into the

Eq. 3.12, resulting in:

$$\begin{aligned} U_{c,m} = \frac{1}{2}\int_S [&N_x(a_{11}(x,y)N_x + a_{12}(x,y)N_y + a_{16}(x,y)N_{xy}) + \\ &+ N_y(a_{12}(x,y)N_x + a_{22}(x,y)N_y + a_{26}(x,y)N_{xy}) + \\ &+ N_{xy}(a_{16}(x,y)N_x + a_{26}(x,y)N_y + a_{66}(x,y)N_{xy})]dS = \\ = \frac{1}{2}\int_S [&a_{11}(x,y)N_x^2 + 2a_{12}(x,y)N_xN_y + a_{22}(x,y)N_y^2 + \\ &+ a_{66}(x,y)N_{xy}^2 + 2a_{16}(x,y)N_xN_{xy} + 2a_{26}(x,y)N_yN_{xy}]dS \end{aligned} \tag{3.13}$$

The complementary work done by the prescribed displacement is [48]:

$$Q_c = \oint_{S_2} (\overline{v}N_y + \overline{u}N_{xy})dx + \oint_{S_2} (\overline{v}N_{xy} + \overline{u}N_x)dy \tag{3.14}$$

where S_2 is the portion of the boundary where the displacements $\overline{u}$ and $\overline{v}$ are prescribed. Note that the prescribed loads $\overline{N}_x$, $\overline{N}_y$, $\overline{N}_{xy}$ do not contribute to the total complementary energy, as they are assumed satisfied a priori.
The expression to be minimized in order to obtain the equilibrium and the compatibility equations is:

$$\Pi_c = U_{c,m} + Q_c \tag{3.15}$$

The resulting equations will have as unknowns the in-plane loads N_x, N_y and N_{xy}. By employing the Airy stress function, the number of unknowns can be reduced from 3 to 1. Therefore, it is possible to express the in-plane load using just one single scalar-valued function.

The membrane complementary energy can be rewritten employing the Airy stress function as:

$$\begin{aligned} U_m = \frac{1}{2}\int_S [&a_{11}(x,y)\phi_{/yy}^2 + 2a_{12}(x,y)\phi_{/xx}^2\phi_{/yy}^2 + a_{22}(x,y)\phi_{/xx}^2 + \\ &+ a_{66}(x,y)\phi_{/xy}^2 - 2a_{16}(x,y)\phi_{/yy}\phi_{/xy} - 2a_{26}(x,y)\phi_{/xx}\phi_{/xy}]dS \end{aligned} \tag{3.16}$$

and the work done by the prescribed displacements is:

$$Q_c = -\oint_{S_2} (\overline{v}\phi_{/yy} - \overline{u}\phi_{/xy})dx + \oint_{S_2} (-\overline{v}\phi_{/xy} + \overline{u}\phi_{/xx})dy \tag{3.17}$$

It is worth noting that the pre-buckling problem of plates and shells are identical: this is due to the assumption of membrane pre-buckling state and negligible out-of-plane displacement.

3.3 Linearised Buckling Formulation

In this Section the energy formulation for the linearised buckling problem of variable-stiffness panels is obtained.

The pre-buckling and buckling problems are very different: the former is a boundary value problem, while the latter is an eigenvalue problem. Accordingly, the underlying variational principles that are used to obtain the governing equations are different each other.
In Section 3.2 it was illustrated the pre-buckling approach under the assumption of purely membrane behaviour, both for plates and shells. When it turns to the buckling analysis, it is necessary to distinguish between the case of plates and shells. In particular, plates can be analysed by exploiting the uncoupling between in-plane and out-of-plane response. On the contrary, shells demand for an analysis approach capable of accounting for the coupled in-plane/out-of-plane behaviour.
It follows that both the membrane and the bending part should be considered in the energy functional.

As introduced in Section 3.2, a Taylor's expansion of the total potential energy can be used to study the equilibrium and the stability of a continuum body: the equilibrium solution is stable if the value of the total potential energy is an absolute minimum at the stationary point. Thus, in order to study the stability of a system, it is necessary to study the sign of the second variation of the total potential energy, that in the case of the Taylor's expansion in Eq. 3.4 is

$$\delta^2\Pi > 0 \tag{3.18}$$

for any admissible kinematic variation (for stability). If the variation is positive for any admissible variation, meaning that the second variation of the total potential energy is positive definite, the solution is stable; if the variation is equal to zero for some kinematically admissible variation then the state is critical; if the variation is

negative, the system is unstable.
At the limit of stability, the second variation ceases to be positive definite, and turns to zero for some choice of the admissible kinematic variations.

An alternative way of formulating the buckling criterion refers to the so-called *Trefftz buckling criterion*, which states that the instability condition can be found by making the second variation of the total potential energy stationary [48]:

$$\delta(\delta^2\Pi) = 0 \tag{3.19}$$

which is also known as *adjacent equilibirum criteria*.
The adjacent equilibrium criteria can be applied by considering a reference equilibirum condition (R), identified by the energy functional $\Pi_{(R)}$. Slightly perturbing this configuration gives:

$$\Pi_{(R)} + \Delta\Pi_{(R)} = \Pi_{(R)} + \delta\Pi_{(R)} + \frac{1}{2!}\delta^2\Pi_{(R)} + \cdots = \Pi_{(R)} + \frac{1}{2!}\delta^2\Pi_{(R)} + \cdots \tag{3.20}$$

where it has been used the condition that $\delta\Pi_{(R)} = 0$ at equilibirum. Now it is possible to introduce another configuration (A) that satisfy the equilibirum requirements and that is adjacent to the configuration (R). The energy of this configuration is then

$$\Pi_{(A)} = \Pi_{(R)} + \Delta\Pi_{(R)} \tag{3.21}$$

Since the adjacent configuration also satisfies the equilibirum conditions

$$\delta\Pi_{(A)} = \delta\Pi_{(R)} + \delta\Delta\Pi_{(R)} = 0 \tag{3.22}$$

and since $\delta\Pi_{(R)} = 0$ and

$$\Delta\Pi_{(R)} = \delta\Pi_{(R)} + \frac{1}{2!}\delta^2\Pi_{(R)} + \cdots = \frac{1}{2!}\delta^2\Pi_{(R)} \tag{3.23}$$

the following condition for the stability is found

$$\delta\Pi_{(A)} = \frac{1}{2!}\delta^2\Pi_{(R)} = 0 \tag{3.24}$$

That correspond to the Trefftz criterion for the stability [48]

$$\delta(\delta^2\Pi_{(R)}) = 0 \tag{3.25}$$

In the present work, the starting point is the following functional, denoted as unitary [27]:

$$\begin{aligned}\Pi_F = &-\frac{1}{2}\int_S [a_{11}(x,y)\phi^2_{/yy} + 2a_{12}(x,y)\phi^2_{/xx}\phi^2_{/yy} + a_{22}(x,y)\phi^2_{/xx} + \\ &+ a_{66}(x,y)\phi^2_{/xy} - 2a_{16}(x,y)\phi_{/yy}\phi_{/xy} - 2a_{26}(x,y)\phi_{/xx}\phi_{/xy}]dS + \\ &+ \frac{1}{2}\int_S [D_{11}(x,y)w^2_{/xx} + 2D_{12}(x,y)w_{/xx}w_{/yy} + D_{22}(x,y)w^2_{/yy} + \\ &+ 4D_{66}(x,y)w^2_{/xy} + 4D_{16}(x,y)w_{/xx}w_{/xy} + 4D_{26}(x,y)w_{/yy}w_{/xy}]dS + \\ &+ \frac{1}{2}\int_S [\phi_{/yy}w^2_{/x} + \phi_{/xx}w^2_{/y} - 2\phi_{/xy}w_{/x}w_{/y}]dS - \\ &- \int_{-b/2}^{+b/2} [\phi_{/yy}\Delta]_{\pm a/2}dy - \int_S \phi_{/xx}\frac{w}{R}dS\end{aligned} \tag{3.26}$$

This nomenclature is aimed at remarking that both the compatibility and the equilibirum equations can be derived by applying the techniques of the calculus of variations. This unitary functional depends upon the Airy stress function and the out-of-plane displacement.
In Eq. 3.26 the following contributions can be identified:

$$\Pi_F = -\Pi_{F,m} + \Pi_{F,b} + \Pi_{F,NL} + P + \Pi_{F,R} \tag{3.27}$$

where $\Pi_{F,m}$ is the membrane complementary energy defined in Eq. 3.13 and P is the complementary work; the contribution $\Pi_{F,b}$ is the bending part and it is defined as:

$$\begin{aligned}\Pi_{F,b} = \frac{1}{2}\int_S [&D_{11}(x,y)w^2_{/xx} + 2D_{12}(x,y)w_{/xx}w_{/yy} + D_{22}(x,y)w^2_{/yy} + \\ &+ 4D_{66}(x,y)w^2_{/xy} + 4D_{16}(x,y)w_{/xx}w_{/xy} + 4D_{26}(x,y)w_{/xy}w_{/yy}]dS\end{aligned} \tag{3.28}$$

The non-linear term $\Pi_{F,NL}$ is

$$\Pi_{F,NL} = \frac{1}{2}\int_S [\phi_{/yy}w^2_{/x} + \phi_{/xx}w^2_{/y} - 2\phi_{/xy}w_{/x}w_{/y}]dS \tag{3.29}$$

This non-linear contribution is the one that provides the non-linear terms in the resulting governing equations. It can be noticed that it doesn't involve any stiffness coefficient.

The last term $\Pi_{F,R}$ is the integral in Eq. 3.26 related to the curvature:

$$\Pi_{F,R} = -\int_S \phi_{/xx}\frac{w}{R}dS \tag{3.30}$$

This term is responsible for the coupled bending-membrane behaviour. Clearly, in the case of flat panels $R \to \infty$, and this contribution goes to zero.

The buckling equations can be derived by introducing a perturbation to the unknowns of the problem. This is done in the form [48]:

$$\phi \to \phi + \delta\phi \tag{3.31}$$

$$w \to w + \delta w \tag{3.32}$$

where the δ identifies the perturbation with respect to the equilibirum condition. The expression in Eq. 3.31 can be substituted in the functional in Eq. 3.26, which can be rewritten in a more compact form as

$$\begin{aligned}\Pi_F = &-\frac{1}{2}\int_S \boldsymbol{f}^T\boldsymbol{a}(x,y)\boldsymbol{f}dS + \frac{1}{2}\int_S \boldsymbol{k}^T D(x,y)\boldsymbol{k}dS + \\ &+\frac{1}{2}\int_S \boldsymbol{f}^T\begin{bmatrix} w^2_{/x} \\ w^2_{/y} \\ w_{/x}w_{/y}\end{bmatrix}dS - \int_{-b/2}^{+b/2}[\phi_{/yy}\Delta]_{\pm a/2}dy - \int_S \phi_{/xx}\frac{w}{R}dS\end{aligned} \tag{3.33}$$

where the vector $\boldsymbol{f}$ collects the Airy stress function derivatives:

$$\boldsymbol{f} = \begin{bmatrix}\phi_{/xx} \\ \phi_{/yy} \\ -2\phi_{/xy}\end{bmatrix} \tag{3.34}$$

and the vector $\boldsymbol{k}$ is the flexural strain vector defined in Eq. 2.4.
The expression in Eq. 3.31 is substituted in the vector $\boldsymbol{f}$:

$$\boldsymbol{f} = \begin{bmatrix}\phi_{/xx} \\ \phi_{/yy} \\ -2\phi_{/xy}\end{bmatrix} \to \boldsymbol{f} + \delta\boldsymbol{f} = \begin{bmatrix}\phi_{/xx} \\ \phi_{/yy} \\ -2\phi_{/xy}\end{bmatrix} + \delta\begin{bmatrix}\phi_{/xx} \\ \phi_{/yy} \\ -2\phi_{/xy}\end{bmatrix} \tag{3.35}$$

Eq. 3.35 can be substituted in the first term of Eq. 3.33:

$$\begin{aligned} -\frac{1}{2}\int_S \boldsymbol{f}^T\boldsymbol{a}(x,y)\boldsymbol{f}dS &= -\frac{1}{2}\int_S (\boldsymbol{f}+\delta\boldsymbol{f})^T\boldsymbol{a}(x,y)(\boldsymbol{f}+\delta\boldsymbol{f})dxdy = \\ &= -\frac{1}{2}\int_S [\boldsymbol{f}^T\boldsymbol{a}\boldsymbol{f} + \delta\boldsymbol{f}^T\boldsymbol{a}\boldsymbol{f} + \boldsymbol{f}^T\boldsymbol{a}\delta\boldsymbol{f} + \delta\boldsymbol{f}^T\boldsymbol{a}\delta\boldsymbol{f}]dS \end{aligned} \tag{3.36}$$

With the same procedure, the vector $\mathbf{k}$ of curvatures can be perturbed and substituted in the part of Eq. 3.33 related to the bending energy:

$$\begin{aligned} \frac{1}{2}\int_S \boldsymbol{k}^T D(x,y)\boldsymbol{k}dxdy &= \frac{1}{2}\int_S (\boldsymbol{k}+\delta\boldsymbol{k})^T D(x,y)(\boldsymbol{k}+\delta\boldsymbol{k})dS = \\ &= \frac{1}{2}\int_S [\boldsymbol{k}^T D\boldsymbol{k} + \delta\boldsymbol{k}^T D\boldsymbol{k} + \boldsymbol{k}^T D\delta\boldsymbol{k} + \delta\boldsymbol{k}^T D\delta\boldsymbol{k}]dS \end{aligned} \tag{3.37}$$

The non-linear term in Eq. 3.33 reads:

$$\begin{aligned} \frac{1}{2}\int_S \boldsymbol{f}^T \begin{bmatrix} w_{/x}^2 \\ w_{/y}^2 \\ w_{/x}w_{/y} \end{bmatrix} dS =& \frac{1}{2}\int_S (\boldsymbol{f}+\delta\boldsymbol{f})^T \begin{bmatrix} (w_{/x}+\delta w_{/x})^2 \\ (w_{/y}+\delta w_{/y})^2 \\ (w_{/x}+\delta w_{/x})(w_{/y}+\delta w_{/y}) \end{bmatrix} dS = \\ =& \frac{1}{2}\int_S \boldsymbol{f}^T \begin{bmatrix} w_{/x}^2 \\ w_{/y}^2 \\ w_{/x}w_{/y} \end{bmatrix} + \boldsymbol{f}^T \begin{bmatrix} 2w_{/x}\delta w_{/x} \\ w_{/y}\delta w_{/y} \\ w_{/x}\delta w_{/y} + \delta w_{/x}w_{/y} \end{bmatrix} + \\ &+ \boldsymbol{f}^T \begin{bmatrix} \delta w_{/x}^2 \\ \delta w_{/y}^2 \\ \delta w_{/y}\delta w_{/x} \end{bmatrix} + \delta\boldsymbol{f}^T \begin{bmatrix} w_{/x}^2 \\ w_{/y}^2 \\ w_{/x}w_{/y} \end{bmatrix} + \\ &+ \delta\boldsymbol{f}^T \begin{bmatrix} 2w_{/x}\delta w_{/x} \\ w_{/y}\delta w_{/y} \\ w_{/x}\delta w_{/y} + \delta w_{/x}w_{/y} \end{bmatrix} + \delta\boldsymbol{f}^T \begin{bmatrix} \delta w_{/x}^2 \\ \delta w_{/y}^2 \\ \delta w_{/y}\delta w_{/x} \end{bmatrix} dS \end{aligned} \tag{3.38}$$

Finally, the perturbation in Eq. 3.31 is substituted in the contribution associated with the imposed displacement of Eq. 3.33:

$$-\int_{-b/2}^{+b/2} [\phi_{/yy}\Delta]_{\pm a/2}dy = -\int_{-b/2}^{+b/2} [(\phi_{/yy}+\delta\phi_{/yy})\Delta]_{\pm a/2}dy \tag{3.39}$$

and in the term related to the curvature R:

$$\begin{aligned} -\int_S \phi_{/xx}\frac{w}{R}dxdy &= -\int_S (\phi_{/xx}+\delta\phi_{/xx})\frac{(w+\delta w)}{R}dS = \\ &= -\frac{1}{R}\int_S [\phi_{/xx}w + \delta\phi_{/xx}\delta w + \delta\phi_{/xx}w + \phi_{/xx}\delta w]dS \end{aligned} \tag{3.40}$$

Collecting the expressions in Eqs. 3.36-3.40, the following contributions are identified:

$$\begin{aligned} \Pi_F = &-\frac{1}{2}\int_S \boldsymbol{f}^T\boldsymbol{a}\boldsymbol{f}dxdy + \frac{1}{2}\int_S \boldsymbol{k}^T D\boldsymbol{k}dS + \\ &+\frac{1}{2}\int_S \boldsymbol{f}^T\begin{bmatrix} w_{/x}^2 \\ w_{/y}^2 \\ w_{/x}w_{/y}\end{bmatrix}dxdy - \int_{-b/2}^{+b/2}[\phi_{/yy}\Delta]_{\pm a/2}dy - \int_S \phi_{/xx}\frac{w}{R}dS \end{aligned} \tag{3.41}$$

which is the same expression of Eq. 3.33,

$$\begin{aligned} \delta\Pi_F = &-\frac{1}{2}\int_S (\delta\boldsymbol{f}^T\boldsymbol{a}\boldsymbol{f} + \boldsymbol{f}^T\boldsymbol{a}\delta\boldsymbol{f})dxdy + \frac{1}{2}\int_S (\delta\boldsymbol{k}^T D\boldsymbol{k} + \boldsymbol{k}^T D\delta\boldsymbol{k})dS + \\ &+\frac{1}{2}\int_S \left[\boldsymbol{f}^T\begin{bmatrix}\delta w_{/x}^2 \\ \delta w_{/y}^2 \\ \delta w_{/y}\delta w_{/x}\end{bmatrix} + \delta\boldsymbol{f}^T\begin{bmatrix} 2w_{/x}\delta w_{/x} \\ w_{/y}\delta w_{/y} \\ w_{/x}\delta w_{/y} + \delta w_{/x}w_{/y}\end{bmatrix}\right]dS - \\ &-\int_{-b/2}^{+b/2}[\delta\phi_{/yy}\Delta]_{\pm a/2}dy - \frac{1}{R}\int_S [\delta\phi_{/xx}w + \phi_{/xx}\delta w]dS \end{aligned} \tag{3.42}$$

and

$$\begin{aligned} \delta^2\Pi_F = &-\frac{1}{2}\int_S \delta\boldsymbol{f}^T\boldsymbol{a}\delta\boldsymbol{f}dxdy + \frac{1}{2}\int_S \delta\boldsymbol{k}^T D\delta\boldsymbol{k}dS + \\ &+\frac{1}{2}\int_S \left[\boldsymbol{f}^T\begin{bmatrix}\delta w_{/x}^2 \\ \delta w_{/y}^2 \\ \delta w_{/y}\delta w_{/x}\end{bmatrix} + \delta\boldsymbol{f}^T\begin{bmatrix} w_{/x}^2 \\ w_{/y}^2 \\ w_{/x}w_{/y}\end{bmatrix} + \delta\boldsymbol{f}^T\begin{bmatrix} 2w_{/x}\delta w_{/x} \\ w_{/y}\delta w_{/y} \\ w_{/x}\delta w_{/y} + \delta w_{/x}w_{/y}\end{bmatrix}\right]dS \\ &-\frac{1}{R}\int_S \delta\phi_{/xx}\delta w dS \end{aligned} \tag{3.43}$$

The expression in Eq. 3.43 is the second variation of the unitary functional in Eq. 3.31, and can be used to derive the buckling problem. By neglecting the high order terms and considering that $w = 0$ due to the membrane pre-buckling assumption,

Eq. 3.43 can be simplified as:

$$\begin{aligned}\delta^2\Pi_F = &-\frac{1}{2}\int_S [a_{11}(x,y)\delta\phi^2_{/yy} + 2a_{12}(x,y)\delta\phi^2_{/xx}\delta\phi^2_{/yy} + a_{22}(x,y)\delta\phi^2_{/xx} + \\ &+ a_{66}(x,y)\delta\phi^2_{/xy} - 2a_{16}(x,y)\delta\phi_{/yy}\delta\phi_{/xy} - 2a_{26}(x,y)\delta\phi_{/xx}\delta\phi_{/xy}]dS + \\ &+ \frac{1}{2}\int_S [D_{11}(x,y)\delta w^2_{/xx} + 2D_{12}(x,y)\delta w_{/xx}\delta w_{/yy} + D_{22}(x,y)\delta w^2_{/yy} + \\ &+ 4D_{66}(x,y)\delta w^2_{0/xy} + 4D_{16}(x,y)\delta w_{/xx}\delta w_{/xy} + 4D_{26}(x,y)\delta w_{/yy}\delta w_{/xy}]dS + \\ &+ \frac{1}{2}\int_S [\phi_{/yy}\delta w^2_{/x} + \phi_{/xx}\delta w^2_{/y} - 2\phi_{/xy}\delta w_{/x}\delta w_{/y}]dS - \\ &- \int_S [\delta\phi_{/xx}\frac{\delta w}{R}]dS\end{aligned} \tag{3.44}$$

The terms $\phi_{/xx}$, $\phi_{/yy}$ and $\phi_{/xy}$ in Eq. 3.44 are the solution of the pre-buckling state, whilst the quantities denoted by the δ symbol define the variation at buckling with respect to the pre-buckling state.
Accordingly to the Trefftz criteria, the differential buckling equations are obtained by minimizing Eq. 3.44.

The expression of Eq. 3.44 can be adopted for analysing the buckling behaviour of shells and, as a particular case, of plates. In this latter case, it can be noted that the membrane and the bending contribution are uncoupled, thus the buckling problem can be solved by considering the bending behaviour alone.

3.4 Post-buckling Formulation

The post-buckling state is characterized by an inherent non-linear coupling between in-plane and out-of-plane response.
One possible approach refers to the formulation in terms of partial differential equations (Donnell-type equations), as classically done in the field of post-buckling literature. Another approach, retained here more suitable for analysing variable-stiffness panels, refers to the variational formulation.
In particular, the unitary functional in Eq. 3.26 is used to derive the out-of-plane equilibrium and the compatibility equations: by applying the Ritz method to the functional is possible to solve the non-linear buckling problem. It can be verified that by means of the calculus of variations and employing the classical

Eulero-Lagrange equation, it is possible to recover the non-linear equilibirum and compatibility equations, i.e. the classical Donnell-type equations.

The post-buckling formulation of perfect panels can be set-up referring to the unitary functional reported in Eq. 3.26. The expression can be further generalized to account for the effect of initial geometric imperfections, which are of crucial importance when dealing with the non-linear post-buckling field.
The necessity of include imperfections is twofold: firstly, imperfections are always present in a real structure, their presence affecting the transition from the pre-buckled state to the post-buckled one. Moreover, for imperfection sensitive structures, such as cylindrical shells, the post-buckling behaviour might be stable or unstable depending on the imperfections' shape.
Secondly, from a numerical stand point the presence of geometrical imperfections is necessary in order to allow the convergence of the numerical procedure. When a bifurcation point is reached, multiple solutions of the non-linear problem, i.e. the equilibrium branches departing from the bifurcation point, are possible. The absence of initial imperfections tends to determine a sequence of equilibirum states characterized by null out-of-plane deflections. Indeed, the equilibirum branch associated with an undeflected pattern is a solution of the problem, although unstable. This is correct from a mathematical point of view, since it is indeed a solution of the non-linear system. However, it is in contrast with experimental observations: after the first instability occurs the structure buckle, and the in-plane and out-of-plane deformations are coupled.
Therefore, an integral related to the geometrical imperfection is added, and the

unitary functional becomes:

$$\begin{aligned}\Pi_F = &-\frac{1}{2}\int_S [a_{11}(x,y)\phi_{/yy}^2 + 2a_{12}(x,y)\phi_{/xx}^2\phi_{/yy}^2 + a_{22}(x,y)\phi_{/xx}^2 + \\ &+ a_{66}(x,y)\phi_{/xy}^2 - 2a_{16}(x,y)\phi_{/yy}\phi_{/xy} - 2a_{26}(x,y)\phi_{/xx}\phi_{/xy}]dS + \\ &+ \frac{1}{2}\int_S [D_{11}(x,y)w_{/xx}^2 + 2D_{12}(x,y)w_{/xx}w_{/yy} + D_{22}(x,y)w_{/yy}^2 + \\ &+ 4D_{66}(x,y)w_{/xy}^2 + 4D_{16}(x,y)w_{/xx}w_{/xy} + 4D_{26}(x,y)w_{/yy}w_{/xy}]dS + \\ &+ \frac{1}{2}\iint_S [\phi_{/yy}w_{/x}^2 + \phi_{/xx}w_{/y}^2 - 2\phi_{/xy}w_{/x}w_{/y}]dS + \\ &- \iint_S \phi_{/xx}\frac{w}{R}dS - \int_{-b/2}^{+b/2}[\phi_{/yy}\Delta]_{\pm a/2}dy - \\ &- \iint_S [\phi_{/yy}w_0w_{/xx} + \phi_{/xx}w_0w_{/yy} - 2\phi_{/xy}w_0w_{/xy}]dS\end{aligned} \tag{3.45}$$

where $w_0(x,y)$ is the function that represents the initial geometric imperfection shape. Since it is not always possible to have proper informations about the imperfection of a panel, especially in the preliminary design phase, a common assumption is to consider linear combinations of the first buckling modes.

3.5 Summary

In this Chapter the approach adopted to derive the linear and non-linear buckling problems have been explained.
The principle of stationary complementary energy has been used to derive the functional for the pre-buckling problem. A linear membrane pre-buckling behaviour has been assumed: thus, to derive the governing equations for the pre-buckling analysis it is necessary to minimize only the membrane complementary energy, together with the complementary work of the prescribed displacement. The membrane complementary energy has been written in terms of the Airy stress function: the in-plane equilibirum is identically satisfied, and the pre-buckling problem is reduced to the complementary equation.

The linearised buckling problem is derived applying the adjacent equilibirum criteria to a so-called unitary functional. This unitary formula is written in terms of a mixed formulation, thus involving the Airy stress function and the out-of-plane

displacement. The governing stability equations for the buckling problem will be then derived by minimizing the second variation of the unitary functional.

The unitary functional can be employed to obtain the non-linear equations describing the post-buckling problem. A contribution related to the initial geometric imperfections has been included in the formulation, in order to account for possible deviation from the panel's nominal shape and to avoid possible convergence problem in the numerical solution.

Chapter 4

Ritz Approach

In this chapter the linear and non-linear buckling analyses of variable-stiffness panels are addressed. The strategy to obtain the discrete governing equations is based on the method of Ritz, which is applied to the energy functional derived in Chapter 3 and follows the approach proposed by Wu et al. [17].
The linear analysis is conceptually divided into two parts: the pre-buckling and the buckling analysis. The pre-buckling problem is firstly solved for obtaining the membrane stress distribution, which is used as input for the buckling analysis. The solution of the linearised buckling problem is then used to determine the shape of the initial imperfection in the post-buckling analysis.
The analyses have been performed for plates and shallow cylindrical shells subjected to compressive loads. The formulation is developed such that force-control and displacement-control can be considered. This two cases will be referred in the chapter as "displacement-control" and "load-control".

First, a brief overview of the Ritz method is given, then the two loading conditions is illustrated, together with a description of the trial functions.
The pre-buckling, buckling and post-buckling governing equations are obtained for variable-stiffness panels in the case of prescribed displacement: the equations are derived by minimizing the energy functional reported in the previous chapter. The equations for the case of prescribed load case are available in the Appendix A.
Finally, a brief description is reported for the algorithm used to perform the analyses.
The results are presented for variable-stiffness plates and shells, and the comparison is illustrated against results in the literature and finite element calculations.

4.1 Ritz Method

The Ritz method, or Ritz *approximation*, has been introduced by Walter Ritz at the beginning of the 20th century [55]. Since then, this method has been employed extensively in the field of the structural analysis and, in the recent past, it has been used in the context of variable-stiffness panels: Leissa and Martin [1] adopted this method in their preliminary study on plates with variable fiber spacing; other authors, such as Wu et al. [17] and Vescovini and Dozio [56], also employed the Ritz method to address the linear buckling behaviour of such panels. Furthermore, the Ritz-method was used to describe the post-buckling behaviour of variable-stiffness plates, for instance by Wu et al. [31], Olvieri and Milazzo [57] and Raju et al. [18],[58].

The idea behind the Ritz method is to convert the continuous problem into a discrete one by approximating the variables of the problem under consideration by means of a series of trial functions defined at global level. For instance, if the unknowns of the problem are, as in the current study, the Airy stress function $\phi(x, y)$ and the out-of-plane displacement $w(x, y)$, the series takes the form of

$$\phi(x, y) = \sum_{i=0}^{I} \Phi_i N_\phi(x, y) \tag{4.1}$$

$$w(x, y) = \sum_{j=0}^{J} W_j N_w(x, y) \tag{4.2}$$

where Φ_i and W_j are the undetermined coefficients of the series and $N_\phi(x, y)$ and $N_w(x, y)$ are suitable trial functions (or admissible functions). Within the framework of the method of Ritz, the trial functions should [59]:

- Satisfy the kinematic boundary conditions.
- Form a complete set in order to attain convergence.
- Be linearly independent.

Once the approximation is substituted into the relevant variational principle, it is possible to derive the set of discrete governing equations imposing the stationarity of the reading variational principle, meaning that the first derivatives with respect

to the Ritz coefficients are set to zero [48]:

$$\begin{cases} \dfrac{\partial \Pi(\Phi_i, W_j)}{\partial \Phi_i} = 0 & i = 1 \dots I \\ \dfrac{\partial \Pi(\Phi_i, W_j)}{\partial W_j} = 0 & j = 1 \dots J \end{cases} \tag{4.3}$$

The system in Eq 4.3 has dimensions $I+J$, and can be in the form of a linear system, eigenvalue problem or non-linear system depending upon the kind of functional being considered.
The method of Ritz guarantees that the accuracy of the solution can be improved as the number of trial functions is increased. However, selecting too many terms may result in very large system, whose solution can be expensive to solve from a computation point of view.
It is well known that different sets of trial functions determine different rates of convergence to the exact solution [60]. With this regard, special care must be given to the selection of the basis of the expansion: a proper choice would indeed allow to keep at minimum the total number of degree of freedom, with clear advantages on the computational time.
The Ritz method is employed here to formulate the pre-buckling, buckling and post-buckling problems. Furthermore, a description of the selected shape functions is also given.

4.2 Loading Cases

In practical applications, thin plates may be subjected to compressive loading conditions of different nature. In some cases, the load introduction could be better simulated by assuming a prescribed axial displacement. This is the case, for instance, of a typical test at panel level, where the load is introduced by means of rigid tabs. In other cases, as for real-life operating conditions of wing panels, the load introduction could be better modelled by assuming prescribed force. For this reason, two different load introduction strategies are considered, and are referred to as displacement-control and force-control. The first loading case refers to a panel loaded with a uniform edge displacement compression, denoted as Δ. The displacement is imposed at $x = \pm a/2$ while the transverse edges ($y = \pm b/2$) are free to deform, thus they are said to be stress-free. The in-plane boundary conditions

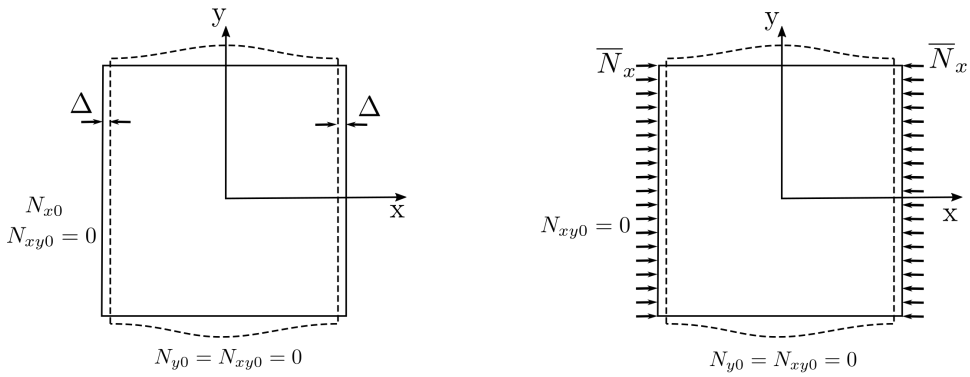

(a) Imposed Displacement case (b) Imposed Load case

Figure 4.1: In-plane boundary conditions and loadings cases analysed.

are:

$$\begin{aligned} x = \pm\frac{a}{2}: \qquad & u = \mp\Delta \qquad & N_{xy0} = 0 \\ y = \pm\frac{b}{2}: \qquad & N_{y0} = 0 \qquad & N_{xy0} = 0 \end{aligned} \tag{4.4}$$

Note that at $x = \pm a/2$ the boundary load $N_x(y)$ is not prescribed and, in general, is not uniform over the edge, due to non constancy of the panel stiffness along y. The force per unit-length $N_x(y)$ is recovered as part of the solution, and it is used during the evaluation of the critical buckling load.

The second loading case consists of a uniform compressive load $\overline{N}_x$ imposed at $x = \pm a/2$. Even in this case the non-compressed edges ($y = \pm b/2$) are free to deform and thus are stress-free. The in-plane boundary conditions are

$$\begin{aligned} x = \pm\frac{a}{2}: \qquad & N_{y0} = \mp\overline{N}_x \qquad & N_{xy0} = 0 \\ y = \pm\frac{b}{2}: \qquad & N_{y0} = 0 \qquad & N_{xy0} = 0 \end{aligned} \tag{4.5}$$

The two loading cases are represented in Figure 4.1.

Concerning the essential boundary conditions for the out-of-plane displacement, each of the edges can either be free, simply-supported or clamped for both loading cases. If the edges are simply-supported (S), the out-of-plane displacement is null

at the borders [54]

$$x = \pm\frac{a}{2}, \quad y = \pm\frac{b}{2} : \qquad w(x,y) = 0 \tag{4.6}$$

If the edges are clamped (C), w and its derivative with respect to x or y are null

$$\begin{aligned} x = \pm\frac{a}{2} : &\quad w(x,y) = 0, \qquad w_{/x}(x,y) = 0 \\ y = \pm\frac{b}{2} : &\quad w(x,y) = 0, \qquad w_{/y}(x,y) = 0 \end{aligned} \tag{4.7}$$

(F), all the boundary conditions are of natural type, and the out-of-plane displacement is $w(x,y) \neq 0$.

4.3 Trial Functions

Following the approach outlined in [17] and [31], the Airy stress function is expressed in a separate form as:

$$\phi(x,y) = \phi_0(x,y) + \phi_1(x,y) \tag{4.8}$$

where $\phi_0(x,y)$ describes the stress distribution along the edges of the plate and thus depends on the boundary conditions. The second term, ϕ_1, satisfies the stress-free boundaries, thus it is null at $x = \pm a/2, y = \pm b/2$. Note that the boundary conditions for ϕ_1 actually corresponds to the ones of clamped edges, meaning that ϕ_1 and its derivatives are null at the boundary:

$$\begin{aligned} x = \pm\frac{a}{2} : &\quad \phi_1(x,y) = 0, \qquad \phi_{1/x}(x,y) = 0 \\ y = \pm\frac{b}{2} : &\quad \phi_1(x,y) = 0, \qquad \phi_{1/y}(x,y) = 0 \end{aligned} \tag{4.9}$$

In the analysed cases the loading conditions (either a displacement or a load) are prescribed only at $x = \pm a/2$. Hence ϕ_0 describes only the boundary force N_x and thus is just a function of y.
The second term in the expansion 4.8 is expanded as

$$\phi_1(x,y) = \sum_{p=0}^{P}\sum_{q=0}^{Q} \Phi_{pq} X_p(x) Y_q(y) \tag{4.10}$$

where Φ_{pq} are the $P \times Q$ unknown coefficients of the series and $X_p(x)$,$Y_q(y)$ are the trial functions, opportunely separated to fulfil the essential boundary conditions along x and y.
The problem can be conveniently formulated in terms of non-dimensional coordinates after introducing the following transformations:

$$x = \frac{a}{2}\xi \quad y = \frac{b}{2}\eta \tag{4.11}$$

and the relation between the derivatives in the physical domain (x, y) and the computational one (ξ, η) are:

$$\frac{\partial}{\partial x} = \frac{2}{a}\frac{\partial}{\partial \xi} \quad \frac{\partial}{\partial y} = \frac{2}{b}\frac{\partial}{\partial \eta} \tag{4.12}$$

Accordingly, the panel's coordinates are defined in the interval $[-1, +1]$

$$\begin{aligned} x = \pm\frac{a}{2} \rightarrow \xi = \pm 1 \\ y = \pm\frac{b}{2} \rightarrow \eta = \pm 1 \end{aligned} \tag{4.13}$$

The in-plane boundary conditions are then rewritten as

$$\xi = \pm 1: \quad u = \mp\Delta \qquad N_{xy0} = 0 \tag{4.14}$$

$$\eta = \pm 1: \quad N_{y0} = 0 \qquad N_{xy0} = 0 \tag{4.15}$$

for the displacement-control case and

$$\begin{aligned} \xi = \pm 1: \qquad & N_{y0} = \mp\overline{N}_x \qquad & N_{xy0} = 0 \\ \eta = \pm 1: \qquad & N_{y0} = 0 \qquad & N_{xy0} = 0 \end{aligned} \tag{4.16}$$

for the force-control case.
The expansion of ϕ in Eq. 4.8 is then

$$\phi_1(x,y) = \phi(\xi,\eta) = \phi_0(\eta) + \phi_1(\xi,\eta) = \phi_0(\xi) + \sum_{p=0}^{P}\sum_{q=0}^{Q} \Phi_{pq} X_p(\xi) Y_q(\eta) \tag{4.17}$$

for the displacement-control case and

$$\phi_1(x,y) = \phi(\xi,\eta) = \phi_0(\eta) + \phi_1(\xi,\eta) = \phi_0(\xi) + \sum_{p=0}^{P}\sum_{q=0}^{Q} \Phi_{pq} X_p(\xi) Y_q(\eta) \tag{4.18}$$

for force-control case.
The expression of ϕ_0 is treated in the sections that deals with the pre-buckling analysis.

The trial functions X_p, Y_q are taken as Legendre polynomials. Due to their non-periodic nature, Legendre polynomials are a good choice for the analysis of variable-stiffness panels as they tend to capture the localised behaviour better than periodic functions as the trigonometric or Fourier series [17].
Legendre Polynomials $L_i(x)$ are the solutions of the Legendre's Differential Equation and are defined in recursive form as [61]:

$$L_i(x) = \frac{1}{2!}\sum_{j=0}^{i} \begin{pmatrix} i \\ j \end{pmatrix}^2 (x-1)^{j-i}(x+1)^j \tag{4.19}$$

where i is the polynomial order. An alternate form is

$$L_i(x) = \sum_{j=0}^{J} (-1)^j \frac{(2i-2j)!}{2^i j!(i-j)!(i-2j)!} x^{i-2j} \tag{4.20}$$

where

$$J = \begin{cases} \dfrac{i}{2} & \text{if } i = 0, 2, 4, \ldots \\ \dfrac{i-1}{2} & \text{if } i = 1, 3, 5, \ldots \end{cases} \tag{4.21}$$

Recursive formulas for the exact derivative of $L_i(x)$ are available in literature. However, in the present work the first derivative $L_i'(x)$ has been approximated using Newton's Difference Quotient as:

$$L_i'(x) = \frac{i}{(x^2-1)}(xL_i(x) - L_{i-1}(x)) \tag{4.22}$$

and the second derivative $L_i''(x)$

$$L_i''(x) = \frac{i}{(x^2-1)^2}[2xL_i(x) + ((i-1)x^2 - i - 1)L_{i-1}(x)] \tag{4.23}$$

Index	Boundary Condition
0	Free (F)
1	Supported (C)
2	Clamped (S)

Table 4.1: Indexes used in the trial functions X_m, Y_n to satisfy the boundary conditions.

The trial functions $X_p(\xi)$, $Y_q(\eta)$ are then expressed using the Legendre polynomials as [17]:

$$\begin{aligned} X_p(\xi) &= (1-\xi^2)^2 L_p(\xi) \\ Y_q(\eta) &= (1-\eta^2)^2 L_q(\eta) \end{aligned} \tag{4.24}$$

The out-of-plane displacement $w(x, y)$ is approximated with a series expansion as:

$$w(x,y) = w(\xi,\eta) = \sum_{m=0}^{M}\sum_{n=0}^{N} W_{mn}\overline{X}_m(\xi)\overline{Y}_n(\eta) \tag{4.25}$$

where the coordinates have been normalized according to Eq. 4.11. The unknowns W_{mn} are the $m \times n$ coefficients of the series, while $\overline{X}_m(x)$,$\overline{Y}_n(y)$ are the trial functions satisfying the essential boundary conditions. The trial functions for w are also expressed by means of Legendre polynomials as

$$\begin{aligned} \overline{X}_m(\xi) &= (1-\xi)^{i_1}(1+\xi)^{i_2} L_m(\xi) \\ \overline{Y}_n(\eta) &= (1-\eta)^{j_1}(1+\eta)^{j_2} L_n(\eta) \end{aligned} \tag{4.26}$$

The indices $i_{1,2}$, $j_{1,2}$ can be either 0, 1, or 2 depending on the boundary conditions. They correspond, respectively, to free, supported and clamped conditions. The indexes and their meaning are reported in Table 4.1.

4.4 Pre-buckling Problem

In this section the governing equations are obtained for the pre-buckling analysis of a panel compressed by means of an imposed uniform displacement.
The panels considered in this work are subjected only to in-plane loading conditions, and the pre-buckling deformation can be considered membrane. In other words,

this means that the out-of-plane displacement derivatives with respect to x and y are zero. From a physical point of view this means that the slope and the curvature of a panel are null during the pre-buckling condition.
Furthermore, with this assumption the transverse displacement w is zero in the pre-buckling deformation part and thus the plate remain flat. The out-of-plane displacement w is then:

$$w = w_{/x} = w_{/y} = 0 \tag{4.27}$$

For this reason, the pre-buckling problem can be considered a flat-equilibirum problem [48]. In the case of shells the in-plane and out-of-plane deformations are coupled in the pre-buckling state. Thus, w should not be assumed null. However, a common assumption is to consider the transverse displacement negligible.

In the case of displacement-control condition, there are no informations about the in-plane load N_x at the edges $x = \pm a/2$. Moreover, due to the variable stiffness properties of the panel, N_x is not uniform along the y direction. Employing the separate form of the Airy stress function given in Eq. 4.8, the normal stress distribution at the panel's boundaries is

$$x = \pm\frac{a}{2}(\xi = \pm 1): \quad N_{x0} = \phi_{/yy} = \frac{4}{b^2}\phi_{0/\eta\eta} = \sum_{k=0}^{K} c_k \psi_k(\eta) \qquad N_{xy0} = 0 \tag{4.28}$$

where c_k are the k unknown coefficients of the series and $\psi_k(\eta)$ are the trial functions of order k. Even for ϕ_0, Legendre polynomials are employed such that

$$\psi_k(\eta) = L_k(\eta) \tag{4.29}$$

Therefore, for the displacement-control formulation the Airy stress function is assumed as:

$$\phi(\xi,\eta) = \phi_0(\eta) + \phi_1(\xi,\eta) = \sum_{k=0}^{K} \int_{-1}^{+1} \int_{-1}^{+1} c_k \psi_k(\eta) d\eta d\eta + \sum_{p=0}^{P}\sum_{q=0}^{Q} \Phi_{pq} X_p(\xi) Y_q(\eta) \tag{4.30}$$

and the unknowns to be determined are the coefficients Φ_{pq} and c_k.

It is now recalled the expression of the complementary energy derived in Section

3.1, and reported, for convenience, here below:

$$\Pi_c = U_m + Q_c \tag{4.31}$$

where U_m is the strain-complementary energy (Eq. 3.16) and Q_c is the external work done by an imposed displacement (Eq. 3.17). By expressing the functional of Eq. 4.31 in terms of the Airy stress function:

$$\begin{aligned}\Pi_c = \frac{1}{2}\int_S [a_{11}(x,y)\left(\phi_{/yy}\right)^2 + 2a_{12}(x,y)\phi_{/xx}\phi_{/yy} + \\ + a_{22}(x,y)\phi_{/xx}^2 + a_{66}(x,y)\phi_{/xy}^2 - \\ - 2a_{16}(x,y)\phi_{/yy}\phi_{/xy} - 2a_{26}(x,y)\phi_{/xx}\phi_{/xy}]dS \\ - \int_{S_2}(\overline{v}\phi_{/yy} - \overline{u}\phi_{/xy})dx - \oint_{S_2}(\overline{u}\phi_{/xx} - \overline{v}\phi_{/xy})dy\end{aligned} \tag{4.32}$$

and considering a uniform displacement acting on the edges $x = \pm a/2$, Π_c becomes:

$$\begin{aligned}\Pi_c = \frac{1}{2}\int_{-a/2}^{+a/2}\int_{-b/2}^{+b/2} [a_{11}(x,y)\left(\phi_{/yy}\right)^2 + 2a_{12}(x,y)\phi_{/xx}\phi_{/yy} + \\ + a_{22}(x,y)\phi_{/xx}^2 + a_{66}(x,y)\phi_{/xy}^2 - \\ - 2a_{16}(x,y)\phi_{/yy}\phi_{/xy} - 2a_{26}(x,y)\phi_{/xx}\phi_{/xy}]dxdy \\ - \int_{-b/2}^{+b/2}[\phi_{/yy}\Delta]_{\pm a/2}dy\end{aligned} \tag{4.33}$$

where Δ is the prescribed uniform compression. Π_c can be then written in terms of the normalized coordinates defined in Eq. 4.11

$$\begin{aligned}\Pi_c = \frac{1}{2}\int_{-1}^{+1}\int_{-1}^{+1} [a_{11}(\xi,\eta)\left(\frac{4}{b^2}\right)^2\phi_{/\eta\eta}^2 + \\ + 2a_{12}(\xi,\eta)\left(\frac{4}{a^2}\right)\left(\frac{4}{b^2}\right)\phi_{/\eta\eta}\phi_{/\xi\xi} + a_{22}(\xi,\eta)\left(\frac{4}{a^2}\right)^2\phi_{/\xi\xi}^2 + \\ + a_{66}(\xi,\eta)\left(\frac{4}{ab}\right)^2\phi_{/\xi\eta}^2 - 2a_{16}(\xi,\eta)\left(\frac{4}{b^2}\right)\left(\frac{4}{ab}\right)\phi_{/\eta\eta}\phi_{/\xi\eta} - \\ - 2a_{26}(\xi,\eta)\left(\frac{4}{a^2}\right)\left(\frac{4}{ab}\right)\phi_{/\xi\xi}\phi_{/\xi\eta}]d\xi d\eta\frac{ab}{4} - \\ - \int_{-1}^{+1}[\frac{4}{b^2}\phi_{/\eta\eta}\Delta]_{\pm 1}d\eta\frac{b}{2}\end{aligned} \tag{4.34}$$

the last expression can be simplified as

$$\begin{aligned}\Pi_c = \frac{2b}{a^3}\int_{-1}^{+1}\int_{-1}^{+1}[\mu^4 a_{11}(\xi,\eta)\phi_{/\eta\eta}^2 + 2\mu^2 a_{12}(\xi,\eta)\phi_{/\eta\eta}\phi_{/\xi\xi} + \\ + a_{22}(\xi,\eta)\phi_{/\xi\xi}^2 + a_{66}(\xi,\eta)\phi_{/\xi\eta}^2 - 2\mu^3 a_{16}(\xi,\eta)\phi_{/\eta\eta}\phi_{/\xi\eta} - \\ - 2\mu a_{26}(\xi,\eta)\phi_{/\xi\xi}\phi_{/\xi\eta}]d\xi d\eta - \frac{2}{b}\int_{-1}^{+1}[\phi_{/\eta\eta}\Delta]_{\pm 1}d\eta\end{aligned} \tag{4.35}$$

where $\mu = a/b$ is a non-dimensional parameter defining the aspect ratio of the panel. The Airy function is expressed in the separate form as described in Eq. 4.17, and Π_c becomes

$$\begin{aligned}\Pi_c = \frac{2b}{a^3}\int_{-1}^{+1}\int_{-1}^{+1}[a_{11}\mu^4(\phi_{1/\eta\eta}^2 + \phi_{0/\eta\eta}^2 - 2\phi_{0/\eta\eta}\phi_{1/\eta\eta}) + \\ + 2a_{12}\mu^2\phi_{1/\xi\xi}(\phi_{0/\eta\eta} + \phi_{1/\eta\eta}) + a_{22}(\phi_{1/\xi\xi})^2 + a_{66}(\phi_{1/\xi\eta})^2 - \\ - 2a_{16}\mu^3\left(\phi_{1/\eta\eta} + \phi_{0/\eta\eta}\right)\phi_{1/\xi\eta} - 2a_{26}\mu\left(\phi_{1/\xi\xi}\phi_{1/\xi\eta}\right)]d\xi d\eta - \\ - \frac{2}{b}\int_{-1}^{+1}[(\phi_{0/\eta\eta} + \phi_{1/\eta\eta})\Delta]_{\pm 1}d\eta\end{aligned} \tag{4.36}$$

Note that the dependence of the membrane compliance terms a_{ij} on ξ, η has been omitted to improve the readability. The integrals are split according to the terms ϕ_1 and ϕ_0

$$\begin{aligned}\Pi_c = &\frac{2b}{a^3}\int_{-1}^{+1}\int_{-1}^{+1}[a_{11}\mu^4\phi_{1/\eta\eta}^2 + 2\mu^2 a_{12}\phi_{1/\xi\xi}\phi_{1/\eta\eta} + \\ &+ a_{22}(\phi_{1/\xi\xi})^2 + a_{66}(\phi_{1/\xi\eta})^2 - 2\mu^3 a_{16}\phi_{1/\eta\eta}\phi_{1/\xi\eta} - \\ &- 2\mu a_{26}\phi_{1/\xi\xi}\phi_{1/\xi\eta}]d\xi d\eta + \frac{2b}{a^3}\int_{-1}^{+1}\int_{-1}^{+1}[-2\mu^4 a_{11}\phi_{0/\eta\eta}\phi_{1/\eta\eta} + \\ &+ 2\mu^2 a_{12}\phi_{1/\xi\xi}\phi_{0/\eta\eta} - 2\mu^3 a_{16}\phi_{0/\eta\eta}\phi_{1/\xi\eta}]d\xi d\eta + \\ &+ \frac{2b}{a^3}\int_{-1}^{+1}\int_{-1}^{+1}a_{11}\mu^4\phi_{0/\eta\eta}^2 d\xi d\eta - \frac{2}{b}\Delta\int_{-1}^{+1}[\phi_{0/\eta\eta}]_{\pm 1}d\eta\end{aligned} \tag{4.37}$$

Three contribution can be highlighted with respect to Eq. 4.37: the first involves only ϕ_1 terms, the second only ϕ_0 terms and the third one contains products of the two. Note that the forcing term integral is evaluated at the panel boundaries where ϕ_1 is null by definition.

Inserting the approximate expansions for ϕ_1 and ϕ_0 in Eq. 4.37 leads to the

following discrete expression of the complementary energy

$$\Pi_c = \frac{2b}{a^3} \sum_{pq\overline{pq}=0}^{PQPQ} U_{pq\overline{pq}} \Phi_{pq} \Phi_{\overline{pq}} + \frac{4b}{a^3} \sum_{pqk=0}^{PQK} U_{C,pqk} \Phi_{pq} c_k + \frac{2b}{a^3} \sum_{k\overline{k}=0}^{KK} C_{k\overline{k}} c_k c_{\overline{k}} - \frac{2}{b} \Delta \sum_{k=0}^{K} P_k c_k \tag{4.38}$$

where the compact notation

$$\sum_{rsmnpq}^{RSMNPQ} = \sum_{r=0}^{R} \sum_{s=0}^{S} \sum_{m=0}^{M} \sum_{n=0}^{N} \sum_{p=0}^{P} \sum_{q=0}^{Q} \tag{4.39}$$

has been used to facilitate reading.
The matrix terms in Eq. 4.38 are

$$\begin{aligned} U_{pq\overline{pq}} = \int_{-1}^{+1} \int_{-1}^{+1} [& a_{11}\mu^4 X_p Y_q'' X_{\overline{p}} Y_{\overline{q}}'' + a_{22} X_p'' Y_q X_{\overline{p}}'' Y_{\overline{q}} + \\ & + 2a_{12}\mu^2 (X_p'' Y_q X_{\overline{p}} Y_{\overline{q}}'' + X_p Y_q'' X_{\overline{p}}'' Y_{\overline{q}}) - \\ & - 2a_{16}\mu^3 (X_p' Y_q' X_{\overline{p}} Y_{\overline{q}}'' + X_p Y_q'' X_{\overline{p}}' Y_{\overline{q}}') - \\ & - 2a_{26}\mu (X_p'' Y_q X_{\overline{p}}' Y_{\overline{q}}' + X_p' Y_q' X_{\overline{p}}'' Y_{\overline{q}}) + \\ & + a_{66} X_p' Y_q' X_{\overline{p}}' Y_{\overline{q}}'] dxdy \end{aligned} \tag{4.40}$$

$$\begin{aligned} U_{C,pqk} = \int_{-1}^{+1} \int_{-1}^{+1} [& a_{11}\mu^4 X_p Y_q'' \psi_k + a_{12}\mu^2 X_p'' Y_q \psi_k - \\ & - a_{16}\mu^3 X_p' Y_q' \psi_k] dxdy \end{aligned} \tag{4.41}$$

$$C_{k\overline{k}} = \int_{-1}^{+1} \int_{-1}^{+1} [a_{11}\mu^4 \psi_k(\eta) \psi_{\overline{k}}(\eta)] dxdy \tag{4.42}$$

$$P_k = 2 \int_{-1}^{+1} \psi_k(\eta) d\eta \tag{4.43}$$

where

$$\begin{aligned} pq, \overline{pq} &= \{0, 1, \ldots, PQ\} \\ k, \overline{k} &= \{0, 1, \ldots, K\} \end{aligned}$$

and $PQ = P(Q+1) + Q$. The notation $(.)'$, $(.)''$ is used to indicate respectively the first and the second derivatives.
It can be worth recalling that the membrane compliance terms a_{ij} are function of

the position. As opposed to the classical case of straight fiber panels, they cannot be taken outside of the integrals. For this reason, the integrals cannot be solved exactly and a numerical procedure is required. A numerical integration based on the Guassian quadrature rule is thus adopted. Further details about the numerical procedure are given in Appendix B.
The set of linear equations governing the pre-buckling response is obtained by minimizing Eq. 4.38 with respect to the coefficients Φ_{pq} and c_k

$$\begin{aligned} \frac{\partial \Pi_c}{\partial \Phi_{pq}} &= 0 \qquad pq = 1, 2, \ldots, PQ \\ \frac{\partial \Pi_c}{\partial c_k} &= 0 \qquad k = 1, 2, \ldots, K \end{aligned} \tag{4.44}$$

and the linear system associated to the pre-buckling problem is

$$\begin{bmatrix} \boldsymbol{U} & \boldsymbol{U_C} \\ \boldsymbol{U_C}^T & \boldsymbol{C} \end{bmatrix} \begin{bmatrix} \boldsymbol{\Phi}_{pq} \\ \boldsymbol{c}_k \end{bmatrix} = \Delta \begin{bmatrix} 0 \\ \boldsymbol{P} \end{bmatrix} \tag{4.45}$$

which is a system of $(PQ \times PQ + PQ \times K)$ linear algebraic equations. The matrix U has dimensions PQ×PQ and is defined as:

$$\boldsymbol{U}(pq, \overline{pq}) = \frac{4b}{a^3} \sum_{pq\overline{pq}=0}^{PQPQ} U_{\overline{pq}}^{pq} \tag{4.46}$$

The matrix U_C has dimension PQ×K and is defined as:

$$\boldsymbol{U_C}(pq, k) = \frac{4b}{a^3} \sum_{pqk=0}^{PQK} U_{C,k}^{pq} \tag{4.47}$$

while the term C is a K×K matrix:

$$\boldsymbol{C}(k, \overline{k}) = \frac{4b}{a^3} \sum_{k\overline{k}=0}^{KK} C_{\overline{k}}^{k} \tag{4.48}$$

Finally, the loading vector P is:

$$\boldsymbol{P}(k) = \frac{2}{b} \sum_{k=0}^{K} P_k \tag{4.49}$$

The unknowns coefficients Φ_{pq} and c_k have been collected in the vectors $\boldsymbol{\Phi}_{pq}$ and $\boldsymbol{c}_k$.
The system in Eq. 4.45 can be easily solved for Φ_{pq} and c_k for a prescribed uniform displacement Δ. The in-plane stress distribution is recovered as

$$N_x = \phi_{/yy} = \frac{4}{b^2}\phi_{/\eta\eta} = \frac{4}{b^2}\left(\sum_{k=0}^{K} c_k\psi_k(\eta) + \sum_{pq=0}^{PQ}\Phi_{pq}X_p(\xi)Y_q''(\eta)\right) \tag{4.50}$$

$$N_y = \phi_{/xx} = \frac{4}{a^2}\phi_{/\xi\xi} = \frac{4}{a^2}\sum_{pq=0}^{PQ}\Phi_{pq}X_p''(\xi)Y_q(\eta) \tag{4.51}$$

$$N_{xy} = -\phi_{/xy} = -\frac{4}{ab}\phi_{/\xi\eta} = -\frac{4}{ab}\sum_{pq=0}^{PQ}\Phi_{pq}X_p'(\xi)Y_q'(\eta) \tag{4.52}$$

A similar approach can be followed to derive the pre-buckling problem in the case of a force-control loading strategy. The equations for this case are reported in Appendix A.

4.5 Buckling Problem

The linearised buckling formulation is presented for a panel compressed by means of an imposed uniform displacement.
As outlined in Section 3.3, the equations are obtained by making the second variation of the unitary functional Π_F, defined in Eq. 3.26, stationary.

The second variation of Π_F has been derived in Section 3.3, and is reported in Eq. 3.44. The expression of $\delta^2\Pi_F$ can be rewritten in terms of the normalized

coordinates ξ and η, defined in Eq. 4.11, as:

$$\begin{aligned}\delta^2\Pi_F = &-\frac{2b}{a^3}\int_{-1}^{+1}\int_{-1}^{+1}[\mu^4 a_{11}(\xi,\eta)\delta\phi^2_{/\eta\eta} + 2\mu^2 a_{12}(\xi,\eta)\delta\phi_{/\eta\eta}\delta\phi_{/\xi\xi} + a_{22}(\xi,\eta)\delta\phi^2_{/\xi\xi}+\\ &+ a_{66}(\xi,\eta)\delta\phi^2_{/\xi\eta} - 2\mu^3 a_{16}(\xi,\eta)\delta\phi_{/\eta\eta}\delta\phi_{/\xi\eta} - 2\mu a_{26}(\xi,\eta)\delta\phi_{/\xi\xi}\delta\phi_{/\xi\eta}]d\xi d\eta+\\ &+\frac{2b}{a^3}\int_{-1}^{+1}\int_{-1}^{+1}[D_{11}(\xi,\eta)\delta w^2_{/\xi\xi} + 2\mu^2 D_{12}(\xi,\eta)\delta w_{/\eta\eta}\delta w_{/\xi\xi} + \mu^4 D_{22}(\xi,\eta)\delta w^2_{/\eta\eta}+\\ &+ 4\mu^2 D_{66}(\xi,\eta)\delta w^2_{/\xi\eta} + 4\mu D_{16}(\xi,\eta)\delta w_{/\xi\xi}\delta w_{/\xi\eta} + 4\mu^3 D_{26}(\xi,\eta)\delta w_{/\eta\eta}\delta w_{/\xi\eta}]d\xi d\eta+\\ &+\frac{2}{ab}\int_{-1}^{+1}\int_{-1}^{+1}[\lambda\phi_{/\eta\eta}\delta w^2_{/\xi} + \lambda\phi_{/\xi\xi}\delta w^2_{/\eta} - 2\lambda\phi_{/\xi\eta}\delta w_{/\xi}\delta w_{/\eta}]d\xi d\eta-\\ &-\frac{1}{\mu R}\int_{-1}^{+1}\int_{-1}^{+1}[\delta\phi_{/\xi\xi}\delta w]d\xi d\eta\end{aligned} \tag{4.53}$$

where $\mu = a/b$ is a non-dimensional parameter defining the aspect ratio of the panel. As defined in Eq. 4.72, the nomenclature ϕ indicates the pre-buckling equilibrium solution evaluated at the critical point, and λ is the buckling load factor. Moreover, due to the assumed membrane pre-buckling behaviour, $w = 0$.
The Ritz approximation of $\delta\phi$, in the separate form given in Eq. 4.30, and δw can be substituted in Eq. 4.53, that becomes:

$$\begin{aligned}\delta^2\Pi_F = &-\frac{2b}{a^3}\sum_{pq\overline{pq}=0}^{PQPQ} U_{pq\overline{pq}}\delta\Phi_{pq}\delta\Phi_{\overline{pq}} - \frac{4b}{a^3}\sum_{pqk=0}^{PQK} U_{C,pqk}\delta\Phi_{pq}\delta c_k-\\ &-\frac{2b}{a^3}\sum_{k\overline{k}=0}^{KK} C_{k\overline{k}}\delta c_k\delta c_{\overline{k}} + \frac{2b}{a^3}\sum_{mn\overline{mn}=0}^{MNMN} K_{mn\overline{mn}}\delta W_{mn}\delta W_{\overline{mn}}+\\ &+\lambda\frac{2}{ab}\sum_{pqmn\overline{mn}=0}^{PQMNMN} L_{1,pqmn\overline{mn}}\phi_{pq}\delta W_{mn}\delta W_{\overline{mn}}+\\ &+\lambda\frac{2}{ab}\sum_{kmn\overline{mn}=0}^{KMNMN} L_{2,kmn\overline{mn}}\delta c_k^{pre}\delta W_{mn}\delta W_{\overline{mn}}+\\ &+\sum_{pq=0}^{PQMN} C_{R,pqmn}\delta\Phi_{pq}\delta W_{mn}\end{aligned} \tag{4.54}$$

with $mn, \overline{mn} = \{0, 1, \ldots, MN\}$ and MN=M(N+1)+N. The compact notation provided in Eq. 4.39 has been employed. The terms in Eq. 4.54 are:

$$\begin{aligned} K_{mn\overline{mn}} = \int_{-1}^{+1}\int_{-1}^{+1} [&D_{11}\overline{X}''_m\overline{Y}_n\overline{X}''_{\overline{m}}\overline{Y}_{\overline{n}} + D_{22}\mu^4\overline{X}_m\overline{Y}''_n\overline{X}_{\overline{m}}\overline{Y}''_{\overline{n}} + \\ &+ 2D_{12}\mu^2(\overline{X}''_m\overline{Y}_n\overline{X}_{\overline{m}}\overline{Y}''_{\overline{n}} + \overline{X}_m\overline{Y}''_n\overline{X}''_{\overline{m}}\overline{Y}_{\overline{n}}) + \\ &+ 4D_{66}\mu^2\overline{X}'_m\overline{Y}'_n\overline{X}'_{\overline{m}}\overline{Y}'_{\overline{n}} + 2D_{16}\mu(\overline{X}''_m\overline{Y}_n\overline{X}'_{\overline{m}}\overline{Y}'_{\overline{n}} + \\ &+ \overline{X}'_m\overline{Y}'_n\overline{X}''_{\overline{m}}\overline{Y}_{\overline{n}}) + 2D_{26}\mu^3(\overline{X}'_m\overline{Y}'_n\overline{X}_{\overline{m}}\overline{Y}''_{\overline{n}} + \\ &+ \overline{X}_m\overline{Y}''_n\overline{X}'_{\overline{m}}\overline{Y}'_{\overline{n}})]d\xi d\eta \end{aligned} \tag{4.55}$$

$$\begin{aligned} L_{1,pqmn\overline{mn}} = \int_{-1}^{+1}\int_{-1}^{+1} [&X_pY''_q\overline{X}'_m\overline{Y}_n\overline{X}'_{\overline{m}}\overline{Y}_{\overline{n}} + \\ &+ X''_pY_q\overline{X}_m\overline{Y}'_n\overline{X}_{\overline{m}}\overline{Y}'_{\overline{n}} - \\ &- 2X'_pY'_q\overline{X}'_m\overline{Y}_n\overline{X}_{\overline{m}}\overline{Y}'_{\overline{n}}]d\xi d\eta \end{aligned} \tag{4.56}$$

$$L_{2,kmn\overline{mn}} = \int_{-1}^{+1}\int_{-1}^{+1} [\psi_k\overline{X}'_m\overline{Y}_n\overline{X}'_{\overline{m}}\overline{Y}_{\overline{n}}]d\xi d\eta \tag{4.57}$$

$$C_{R,pqmn} = -\frac{1}{\mu R}\int_{-1}^{+1}\int_{-1}^{+1} X''_p(\xi)Y_q(\eta)\overline{X}_m(\xi)\overline{Y}_n(\eta)d\xi d\eta \tag{4.58}$$

while $U_{pq\overline{pq}}$, $U_{C,pqk}$ and $C_{k\overline{k}}$ are defined in Section 4.4.

The stability equation can be obtained by minimizing Eq. 4.54 with respect to the unknown coefficients $\delta\Phi_{pq}$, δc_k and δW_{mn}.
Differentiating with respect to $\delta\Phi_{pq}$ and δc_k gives

$$\begin{aligned} \frac{\partial\delta^2\Pi_F}{\partial\delta\Phi_{pq}} &= -\boldsymbol{U}\delta\boldsymbol{\Phi}_{pq} - \boldsymbol{U_C}\delta\boldsymbol{c}_k + \boldsymbol{C_R}^T\delta\boldsymbol{W}_{mn} = 0 \\ \frac{\partial\delta^2\Pi_F}{\partial\delta c_k} &= -\boldsymbol{U_C}^T\delta\boldsymbol{\Phi}_{pq} - \boldsymbol{C}\delta\boldsymbol{c}_k = 0 \end{aligned} \tag{4.59}$$

where the matrices U, U_C and C are given in Eqs. 4.46, 4.47 and 4.48. The unknowns coefficients $\delta\Phi_{pq}$, δc_k and δW_{mn} have been collected in the vectors $\delta\boldsymbol{\Phi}_{pq}$, $\delta\boldsymbol{c}_k$ and $\delta\boldsymbol{W}_{mn}$. The matrix $\boldsymbol{C_R}$ is defined as:

$$\boldsymbol{C_R}(mn, pq) = \sum_{pqmn=0}^{PQMN} C_{R,pqmn} \tag{4.60}$$

and has dimensions MN×PQ.
Minimizing Eq. 4.54 with respect to the transverse displacement series coefficients δW_{mn} results in:

$$\frac{\partial \delta^2 \Pi_F}{\partial \delta W_{mn}} = \boldsymbol{K}\delta \boldsymbol{W}_{\overline{mn}} + \lambda \boldsymbol{L_1}\delta \boldsymbol{W}_{\overline{mn}} + \lambda \boldsymbol{L_2}\delta \boldsymbol{W}_{\overline{mn}} + \boldsymbol{C_R}\delta \boldsymbol{\Phi}_{pq} = 0 \tag{4.61}$$

where $\boldsymbol{K}$ is a MN×MN matrix defined as:

$$\boldsymbol{K}(mn, \overline{mn}) = \frac{2b}{a^3} \sum_{mn\overline{mn}=0}^{MNMN} K^{mn}_{\overline{mn}} \tag{4.62}$$

and $\boldsymbol{L_1}$, $\boldsymbol{L_2}$ are vectors of size MN defined as:

$$\boldsymbol{L_1}(mn) = \frac{2}{ab} \sum_{pqmn\overline{mn}=0}^{PQMNMN} L^{mn}_{1,pq\overline{mn}} \Phi_{pq} \tag{4.63}$$

$$\boldsymbol{L_2}(mn) = \frac{2}{ab} \sum_{kmn\overline{mn}=0}^{KMNMN} L^{mn}_{2,k\overline{mn}} c_k \tag{4.64}$$

Note that $\boldsymbol{L_1}$, $\boldsymbol{L_2}$ includes the pre-buckling solution Φ_{pq} and c_k.
The buckling problem is obtained in the form of the following set of equations:

$$\begin{aligned} -\boldsymbol{U}\delta \boldsymbol{\Phi}_{pq} - \boldsymbol{U_C}\delta \boldsymbol{c}_k + \boldsymbol{C_R}^T \delta \boldsymbol{W}_{mn} &= 0 \\ \boldsymbol{U_C}^T \delta \boldsymbol{\Phi}_{pq} + \boldsymbol{C}\delta \boldsymbol{c}_k &= 0 \\ \boldsymbol{K}\delta \boldsymbol{W}_{mn} + \lambda(\boldsymbol{L_1} + \boldsymbol{L_2})\delta \boldsymbol{W}_{mn} + \boldsymbol{C_R}\delta \boldsymbol{\Phi}_{pq} &= 0 \end{aligned} \tag{4.65}$$

From the second equation in 4.65

$$\delta \boldsymbol{c}_k = -\boldsymbol{C}^{-1}\boldsymbol{U_C}^T \delta \boldsymbol{\Phi}_{pq} \tag{4.66}$$

which can be substituted in the first equation of 4.65, resulting in:

$$\delta \boldsymbol{\Phi}_{pq} = -(\boldsymbol{U} - \boldsymbol{U_C}\boldsymbol{C}^{-1}\boldsymbol{U_C}^T)^{-1}\boldsymbol{C_R}^T \delta \boldsymbol{W}_{mn} \tag{4.67}$$

that can be substituted in the third equation of 4.65. The following eigenvalue problem is obtained:

$$[\boldsymbol{K} + \boldsymbol{U_R} + \lambda(\boldsymbol{L_1} + \boldsymbol{L_2})]\delta \boldsymbol{W}_{mn} = 0 \tag{4.68}$$

where the matrix $\boldsymbol{U_R}$ has the same dimensions of K and is

$$\boldsymbol{U_R}(mn, \overline{mn}) = -\boldsymbol{C_R}[(\boldsymbol{U} - \boldsymbol{U_C}\boldsymbol{C}^{-1}\boldsymbol{U_C}^T)^{-1}\boldsymbol{C_R}^T] \tag{4.69}$$

By solving Eq. 4.68, MN eigencouples $(\lambda, \delta\boldsymbol{W}_{mn})_{mn}$ are found. The solution corresponding to the smallest eigenvalue represent the buckling factor λ and the bucking mode δW_{mn} of a variable-stiffness shell.

From the expression of the buckling problem in Eq. 4.68 it is possible to obtain the buckling problem for a plate. In the case of a flat panel $R \to \infty$, and the matrix C_R goes to zero. When C_R is zero, the membrane part is decoupled from the bending one, and Eq. 4.68 reduces to:

$$[\boldsymbol{K} + \lambda(\boldsymbol{L_1} + \boldsymbol{L_2})]\delta\boldsymbol{W}_{mn} = 0 \tag{4.70}$$

which is the eigenvalue equation associated to the buckling problem of a plate.

The buckling condition is then identified by the critical displacement Δ_{cr}, that is computed as:

$$\Delta_{cr} = \lambda\Delta \tag{4.71}$$

Therefore, the in-plane stress at the critical point is given by

$$\phi_{cr} = \lambda\phi \tag{4.72}$$

which is:

$$\phi_{cr} = \lambda(\phi_0 + \phi_1) = \lambda\left(\sum_{k=0}^{K}\int_{-1}^{+1}\int_{-1}^{+1} c_k\psi_k(\eta) + \sum_{p=0}^{P}\sum_{q=0}^{Q}\Phi_{pq}X_p(\xi)Y_q(\eta)\right) \tag{4.73}$$

From the solution of the pre- and buckling problems, the buckling load N_x^{cr} can be computed as:

$$N_x^{cr} = \frac{\lambda}{b}\int_{-b/2}^{+b/2}\phi_{0/yy}dy = \frac{2\lambda}{b^2}\int_{-1}^{+1}\phi_{0/\eta\eta}d\eta = \frac{2\lambda}{b^2}\sum_{k=0}^{K}c_k\int_{-1}^{+1}\psi(\eta)d\eta \tag{4.74}$$

By following the same approach it is also possible to derive the load-control formulation for the buckling problem. The equations are reported in Appendix A.

4.6 Post-buckling Problem

In this section the governing non-linear equations for the post-buckling analysis are obtained for a panel compressed by means of an imposed uniform displacement. As mentioned in Section 3.4, the set of non-linear equations will be obtained by means of the unitary functional given in Eq. 3.45, which is written in terms of the out-of-plane displacement w and the Airy stress function ϕ: with this formulation the in-plane equilibirum is automatically satisfied, therefore it is necessary to satisfy only the out-of-plane equilibrium and the compatibility.
In the following, the equations are derived by applying the Ritz method to the unitary functional Π_F: the resulting set of equations are non-linear, thus a numerical solution is required. After deriving the equations, a brief overview on the numerical techniques adopted to solve the post-buckling problem will be presented.

The unitary functional of Eq. 3.45 can be organized by separating the different contributions. In particular, the functional is organized as:

$$\Pi_F = -\Pi_{F,m} + \Pi_{F,b} + \Pi_{F,NL} + \Pi_{F,0} + P + \Pi_{F,R} \tag{4.75}$$

where $\Pi_{F,m}$ is the membrane complementary energy defined in Eq. 3.16 and $\Pi_{F,b}$ is the bending part of the total potential energy. The contribution $\Pi_{F,NL}$ is

$$\Pi_{F,NL} = \frac{1}{2}\int_S [\phi_{/yy} w_{/x}^2 + \phi_{/xx} w_{/y}^2 - 2\phi_{/xy} w_{/x} w_{/y}] dS \tag{4.76}$$

Note that the last integral is non-linear, as it involves ϕ and the quadratic terms in w: this integral is the one that provides the non-linear terms in the resulting governing equations. It is worth noting that it doesn't involve any stiffness coefficient.
The $\Pi_{F,0}$ contribution is the integral related to the geometrical imperfections, while the term P is the complementary work related to the imposed displacement Δ.
Finally, the contribution $\Pi_{F,R}$ is the part of the functional related to the curvature R of the panel.

To derive the governing equations, the unitary functional is rewritten in terms of

the normalized coordinates, given in Eq. 4.11, as:

$$\begin{aligned}\Pi_F = &-\frac{2b}{a^3}\int_{-1}^{+1}\int_{-1}^{+1}[\mu^4 a_{11}\phi_{/\eta\eta}^2 + 2\mu^2 a_{12}\phi_{/\eta\eta}\phi_{/\xi\xi}+\\ &+ a_{22}\phi_{/\xi\xi}^2 + a_{66}\phi_{/\xi\eta}^2 - 2\mu^3 a_{16}\phi_{/\eta\eta}\phi_{/\xi\eta}-\\ &- 2\mu a_{26}\phi_{/\xi\xi}\phi_{/\xi\eta}]d\xi d\eta+\\ &+\frac{2b}{a^3}\int_{-1}^{+1}\int_{-1}^{+1}[D_{11}w_{/\xi\xi}^2 + 2D_{12}\mu^2 w_{/\eta\eta}w_{/\xi\xi}+\\ &+ D_{22}\mu^4 w_{/\eta\eta}^2 + 4D_{66}\mu^2 w_{/\xi\eta}^2+\\ &+ 4D_{16}\mu w_{/\xi\xi}w_{/\xi\eta} + 4D_{26}\mu^3 w_{/\eta\eta}w_{/\xi\eta}]d\xi d\eta+\\ &+\frac{2}{ab}\int_{-1}^{+1}\int_{-1}^{+1}[\phi_{/\eta\eta}w_{/\xi}^2 + \phi_{/\xi\xi}w_{/\eta}^2 - 2\phi_{/\xi\eta}w_{/\xi}w_{/\eta}]d\xi d\eta+\\ &-\frac{2}{ab}\int_{-1}^{+1}\int_{-1}^{+1}\phi_{/\xi\xi}\frac{w}{R}d\xi d\eta - \frac{2}{b}\int_{-1}^{+b/2}[\phi_{/yy}\Delta]_{\pm a/2}d\eta-\\ &-\int_{-1}^{+1}\int_{-1}^{+1}[\phi_{/\eta\eta}w_0 w_{/\xi\xi} + \phi_{/\xi\xi}w_0 w_{/\eta\eta} - 2\phi_{/\xi\eta}w_0 w_{/\xi\eta}]d\xi d\eta\end{aligned} \tag{4.77}$$

The Ritz approximation of ϕ and w can be inserted in Eq. 4.77, and the resulting expression can be minimized with respect to the coefficient of the series expansion. In order to simplify the reading, the different contributions of the unitary functional are hereafter considered separately.

Membrane Contribution The membrane complementary energy has already been treated in Section 4.4, and the minimization procedure is not reported here for the sake of conciseness. The separate expression of ϕ given in Eq. 4.30 is substituted in $\Pi_{F,m}$. The resulting discrete form of the membrane contribution can be differentiated with respect to the coefficients Φ_{pq} and c_k as:

$$\begin{aligned}\frac{\partial \Pi_{F,m}}{\partial \Phi_{pq}} &= -\boldsymbol{U}\boldsymbol{\Phi}_{pq} - \boldsymbol{U_C}\boldsymbol{c}_k\\ \frac{\partial \Pi_{F,m}}{\partial c_k} &= -\boldsymbol{U_C}\boldsymbol{\Phi}_{pq} - \boldsymbol{C}\boldsymbol{c}_k\end{aligned} \tag{4.78}$$

where the matrices $\boldsymbol{U}$, $\boldsymbol{U_C}$ and $\boldsymbol{C}$ are defined in Eqs. 4.46, 4.47 and 4.48. The vectors $\boldsymbol{\Phi}_{pq}$ and $\boldsymbol{c}_k$ collects the unknowns coefficients of the series expansions of ϕ and c.

Bending Contribution The bending energy contribution $\Pi_{F,b}$ is written in a discrete form by inserting the series expansion of the out-of-plane displacement given in Eq. 5.11. By minimizing the resulting expression with respect to the coefficients W_{mn}, the following expression is obtained:

$$\frac{\partial \Pi_{F,b}}{\partial W_{mn}} = \boldsymbol{K}\boldsymbol{W}_{mn} \tag{4.79}$$

where the stiffness matrix $\boldsymbol{K}$ is defined in Eq. 4.62 and the vector $\boldsymbol{W}_{mn}$ collects the unknowns coefficients W_{mn}.

Non-linear Contribution The non-linear integral $\Pi_{F,NL}$ is rewritten by substituting the separate form of ϕ, given in Eq. 4.30, as:

$$\begin{aligned}
\Pi_{F,NL} &= +\frac{2}{ab}\int_{-1}^{+1}\int_{-1}^{+1}[\phi_{0/\eta\eta} + \phi_{1/\eta\eta}w_{/\xi}^2 + \phi_{1/\xi\xi}w_{/\eta}^2 - 2\phi_{1/\xi\eta}w_{/\xi}w_{/\eta}]d\xi d\eta = \\
&= +\frac{2}{ab}\int_{-1}^{+1}\int_{-1}^{+1}[\phi_{1/\eta\eta}w_{/\xi}^2 + \phi_{1/\xi\xi}w_{/\eta}^2 - 2\phi_{1/\xi\eta}w_{/\xi}w_{/\eta}]d\xi d\eta + \\
&\quad + \frac{2}{ab}\int_{-1}^{+1}\int_{-1}^{+1}[\phi_{0/\eta\eta}w_{/\xi}^2]d\xi d\eta
\end{aligned} \tag{4.80}$$

The Ritz approximation of ϕ_0, ϕ_1 and w are substituted in Eq. 4.80, that becomes:

$$\begin{aligned}
\Pi_{F,NL} = +\frac{2}{ab}\int_{-1}^{+1}\int_{-1}^{+1}[&\sum_{pq=0}^{PQ} X_p Y_q'' \Phi_{pq} \sum_{mn=0}^{MN}\sum_{\overline{mn}=0}^{MN} \overline{X}'_m \overline{Y}_n W_{mn} \overline{X}'_{\overline{m}} \overline{Y}_{\overline{n}} W_{\overline{mn}} + \\
&+ \sum_{pq=0}^{PQ} X_p'' Y_q \Phi_{pq} \sum_{mn=0}^{MN}\sum_{\overline{mn}=0}^{MN} \overline{X}_m \overline{Y}'_n W_{mn} \overline{X}_{\overline{m}} \overline{Y}'_{\overline{n}} W_{\overline{mn}} - \\
&- 2\sum_{pq=0}^{PQ} X_p' Y_q' \Phi_{pq} \sum_{mn=0}^{MN}\sum_{\overline{mn}=0}^{MN} \overline{X}'_m \overline{Y}_n W_{mn} \overline{X}_{\overline{m}} \overline{Y}'_{\overline{n}} W_{\overline{mn}}]d\xi d\eta + \\
&+ \frac{2}{ab}\int_{-1}^{+1}\int_{-1}^{+1}[\sum_{k=0}^{K}\psi_k c_k \sum_{mn=0}^{MN}\sum_{\overline{mn}=0}^{MN} \overline{X}'_m \overline{Y}_n W_{mn} \overline{X}'_{\overline{m}} \overline{Y}_{\overline{n}} W_{\overline{mn}}]d\xi d\eta
\end{aligned} \tag{4.81}$$

It is possible to identify two different contributions: one that involves ϕ_0 and one that involves ϕ_1. Eq. 4.81 can be rewritten in terms of components as:

$$\Pi_{F,NL} = \sum_{pqmn\overline{mn}}^{\text{PQMNMN}} L_{1,pqmn\overline{mn}} \Phi_{pq} W_{mn} W_{\overline{mn}} + \sum_{kmn\overline{mn}}^{\text{KMNMN}} L_{2,kmn\overline{mn}} c_k W_{mn} W_{\overline{mn}} \tag{4.82}$$

where $L_{1,pqmn\overline{mn}}$ is:

$$\begin{aligned} L_{1,pqmn\overline{mn}} = &+ \frac{2}{ab} \int_{-1}^{+1} \int_{-1}^{+1} [X_p Y_q'' \overline{X}'_m \overline{Y}_n \overline{X}'_{\overline{m}} \overline{Y}_{\overline{n}} + \\ &+ X_p'' Y_q \overline{X}_m \overline{Y}'_n \overline{X}_{\overline{m}} \overline{Y}'_{\overline{n}} - \\ &- 2 X'_p Y'_q \overline{X}'_m \overline{Y}_n \overline{X}_{\overline{m}} \overline{Y}'_{\overline{n}}] d\xi d\eta \end{aligned} \tag{4.83}$$

and $L_{2,kmn\overline{mn}}$ is:

$$L_{2,kmn\overline{mn}} = + \frac{2}{ab} \int_{-1}^{+1} \int_{-1}^{+1} [\psi_k \overline{X}'_m \overline{Y}_n \overline{X}'_{\overline{m}} \overline{Y}_{\overline{n}}] d\xi d\eta \tag{4.84}$$

Differentiating with respect to the unknown coefficients:

$$\begin{aligned} \frac{\partial \Pi_{F,NL}}{\partial \Phi_{pq}} &= \boldsymbol{L_1}^{pq} \boldsymbol{W}_{mn} \boldsymbol{W}_{\overline{mn}} \\ \frac{\partial \Pi_{F,NL}}{\partial c_k} &= \boldsymbol{L_2}^{k} \boldsymbol{W}_{mn} \boldsymbol{W}_{\overline{mn}} \\ \frac{\partial \Pi_{F,NL}}{\partial W_{il}} &= \boldsymbol{L_1}^{mn} \boldsymbol{\Phi}_{pq} \boldsymbol{W}_{\overline{mn}} + \boldsymbol{L_2}^{mn} \boldsymbol{c}_k \boldsymbol{W}_{\overline{mn}} \end{aligned} \tag{4.85}$$

where the following notation has been used:

$$\boldsymbol{L_1}^{ij} \boldsymbol{B}_{kl} \boldsymbol{C}_{rs} = \sum_{kl}^{\text{KL}} \sum_{rs}^{\text{RS}} \frac{\partial}{\partial A_{ij}} (L_{1,ijklmn} A_{ij} B_{kl} C_{rs}) \tag{4.86}$$

Note that the unknowns coefficients have been collected in vectorial form.

Imperfection Contribution In this work the initial geometric imperfection, w_0, is assumed to have the same shape of the first buckling mode of the panel:

$$w_0(\xi, \eta) = \sum_{t=0}^{T} \sum_{u=0}^{U} W_{0tu} X_{0m}(\xi) Y_{0n}(\eta) \tag{4.87}$$

where the same admissible functions used for $w(x,y)$ are used for X_0 and Y_0. The coefficients W_{0tu} correspond to the first eigenvector obtained from the buckling problem in Eq. 4.68.
The Ritz approximation of w, $w0$ and ϕ is then substituted as

$$\begin{aligned}\Pi_{F,0} = &-\frac{4}{ab}\int_{-1}^{+1}\int_{-1}^{+1}[\sum_{k=0}^{K} c_k\psi_k \sum_{tu=0}^{TU} W_{0tu}X_{0t}Y_{0u}\sum_{mn=0}^{MN} W_{mn}\overline{X}''_m\overline{Y}_n]d\xi d\eta - \\ &-\frac{4}{ab}\int_{-1}^{+1}\int_{-1}^{+1}[\sum_{pq=0}^{PQ}\Phi_{pq}X_pY''_q\sum_{tu=0}^{TU} W_{0tu}X_{0t}Y_{0u}\sum_{mn=0}^{MN} W_{mn}\overline{X}''_m\overline{Y}_n + \\ &+\sum_{pq=0}^{PQ}\Phi_{pq}X''_pY_q\sum_{tu=0}^{TU} W_{0tu}X_{0t}Y_{0u}\sum_{mn=0}^{MN} W_{mn}\overline{X}_m\overline{Y}''_n - \\ &-2\sum_{pq=0}^{PQ}\Phi_{pq}X'_pY'_q\sum_{tu=0}^{TU} W_{0tu}X_{0t}Y_{0u}\sum_{mn=0}^{MN} W_{mn}\overline{X}'_m\overline{Y}'_n]d\xi d\eta\end{aligned} \tag{4.88}$$

Eq. 4.88 can be written in terms of components as:

$$\Pi_{F,0} = \sum_{pqmntu}^{\text{PQMNTU}} L_{01,pqmntu}\Phi_{pq}W_{mn}W_{0tu} + \sum_{kmntu}^{\text{KMNTU}} L_{02,kmntu}c_kW_{mn}W_{0tu} \tag{4.89}$$

where

$$\begin{aligned}L_{01,pqmntu} = &-\frac{4}{ab}\int_{-1}^{+1}\int_{-1}^{+1}[X_pY''_qX_{0t}Y_{0u}\overline{X}''_m\overline{Y}_n + \\ &+X''_pY_qX_{0t}Y_{0u}\overline{X}_m\overline{Y}''_n - \\ &-2X'_pY'_qX_{0t}Y_{0u}\overline{X}'_m\overline{Y}'_n]d\xi d\eta\end{aligned} \tag{4.90}$$

$$L_{02,kmntu} = -\frac{4}{ab}\int_{-1}^{+1}\int_{-1}^{+1}[\psi_kX_{0t}Y_{0u}\overline{X}''_m\overline{Y}_n]d\xi d\eta \tag{4.91}$$

Differentiating with respect to the coefficient W_{mn} and Φ_{pq} gives:

$$\begin{aligned}\frac{\partial\Pi_{F,0}}{\partial\Phi_{pq}} &= \boldsymbol{L_{01}}^{pq}\boldsymbol{W}_{0tu}\boldsymbol{W}_{mn} \\ \frac{\partial\Pi_{F,0}}{\partial c_k} &= \boldsymbol{L_{02}}^{k}\boldsymbol{W}_{0tu}\boldsymbol{W}_{mn} \\ \frac{\partial\Pi_{F,0}}{\partial W_{mn}} &= \boldsymbol{L_{01}}^{mn}\boldsymbol{\Phi}_{pq}\boldsymbol{W}_{0tu} + \boldsymbol{L_{02}}^{mn}\boldsymbol{c}_k\boldsymbol{W}_{0tu}\end{aligned} \tag{4.92}$$

where the notation in Eq. 4.86 has been adapted to $L_{01,pqmntu}$ and $L_{02,kmntu}$. The unknown coefficients W_{mn}, Φ_{pq} and c_k have been collected in the vectors $\boldsymbol{W}_{mn}$, $\boldsymbol{\Phi}_{pq}$ and $\boldsymbol{c}_k$.

Load Contribution The contribution related to the imposed displacement Δ is:

$$\begin{aligned} P &= -\int_{C_2} \left[\phi_{/yy} 2\Delta\right]_{x=-a/2}^{x=a/2} dy = \\ &= -\frac{4}{b}\Delta \int_{C_2} \left[\phi_{0/\eta\eta}\right] d\eta \end{aligned} \tag{4.93}$$

By substituting the series expansion of ϕ_0, Eq. 4.93 becomes:

$$P_k = -\frac{4}{b}\Delta \int_{C_2} \left[\sum_k^K c_k \psi_k(\eta)\right] d\eta \tag{4.94}$$

and by differentiating the expression above with respect to the coefficients c_k

$$\frac{\partial P_k}{\partial c_k} = \Delta \boldsymbol{P} \tag{4.95}$$

Curvature Contribution The Ritz approximations of the Airy stress function and the out-of-plane displacement are substituted in the contribution related to the curvature R as:

$$\begin{aligned} \Pi_{F,R} &= -\frac{a^2}{2R} \sum_{pqmn=0}^{PQMN} \int_{-1}^{+1} \int_{-1}^{+1} \Phi_{pq} X_p''(\xi) Y_q(\eta) W_{mn} \overline{X}_m(\xi) \overline{Y}_n(\eta) d\xi d\eta \\ &= -\frac{a^2}{2R} \sum_{pqmn=0}^{PQMN} C_{R,pqmn} \Phi_{pq} W_{mn} \end{aligned} \tag{4.96}$$

Differentiating Eq. 4.58 with respect to Φ_{pq} and W_{mn}

$$\begin{aligned} \frac{\partial \Pi_{F,R}}{\partial \Phi_{pq}} &= \boldsymbol{C_R}^T \boldsymbol{W}_{mn} \\ \frac{\partial \Pi_{F,R}}{\partial W_{mn}} &= \boldsymbol{C_R} \boldsymbol{\Phi}_{pq} \end{aligned} \tag{4.97}$$

where the matrix C_R is:

$$\boldsymbol{C_R}(pq, mn) = -\frac{a^2}{2R} \sum_{pqmn=0}^{PQMN} C_{R,pq}^{mn,T} \tag{4.98}$$

The unknown coefficients W_{mn}, Φ_{pq} have been collected in the vectors $\boldsymbol{W}_{mn}$, $\boldsymbol{\Phi}_{pq}$.

By collecting the different contributions it is possible to write the set of non-linear equations that models the post-buckling response of a variable stiffness shell. The following non-linear system is obtained:

$$\begin{cases} \boldsymbol{U}\boldsymbol{\Phi}_{pq} + \boldsymbol{U_C}\boldsymbol{c}_k + \boldsymbol{L_1}^{pq}\boldsymbol{W}_{mn}\boldsymbol{W}_{\overline{mn}} + \boldsymbol{L_{01}}^{pq}\boldsymbol{W}_{mn}\boldsymbol{W}_{tu} + \boldsymbol{C_R}^T\boldsymbol{W}_{mn} = 0 \\ \boldsymbol{U_C}\boldsymbol{\Phi}_{pq} + \boldsymbol{C}\boldsymbol{c}_k + \boldsymbol{L_2}^{k}\boldsymbol{W}_{mn}\boldsymbol{W}_{\overline{mn}} + \boldsymbol{L_{02}}^{k}\boldsymbol{W}_{mn}\boldsymbol{W}_{tu} - \Delta\boldsymbol{P} = 0 \\ \boldsymbol{K}\boldsymbol{W}_{\overline{mn}} + \boldsymbol{L_1}^{mn}\boldsymbol{\Phi}_{pq}\boldsymbol{W}_{\overline{mn}} + \boldsymbol{L_2}^{mn}\boldsymbol{c}_k\boldsymbol{W}_{\overline{mn}} + \boldsymbol{L_{01}}^{mn}\boldsymbol{\Phi}_{pq}\boldsymbol{W}_{tu} + \boldsymbol{L_{02}}^{mn}\boldsymbol{c}_k\boldsymbol{W}_{\overline{mn}} + \boldsymbol{C_R}\boldsymbol{\Phi}_{pq} = 0 \end{cases} \tag{4.99}$$

The first and the second equations in Eq. 4.99 are sets of PQ and K equations respectively, and represent the compatibility condition. The third set of MN equations represents the out-of-plane equilibirum equation.
Note that from the expression of the non-linear system in Eq. 4.99 it is possible to derive the post-buckling problem for variable-stiffness plates: in the case of a flat panel the matrix $\boldsymbol{C_R}$ goes to zero.

A similar approach can be followed to derive the pre-buckling problem in the case of a force-control loading strategy. The equations for this case are reported in Appendix A.

4.7 Numerical Solution

The non-linear system in Eq. 4.99 demands for a numerical solution strategy. In order to trace the equilibirum steps at different load levels, the load can be progressively increased from zero up to the desired load level. In the proposed implementation, two strategies are discussed, based on the Newton-Raphson approach and the arc-length solution strategy.

Using a compact notation, the non-linear system derived in Section 4.6 can be solved in order to obtain the post-buckling response: the system is solved for various load levels in order to compute the equilibirum states, and the results can be visualized in terms of load-displacement curve, as described in Section 2.3.

The non-linear system in Eq. 4.99 can be expressed as:

$$\boldsymbol{R}(\boldsymbol{x}, \lambda) = \boldsymbol{F}(\boldsymbol{x}) - \lambda \boldsymbol{q} = 0 \tag{4.100}$$

where λ is the load parameter, $\boldsymbol{q}$ is the vector defining the shape of the load and $\boldsymbol{x}$ is the vector collecting the unknown amplitudes of the Airy stress function and the out-of-plane displacement as:

$$\boldsymbol{x} = \begin{bmatrix} \boldsymbol{\Phi}_{pq} \\ \boldsymbol{c}_k \\ \boldsymbol{W}_{mn} \end{bmatrix} \tag{4.101}$$

The vector $\boldsymbol{F}(\boldsymbol{x})$ is defined as:

$$\boldsymbol{F}(\boldsymbol{x}) = \begin{cases} \boldsymbol{U}\boldsymbol{\Phi}_{pq} + \boldsymbol{U_C}\boldsymbol{c}_k + \boldsymbol{L_1}^{pq}\boldsymbol{W}_{mn}\boldsymbol{W}_{\overline{mn}} + \boldsymbol{L_{01}}^{pq}\boldsymbol{W}_{mn}\boldsymbol{W}_{tu} + \boldsymbol{C_R}^T\boldsymbol{W}_{mn} \\ \boldsymbol{U_C}\boldsymbol{\Phi}_{pq} + \boldsymbol{C}\boldsymbol{c}_k + \boldsymbol{L_2}^k\boldsymbol{W}_{mn}\boldsymbol{W}_{\overline{mn}} + \boldsymbol{L_{02}}^k\boldsymbol{W}_{mn}\boldsymbol{W}_{tu} \\ \boldsymbol{K}\boldsymbol{W}_{mn} + \boldsymbol{L_1}^{mn}\boldsymbol{\Phi}_{pq}\boldsymbol{W}_{mn} + \boldsymbol{L_2}^{mn}\boldsymbol{c}_k\boldsymbol{W}_{mn} + \boldsymbol{L_{01}}^{mn}\boldsymbol{\Phi}_{pq}\boldsymbol{W}_{tu} + \boldsymbol{L_{02}}^{mn}\boldsymbol{c}_k\boldsymbol{W}_{mn} + \boldsymbol{C_R}\boldsymbol{\Phi}_{pq} \end{cases} \tag{4.102}$$

and the reference loading vector $\boldsymbol{q}$ is

$$\boldsymbol{q} = \begin{bmatrix} \boldsymbol{0} \\ \boldsymbol{P} \\ \boldsymbol{0} \end{bmatrix} \tag{4.103}$$

If the problem in Eq. 4.100 is defined by n degree of freedom, there are $n+1$ unknowns. However, there are only n equations, and an additional constraint equation shall be added to complete the system. This constraint equation relates the unknowns $\boldsymbol{x}$ to the load parameter λ, and, in general, can be written as:

$$f(\boldsymbol{x}, \lambda) = 0 \tag{4.104}$$

This last equations depends on the strategy adopted.
To solve the non-linear system in Eq. 4.99, iterative solution techniques are required: at every i-th iteration the unknowns $\boldsymbol{x}$ and the imposed displacement λ are

$$\begin{aligned} \boldsymbol{x}_{i+1} &= \boldsymbol{x}_i + \Delta\boldsymbol{x}_i \\ \lambda_{i+1} &= \lambda_i + \Delta\lambda_i \end{aligned} \tag{4.105}$$

where the terms $\Delta \boldsymbol{x}_i$ and $\Delta\lambda_i$ are the correction of the unknowns states $\boldsymbol{x}$ and the load factor. Note that $\Delta(\cdot)$ is an incremental quantity, and should not be confused with the imposed displacement Δ.
In general, at every iteration the following system is solved

$$\begin{aligned} \boldsymbol{R}(\boldsymbol{x}_{i+1}, \lambda_{i+1}) = F(\boldsymbol{x}_i) - \lambda_i \boldsymbol{q} = 0 \\ f(\boldsymbol{x}_{i+1}, \lambda_{i+1}) = 0 \end{aligned} \tag{4.106}$$

The difference between the various techniques is mainly related to the way the corrections in Eq. 4.105 are evaluated. In the Newton-Raphson method, the correction $\Delta \boldsymbol{x}$ is evaluated separately from $\Delta\lambda$, which is null: the load vector is fixed at every evaluation, and it is in general imposed by the user. The solution of the system in Eq. 4.106 is thus restricted to the first set of equations, while the last one is dropped out. In contrast, the arc-length approach requires the solution of the complete system in Eq. 4.106, including the constraint equation. In this case, the load parameter is an unknown of the problem and, as such, has to be determined as part of the solution.
In the following, the Newton-Raphson and the arc-length methods are briefly outlined, together with the algorithms developed to solve the non-linear system obtained in Section 4.6.

Newton-Raphson Method

In the classical Newton-Raphson method, the solution of the non-linear system of Eq. 4.100 is obtained by means of an iterative procedure based on successive linearisations of the problem:

$$\boldsymbol{R}(\boldsymbol{x}_i, \lambda_j) = \boldsymbol{R}(\boldsymbol{x}_i, \lambda_j) + \boldsymbol{J}(\boldsymbol{x}_i)\Delta x_i \tag{4.107}$$

where $\boldsymbol{J}(\boldsymbol{x}_i)$ is the Jacobian matrix, defined as:

$$\boldsymbol{J}(\boldsymbol{x}_i) = \left[\frac{\partial \boldsymbol{R}(\boldsymbol{x}_i, \lambda_j)}{\partial \boldsymbol{x}}\right]_{\boldsymbol{x}_i} \tag{4.108}$$

Then, at every iteration, the increment $\Delta \boldsymbol{x}_i$ is evaluated as:

$$\Delta \boldsymbol{x}_i = -\boldsymbol{J}^{-1}(\boldsymbol{x}_i)\boldsymbol{R}(\boldsymbol{x}_i, \lambda_i) \tag{4.109}$$

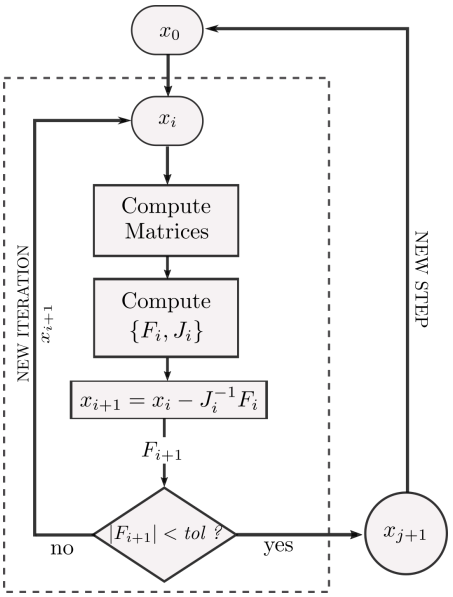

Figure 4.2: Work-flow of the Newton-Raphson method.

and the solution at the iteration $i + 1$ is:

$$\boldsymbol{x}_{i+1} = \boldsymbol{x}_i + \Delta\boldsymbol{x}_{i+1} = \boldsymbol{x}_i - \boldsymbol{J}^{-1}(\boldsymbol{x}_i)\boldsymbol{R}(\boldsymbol{x}_i, \lambda_j) \tag{4.110}$$

The Newton-Raphson solution procedure is implemented as outlined in Figure 4.2. In particular, at every step j the loading condition λ_j is prescribed, and the iteration is carried out to determine the convergence of the solution according to a given criterion. For every i-th iteration, the matrices of the non-linear system and the Jacobian matrix are evaluated, and the solution $\boldsymbol{x}_{i+1}$ is computed according to Eq. 4.110. The convergence criteria is defined by evaluating the norm of the residual as:

$$\|\boldsymbol{R}_{i+1} - \boldsymbol{R}_i\| < \text{tol} \tag{4.111}$$

where *tol* is the tolerance defined by the user. The iteration is arrested when the condition of Eq. 4.111 is met, and a new load step is applied as:

$$\lambda_j = \frac{\lambda_{cr}}{\tau} + \lambda_{j-1} \tag{4.112}$$

where λ_{cr} is the critical buckling load, available from the linear buckling analysis, and τ is an integer value defining the step size. Good choices of τ, based on a number of tests, are $20 - 30$: this leads to a good compromise between accuracy and computational time.

The post-buckling response is computed until the desired load level is reached.

The Jacobian matrix is computed at every iteration i: this can be done numerically or analytically. To improve the computational efficiency, the latter option is chosen. The Jacobian matrix is computed as:

$$\boldsymbol{J} = \begin{bmatrix} \frac{\partial \boldsymbol{R}_i^1}{\partial \Phi_{pq}} & \frac{\partial \boldsymbol{R}_i^1}{\partial c_k} & \frac{\partial \boldsymbol{R}_i^1}{\partial W_{mn}} \\ \frac{\partial \boldsymbol{R}_i^2}{\partial \Phi_{pq}} & \frac{\partial \boldsymbol{R}_i^2}{\partial c_k} & \frac{\partial \boldsymbol{R}_i^2}{\partial W_{mn}} \\ \frac{\partial \boldsymbol{R}_i^3}{\partial \Phi_{pq}} & \frac{\partial \boldsymbol{R}_i^3}{\partial c_k} & \frac{\partial \boldsymbol{R}_i^3}{\partial W_{mn}} \end{bmatrix} = \\ = \begin{bmatrix} \boldsymbol{U} & \boldsymbol{U_C} & (\boldsymbol{L_1}^{pq,J} + \boldsymbol{L_{01}}^{pq,J} + \boldsymbol{C_R}^T) \\ \boldsymbol{U_C} & \boldsymbol{C} & (\boldsymbol{L_2}^{k,J} + \boldsymbol{L_{02}}^{k,J}) \\ (\boldsymbol{L_1}^{mn,J} + \boldsymbol{L_{01}}^{mn,J} + \boldsymbol{C_R}^T) & (\boldsymbol{L_2}^{mn,J} + \boldsymbol{L_{02}}^{mn,J}) & \boldsymbol{K} + \boldsymbol{L_{12}}^{mn,J} \end{bmatrix} \tag{4.113}$$

which is a matrix of dimensions (PQ+K+MN)×(PQ+K+MN).
For a detailed description of the matrices entering Eq. 4.113 see Appendix C.

Once the response is computed, is possible to retrieve results in terms of in-plane stress distribution and out-of-plane displacement.

Arc-length Method

The arc-length method is a solution technique which is often used to compute the response of structures exhibiting post-buckling responses characterized by snap-back or snap-through.
Different formulations have been proposed in the years, including strategies capable of combining geometric and materials non-linearities, for instance Verhoosel et al. [62] and Bellora and Vescovini [63]. A useful review is available in [64]. The strategy adopted here is purely geometrical, and is based on the version of the method proposed by Crisfield [65]. An overview of the procedure is presented in Figure 4.3.

In the arc-length method the load factor λ becomes part of the unknowns to be determined. The variables $\boldsymbol{x}$ and λ can be parametrized as a function of a

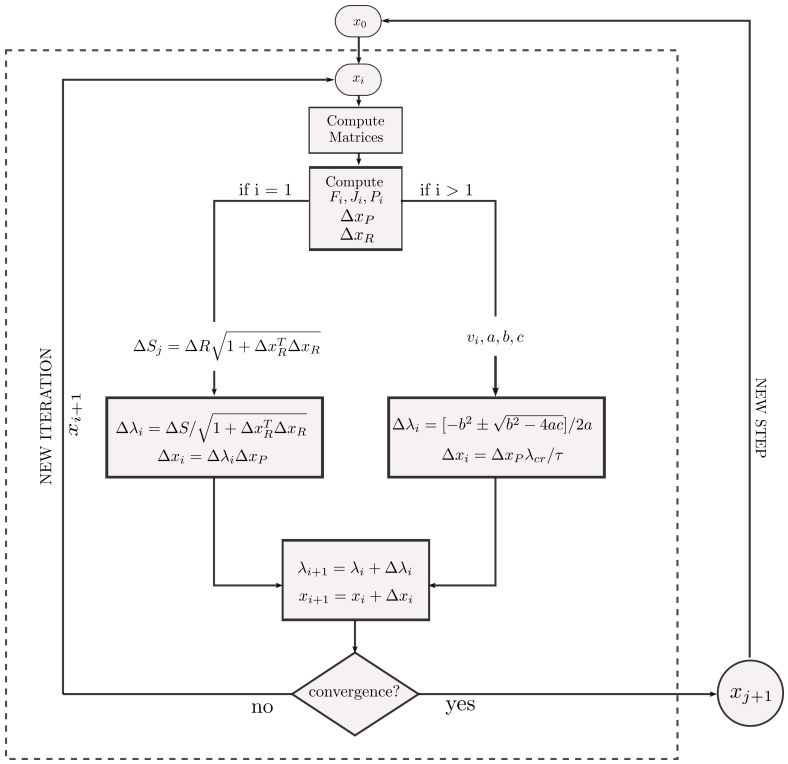

Figure 4.3: Work-flow of the arc-length method.

curvilinear coordinate s along the general force-displacement response curve:

$$\boldsymbol{x} = \boldsymbol{x}(s); \qquad \lambda = \lambda(s) \tag{4.114}$$

The non-linear equilibrium system of Eq. 4.100 is thus expressed as a function of s, and can be derived as

$$\frac{\partial \boldsymbol{R}(s)}{\partial s} = -\boldsymbol{J}\frac{\partial \boldsymbol{x}}{\partial s} + \frac{\partial \lambda}{\partial s}\frac{\partial \boldsymbol{R}}{\partial \lambda} \tag{4.115}$$

where $\boldsymbol{J}$ is the Jacobian matrix defined in Eq. 4.108. The derivatives in Eq. 4.115 are written in a discrete form as

$$\frac{\partial \boldsymbol{x}}{\partial s} \approx \frac{\Delta \boldsymbol{x}}{\Delta S}; \qquad \frac{\partial \lambda}{\partial s} \approx \frac{\Delta \lambda}{\Delta S} \tag{4.116}$$

where ΔS is a finite increment of the arc-length. Considering that $\partial \boldsymbol{R}(s)/\partial \lambda = P$, Eq. 4.115 becomes:

$$\boldsymbol{J}\Delta \boldsymbol{x} + \Delta\lambda \boldsymbol{P} = 0 \tag{4.117}$$

Moreover, the constrain of 4.104 is derived as

$$\Delta \boldsymbol{x}^T \Delta \boldsymbol{x} + (\Delta\lambda)^2 = (\Delta S)^2 \tag{4.118}$$

Equations 4.117 and 4.118 are the $n+1$ relations required to solve the non-linear problem.

The arc-length method is implemented, similarly to the case of the Newton-Raphson iterations, such that the solution is obtained for j equilibirum steps and, at every step, i iterations are performed until convergence is achieved.
At the end of every step j, the solution is evaluated as

$$\begin{aligned} \lambda_{j+1} &= \lambda_j + \Delta\lambda_j \\ \boldsymbol{x}_{j+1} &= \boldsymbol{x}_j + \Delta\boldsymbol{x}_j \end{aligned} \tag{4.119}$$

with

$$\Delta \boldsymbol{x}_j = \Delta\lambda_j \boldsymbol{J}^{-1}\boldsymbol{P} = \Delta\lambda_j \Delta\boldsymbol{x}_P \tag{4.120}$$

$$\Delta\lambda_j = \frac{\pm\Delta S}{\sqrt{\Delta\boldsymbol{x}_P^T \Delta\boldsymbol{x}_P + 1}} \tag{4.121}$$

where $\Delta\boldsymbol{x}_P = \boldsymbol{J}^{-1}\boldsymbol{P}$. The root in Eq. 4.121 is selected with a criterion based on the least positive cosine value for the angle between the solution of the current iterartion and the last converged value:

$$\cos\theta^{\pm} = \frac{\boldsymbol{x}_p^{i-1,T}\boldsymbol{x}_{p,\pm}^{i}}{\|\boldsymbol{x}_p^{i-1,T}\boldsymbol{x}_{p,\pm}^{i}\|} \tag{4.122}$$

where the vector $\boldsymbol{x}_p^{i-1}$ is computed as:

$$\boldsymbol{x}_p^{i-1} = x_{i-1} - x_{j-1} \tag{4.123}$$

and the vectors $\boldsymbol{x}_{p,\pm}^{i}$ are evaluated using both the roots of Eq. 4.121 as:

$$\boldsymbol{x}_{p,\pm}^{i} = x_{i,\pm} - x_{j-1} \tag{4.124}$$

The solution is selected as the one corresponding to the minimum value of Eq. 4.122. In the Crisfield version of the arc-length method, at every j-th step, the i-th

iteration is evaluated as

$$\boldsymbol{x}^i_{j+1} = \boldsymbol{x}^i - \boldsymbol{x}_j + \Delta\boldsymbol{x}^i \tag{4.125}$$

where the term $\Delta\boldsymbol{x}^i$ is split in two contributions

$$\Delta\boldsymbol{x}^i = -\boldsymbol{J}^{i,-1}\boldsymbol{R}^i + \Delta\lambda\boldsymbol{J}^{i,-1}\boldsymbol{P} = \Delta\boldsymbol{x_R}^i + \Delta\lambda\Delta\boldsymbol{x_P}^i \tag{4.126}$$

and Eq. 4.118 is rewritten as [64]

$$a(\Delta\lambda^i)^2 + 2b\Delta\lambda^i + c = 0 \tag{4.127}$$

with

$$a = \Delta\boldsymbol{x_P}^{i,T}\Delta\boldsymbol{x_P}^i \tag{4.128}$$

$$b = \Delta\boldsymbol{x_P}^{i,T}\boldsymbol{v}^i \tag{4.129}$$

$$c = \boldsymbol{v}^{i,T}\boldsymbol{v}^i - \Delta S^2 \tag{4.130}$$

$$v^i = \Delta\boldsymbol{x}^i_R + \boldsymbol{x}^i_j \tag{4.131}$$

The roots of Eq. 4.127 are calculated at every step, and the smallest positive value is kept according to the cosine criterion.
The i-th solution is assumed to be converged when the following convergence criteria is met

$$\frac{\Delta\boldsymbol{x}^i}{\boldsymbol{x}^i} < tol \quad \text{and} \quad \frac{\Delta\lambda^i}{\lambda^i} < tol \tag{4.132}$$

where tol is a tolerance selected in advance. It has been found that a value of $tol = 10^{-5}$ is generally an adequate choice in terms of balance between number of iterations and accuracy of the solution.

4.8 Implementation

The buckling and post-buckling formulations have been implemented in a Matlab language program [66].
The code allows to select between three solution procedures –pre-, buckling, and post-buckling–, and different panel types: flat plates and cylindrical shells. Furthermore, it is possible to simulate both the displacement-control and force-control loading cases. The variation of fibers angles can be either linear or non-linear. In

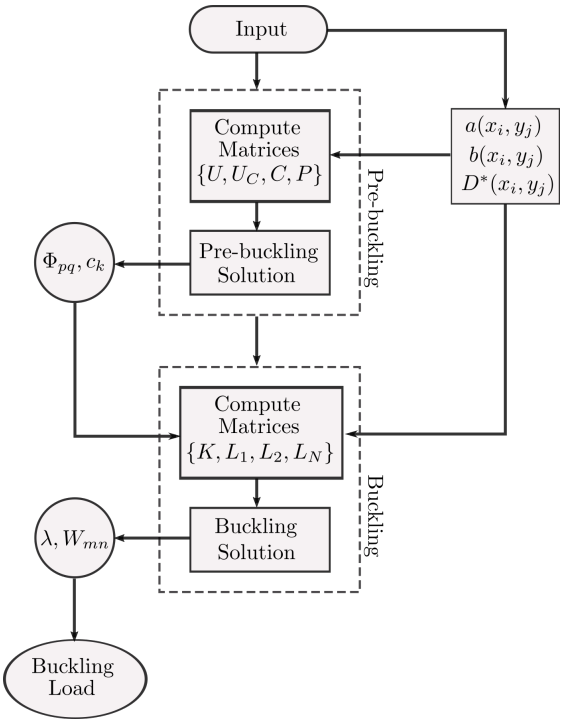

Figure 4.4: Work-flow of the algorithm used for the linear analysis.

the second case, the non-linear reference path is prescribed by means of Lagrangian polynomials.
A numerical scheme based on the Gauss-quadrature method has been employed to perform the integration of the matrices.
The following data are required as input:

- Material Properties (in terms of engineering constants)
- Plate/Shell Geometry
- Lamination Sequence
- Load Magnitude
- Essential boundary conditions (Free/Supported/Clamped edges)
- Number of terms for the series expansion (P, M, K)
- Number of Gaussian grid points for the numerical integration

The pre-buckling procedure provides the in-plane stresses, as outlined in Section 4.4. It can be selected to perform a linear analysis –in this case pre-buckling is

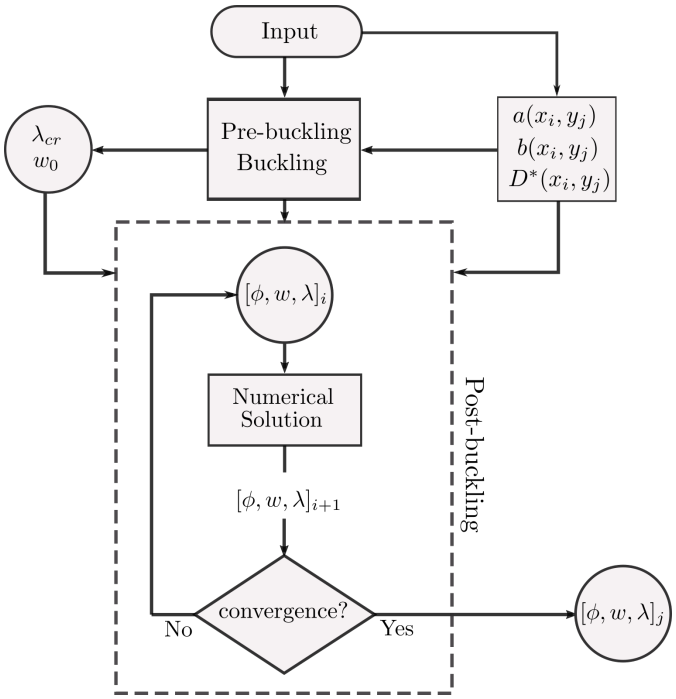

Figure 4.5: Work-flow of the algorithm used for the non-linear analysis.

a rather improper name, as the analysis is not followed by a successive buckling analysis. A second possibility consists in selecting a buckling analysis, which is indeed a two-step procedure, as illustrated in the sketch in Figure 4.4. At first, a pre-buckling analysis is performed, then the buckling eigenvalue problem is solved. The smallest among the calculated eigenvalues defines the buckling conditions and the corresponding eigenvector provides the buckling shape.
The outputs of the program can be chosen among the following options: normalized buckling coefficients, in-plane stress distribution, buckling shape, force distribution along the loaded edges.

The algorithm for the post-buckling analysis is organized as illustrated in Figure 4.5. In particular, it performs the following steps: the pre-buckling and buckling problems are solved to obtain the critical buckling load. The algorithm then starts the post-buckling loop. Depending on the selected solution method (Newton-Raphson or arc-length), the step size can be selected: in the case of the Newton-Raphson method, the imposed loading condition is constantly increased until a pre-defined load value is reached; in the case of the arc-length method, the algorithm automatically defines the load levels at which the solution is computed, and it stops when a pre-specified number of steps is reached. The matrices required for the

post-buckling analysis are computed at every i-th iteration of the solution process. Then, at every converged step, the solution is computed in terms of in-plane stress distribution and out-of-plane displacement.
The results are then post-processed to obtain the average axial load (or the average edge displacement in the force-control case) and the maximum out-of-plane displacement at every step.
The following results can be requested: in-plane stress distribution, out-of-plane displacement field, load-displacement curve, maximum out-of-plane displacement at every step.

4.9 Results

In this Section the linear and non-linear behaviour of variable-stiffness panels is investigated. The accuracy of the Ritz solutions are checked against results from literature and finite element computations. To this aim, the commercial finite element code Abaqus [67] is used. The comparison is presented in terms of pre-buckling stress distribution, buckling eigenvalue predictions and post-buckling response.

Finite Element Model

The finite element models are realised using S4R shell elements with a mesh-density of 50×50 elements, chosen on the basis of a preliminary convergence analysis. For this reason, all the results reported in this thesis are obtained with this mesh density.
To model the fiber variation along the panel domain, each element is equipped with a given orientation, established on the basis of the orientation angle at the position corresponding to the centroid of the element itself. This means that the angle variation is not continuous, but is changed in a step-wise manner from element to element. For properly refined meshes, this assumption is not too restrictive, and the orientation field is described with a satisfactory degree of accuracy.

Materials Two different materials are considered in the examples reported next: an orthotropic one, namely *Material A* –whose properties are reported in Table 4.2– and an isotropic one. The latter is an aluminium alloy whose elastic

Material	E_1 [GPa]	E_2 [GPa]	G_{12} [GPa]	ν_{12}	h_{ply} [mm]
Material A[17]	181	10.273	7.1705	0.28	0.1272

Table 4.2: Properties of the materials employed in the analyses. h_{ply} is the thickness of a single ply.

properties are:

$$E = 70\,\text{GPa} \qquad \nu = 0.3 \tag{4.133}$$

In the case of isotropic plates, the thickness is 0.8 mm.

Convergence Analysis A preliminary study is conducted to establish the number of terms to be used in the series of ϕ and w, and to assess their effect on the accuracy of the solution.
The convergence analysis is conducted by considering the case analysed by Raju et al. [18]. The plate is square, with dimensions ($a = b = 1000\,\text{mm}$) and is simply-supported along the four edges. The load is applied in the form of an edge compression $\Delta = 0.5\,mm$. The plate is made of 12 plies, stacked with the lamination sequence $[90 \pm \langle 0, 75 \rangle]_{3S}$. The results are compared in terms of non-dimensional buckling coefficient, defined as

$$K_{cr} = \frac{N_x^{cr} a^2}{E_1 h^3} \tag{4.134}$$

where N_x^{cr} is the critical buckling load, as defined in Eq. 4.74.
The analysis is performed by varying the number of functions P and M. More specifically, P is the number of terms used in the series expansion of ϕ_1 (as defined in Eq. 4.10). For simplicity, the same number of terms is assumed in the x and y directions, which is Q=P. Moreover, the same number of terms is used to approximate ϕ_0, and K=P (see Eq. 4.30). For instance, if P=5, it means that P=Q=K=5. Thus, the number of terms used for ϕ_0 is K=5 while it is P×Q=25 for ϕ_1.
Likewise, M is the number of terms used to approximate w, as shown in Eq. 4.25. As above, the expansion is taken by assuming N=M and the total number of terms used to approximate w is M×N. The dimension of the pre-buckling problem is equal to P×P+P, while for the buckling problem it is M×M.

As seen in Table 4.3, the Ritz results are in close matching with those reported by

$^P/_M$	0	2	4	6	8	12
0	2.5944	2.0032	1.8553	1.8229	1.8205	
2	3.5006	3.2269	3.0218	2.9922	2.9861	
4	3.3641	3.1189	3.1090	3.0742	3.0668	
6	3.3672	3.1215	3.1117	3.0769	3.0692	
8	3.3685	3.1229	3.1131	3.0785	3.0708	
12						3.0703
Abaqus			3.0747			
DQM [18]			3.067			
FEM [18]			3.077			

Table 4.3: Convergence analysis for the buckling coefficient K_{cr} of a square simply-supported plate with lamination sequence $[90 \pm \langle 0, 75 \rangle]_{3S}$. P, Q: number of functions of ϕ_1 and w, respectively.

Raju et al. [18]: using 12 terms for all the series, the normalized buckling coefficient is $K_{cr} = 3.0703$. The non-dimensional buckling coefficient differs by 0.10% from the one obtained in Ref. [18] with the DQM, revealing good agreement between the two approaches. In addition, the Ritz results are close to the finite element ones, with a difference of about 0.21% from the reference results of Ref. [18] and of 0.14% from the result obtained with the present finite element model. It can be noted that the Ritz model is slightly stiffer with respect to the finite element one. As seen from Table 4.3, convergence is obtained when a large value of M is chosen, while the requirements for P are less strict, and a smaller number of terms suffices for guaranteeing a satisfactory level of accuracy. Note that 7-8 terms are sufficient to obtain a result similar to the one obtained with a larger number of terms.

The results of the convergence analysis are plotted in Figure 4.6, where the influence of the number of M and P terms on K_{cr} is shown: the convergence rate is from above or from the bottom, depending on the number of term which are increased: increasing the number of terms of the Airy stress function, the compatibility requirement is satisfied better and better, resulting in a stiffer system (convergence from the bottom); increasing the number of terms of the out-of-plane displacement approximation the system becomes more and more flexible, and the buckling load decreases (convergence from above).

The results of the buckling analysis are reported in Figure 4.7, where the comparison is illustrated between Ritz and FEM results. Note that, for guaranteeing a clearer comparison between the two techniques, Abaqus results are illustrated

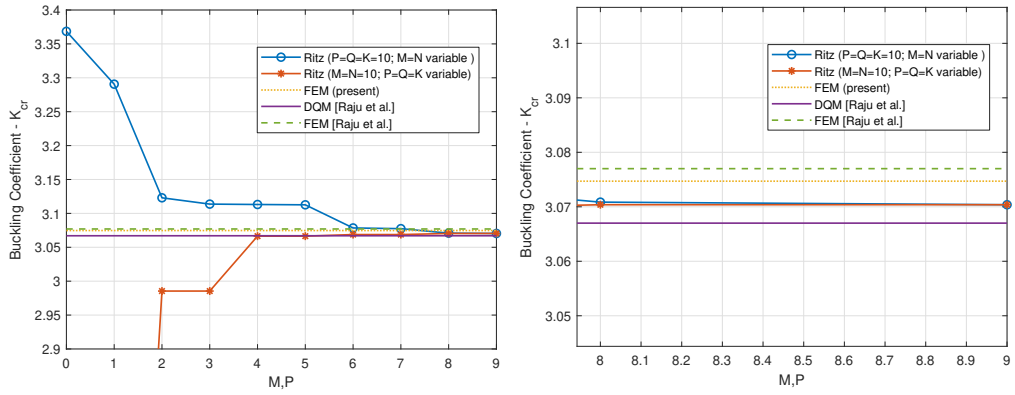

(a) (b)

Figure 4.6: Convergence analysis for square, simply-supported plate with lay-up $[0 \pm \langle 45, 0\rangle]_{3S}$: 4.6a convergence rate, 4.6b: zoom.

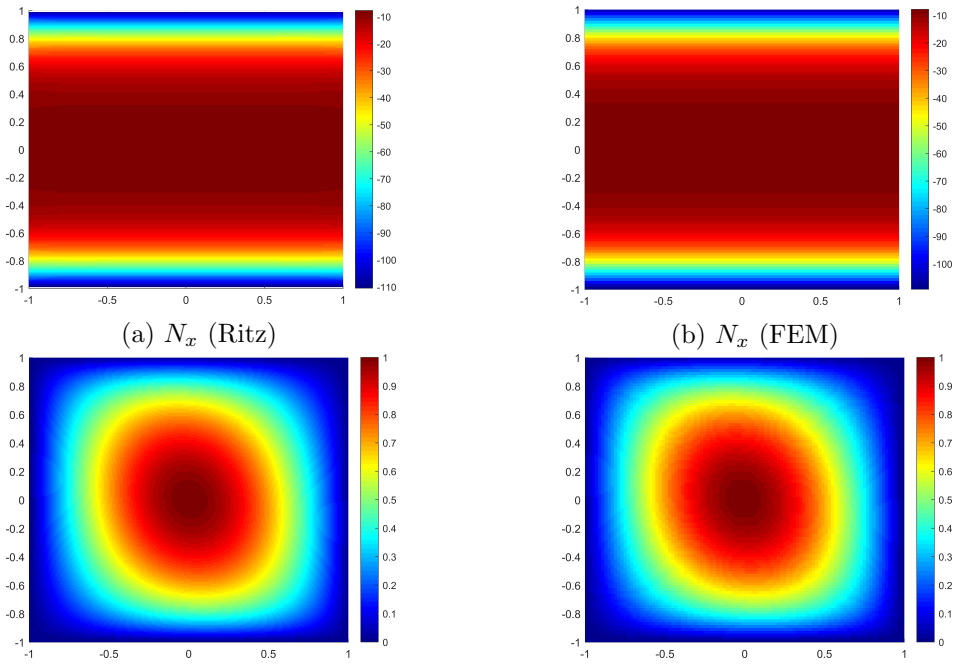

(a) N_x (Ritz) (b) N_x (FEM)

(c) Buckling Shape (Ritz) (d) Buckling Shape (FEM)

Figure 4.7: Simply-supported square plate $[0 \pm \langle 45, 0\rangle]_{3S}$. (a),(b): Stress resultant [N/mm], imposed displacement Δ=0.5 mm. (c),(d): buckling shape. Abaqus results are post-processed with Matlab.

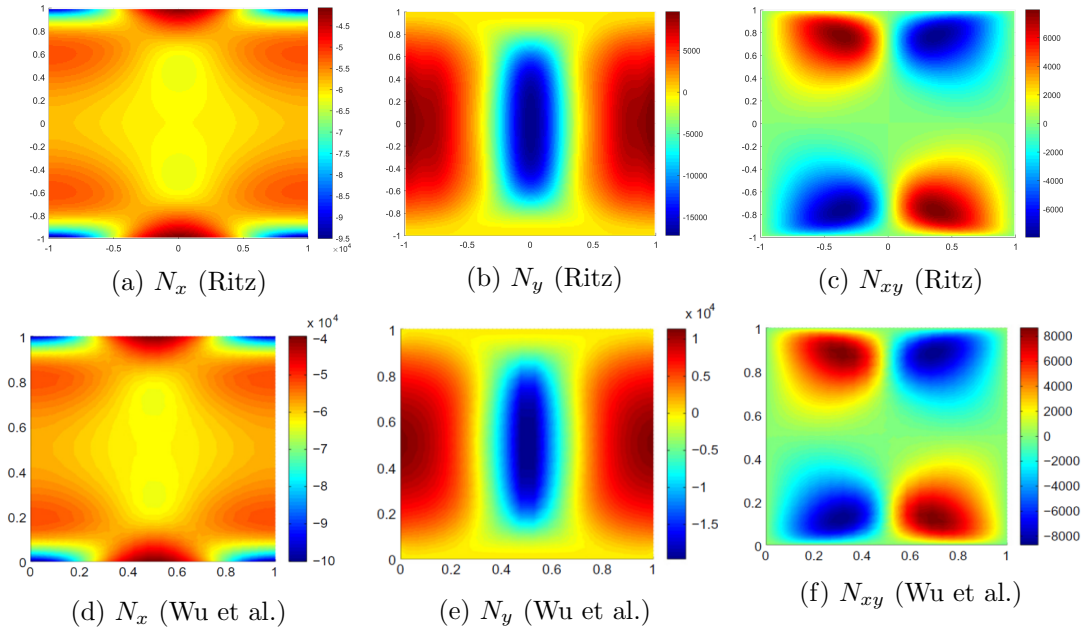

(a) N_x (Ritz) (b) N_y (Ritz) (c) N_{xy} (Ritz)

(d) N_x (Wu et al.) (e) N_y (Wu et al.) (f) N_{xy} (Wu et al.)

Figure 4.8: In-plane stress distribution of a variable stiffness panel (SSSS) with lamination sequence $[0 \pm \langle 45, 0 \rangle]_{3S}$.

by performing the post-processing operations in Matlab. The contours are thus reported in the same Matlab environment. The plot of Figure 4.7a and 4.7b are relative to the pre-buckling internal forces distributions, whilst the buckled shapes are depicted in Figure 4.7c and 4.7d.

Example 1: In-plane stress distribution of a variable-stiffness panel
The in-plane stress distribution of a square plate ($a = b = 1000\,\text{mm}$) with lamination sequence $[0 \pm \langle 45, 0 \rangle]_{3S}$ is compared with results obtained by Raju et al. [18]. The panel is compressed by means of a $\Delta = 500\,\text{mm}$ [sic] uniform edge displacement. For the approximation of the Airy stress function $P, Q, K = 8$ terms have been used.

The stress distribution obtained with the Ritz method is compared against the results obtained in Ref. [18] using the DQM in Figure 4.8. As seen, the stress distribution are in close agreement.

In Figure 4.9 the in-plane stress distribution is also compared with the results obtained with Abaqus. Furthermore, a comparison is reported in Figure 4.10 in terms of stress resultant at the plate's border, that is $x = \pm a/2$. It can be noticed that the distribution is not uniform: this was expected, since the distribution of

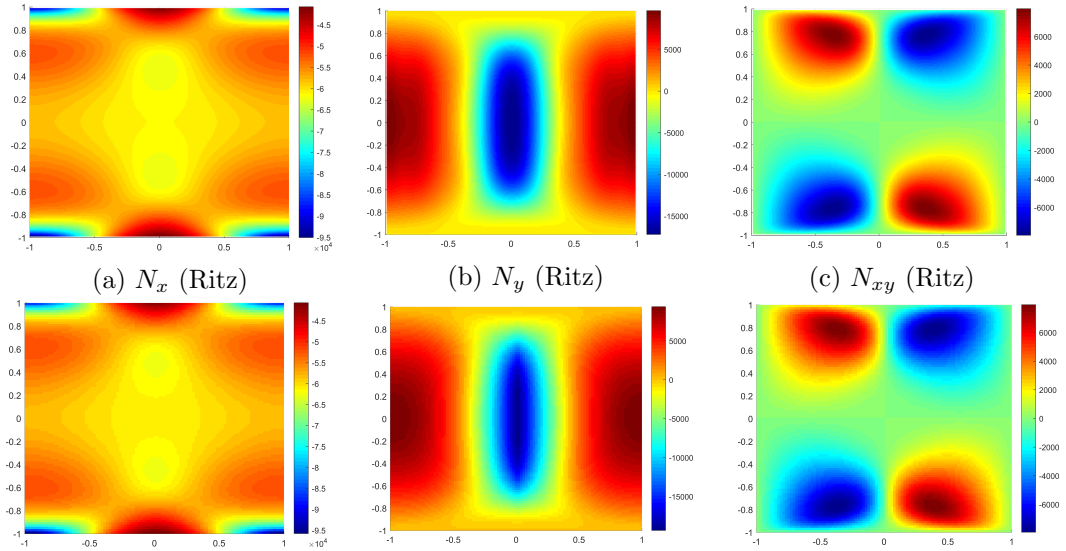

(a) N_x (Ritz) (b) N_y (Ritz) (c) N_{xy} (Ritz)

(d) N_x (FEM) (e) N_y (FEM) (f) N_{xy} (FEM)

Figure 4.9: In-plane stress distribution of a variable stiffness panel (SSSS) with lamination sequence $[0 \pm \langle 45, 0 \rangle]_{3S}$.

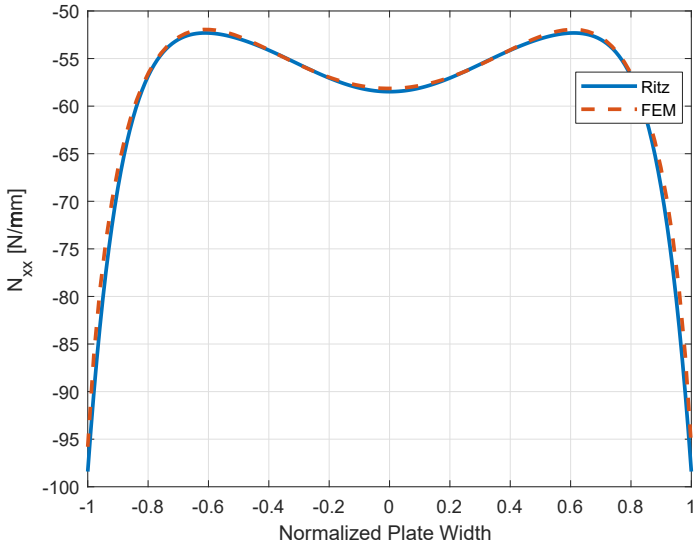

Figure 4.10: Non-uniform stress resultant of a simply-supported plate with lamination sequence $[90 \pm \langle 0, 75 \rangle]_{3S}$, evaluated at $x = \pm a/2$.

N_x is not uniform as well.
The non uniform stress distribution is one of the effects of the non-constant orientation of fibers. This property can be exploited to achieve pre-buckling stress as well as bending stiffness distributions that can improve the buckling response. With a similar philosophy - although examples are not reported in the present investigation -, the tailoring opportunities can be exploited to design the load paths in proximity of cut-outs or geometric discontinuities.

Example 2: Effect of fibers orientation on the buckling load The effect of different fiber angle distributions on the buckling response of the panel are now investigated.

To this aim, a simply-supported square plate ($a = b = 1000\,\text{mm}$) with 8 symmetric plies is considered. The variation of fibers orientation is linear. Buckling loads are computed for different combinations of the parameters T_0 and T_1. Results are compared against those of a square panel with lamination sequence $[\pm 45]_{2S}$ with same dimensions and boundary conditions. For this classical laminate, the buckling load is $N^{cr}_{x,\text{straight}} = 1.097\,N/\text{mm}$.
The plates considered are characterized by a $[\pm(90\,\langle T_0, T_1\rangle)]_{3S}$ lamination sequence. For simplicity, the values of T_1 are taken with a step of 10 degrees, as:

$$T_1 \in \{0, 10, 20, 30, 40, 50, 60, 70, 80, 90\}$$

while only four T_0 are tried:

$$T_0 \in \{0, 20, 40, 60\}$$

It has been found that the maximum buckling load is obtained for $(T_0, T_1) = (0, 80)$, which correspond to a buckling load of $N^{cr}_x = 1.89\,N/\text{mm}$. It is worth remarking that technological restrictions are not accounted for in the present investigation. With this regard, the extreme steering of the optimal configuration would be probably hard to achieve.
This value is almost 70% higher than the one associated with the optimal straight fiber one. The advantages offered by the tailoring opportunities given by the steering of the fibers are thus clear.

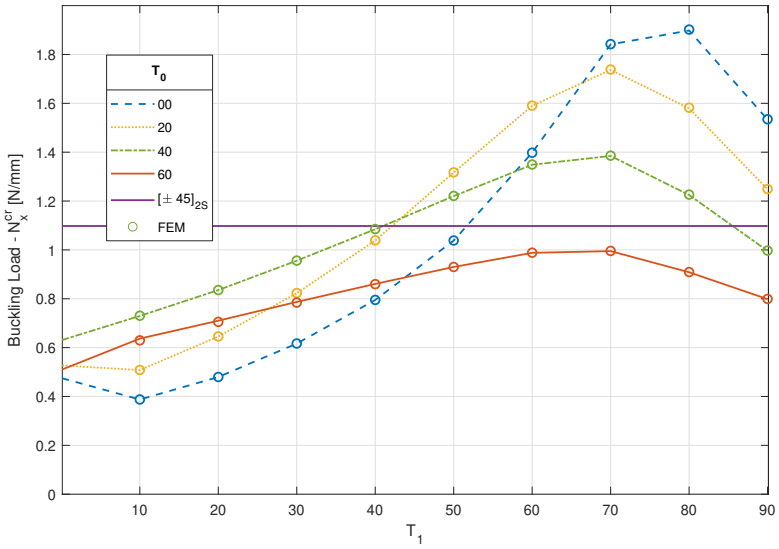

Figure 4.11: Buckling coefficient plotted for a simply-supported VS plate with lamination sequence $[\pm(90\,\langle T_0, T_1\rangle)]_{3S}$ for different combinations of T_0 and T_1.

The carpet plot relative to the combinations previously assessed is illustrated in Figure 4.11. As it can be noticed, the effects of T_0 and T_1 are extremely significant. Moreover, it is possible to appreciate the agreement of the results with Abaqus.

Example 3: Buckling analysis of a variable-stiffness panel: force-control case A simply-supported square plate is considered subjected to a prescribed uniform compression force per unit length. Dimensions are $a = b = 1000\,\text{mm}$ and the elastic properties of the plies composing the stack are the ones of *Material A*. Two different lamination sequence with 8 plies have been considered, namely:

- Layup 1: $[0]_8$
- Layup 2: $[0 \pm \langle 45, 0\rangle]_{2S}$

The results have been compared in terms of buckling load $[N/\text{mm}]$, which is computed as

$$N_x^{cr} = \lambda \overline{N}_x \tag{4.135}$$

where $\overline{N}_x$ is the pre-buckling average compression load. In the current analysis, $\overline{N}_x$=1.

The buckling loads are reported in Table 4.4 for the case Layup 1. Results obtained with the Ritz method are shown for different values of M, and are compared against

$^P/_M$	0	2	4	6	8
0	0.2327	0.1964	0.1963	0.1963	0.1963
2	0.2327	0.1964	0.1963	0.1963	0.1963
4	0.2327	0.1964	0.1963	0.1963	0.1963
6	0.2327	0.1964	0.1963	0.1963	0.1963
8	0.2327	0.1964	0.1963	0.1963	0.1963
FEM	0.1965 [N/mm]				

Table 4.4: Convergence analysis for the buckling load N_x^{cr} of a simply-supported plate, with lamination sequence $[0]_4$ (force-control)

those available from Abaqus analyses. It can be noticed that the convergence of the solution does not depends on the number of terms approximating the Airy stress function. This is related to the in-plane stress distribution, which is uniform in the case of a straight fibers laminate subjected to force-control loading. Moreover, the magnitude of N_x is directly the magnitude of the imposed load $\overline{N}_x$.
In the force-control case the separate form of the Airy stress function reads:

$$\phi(\xi,\eta) = \phi_0(\xi) + \phi_1(\xi,\eta) = \frac{b^2}{4}\frac{\overline{N}_x\eta}{2} + \sum_{p=0}^{P}\sum_{q=0}^{Q} X_p(\xi)Y_q(\eta)\Phi_{pq} \tag{4.136}$$

By looking at Eq. 4.136, it is plain to see that only the first part (which is ϕ_0) contributes to the stress distribution. Therefore, the coefficients Φ_{pq} are expected to be zero, thus not affecting the solution of the buckling problem.

A different behaviour is experienced by variable stiffness panels, irrespectively on the modality for the load introductions. This behaviour can be explained with the following qualitative description: the variable stiffness panel can be seen as the assembly of parallel infinitesimal strips, each characterized by a different axial stiffness due to the variability of the orientation angle. When a load is introduced, each strip should, if operating as a self-standing element, undergo different axial shortening. This clearly violates the compatibility which is restored through a non-uniform stress distribution.
For this reason, the convergence of the buckling load is related also to the number of terms used in the expansion of ϕ_1, as it can be appreciated in Table 4.5, where the critical load is reported with computed for different values of P and M.

The stress distribution in the x-direction is reported for the two layups in Figure

$^P/_M$	0	2	4	6	8
0	0.2534	0.2074	0.2043	0.2040	0.2038
2	0.2513	0.2050	0.2018	0.2014	0.2012
4	0.2508	0.2044	0.2012	0.2007	0.2005
6	0.2506	0.2043	0.2010	0.2006	0.2003
8	0.2506	0.2042	0.2010	0.2005	0.2003
FEM			0.1999 [N/mm]		

Table 4.5: Buckling load N_x^{cr} [N/mm] of a simply-supported variable-stiffness plate, with lamination sequence $[0 \pm \langle 45, 0 \rangle]_{2S}$ (force-control case)

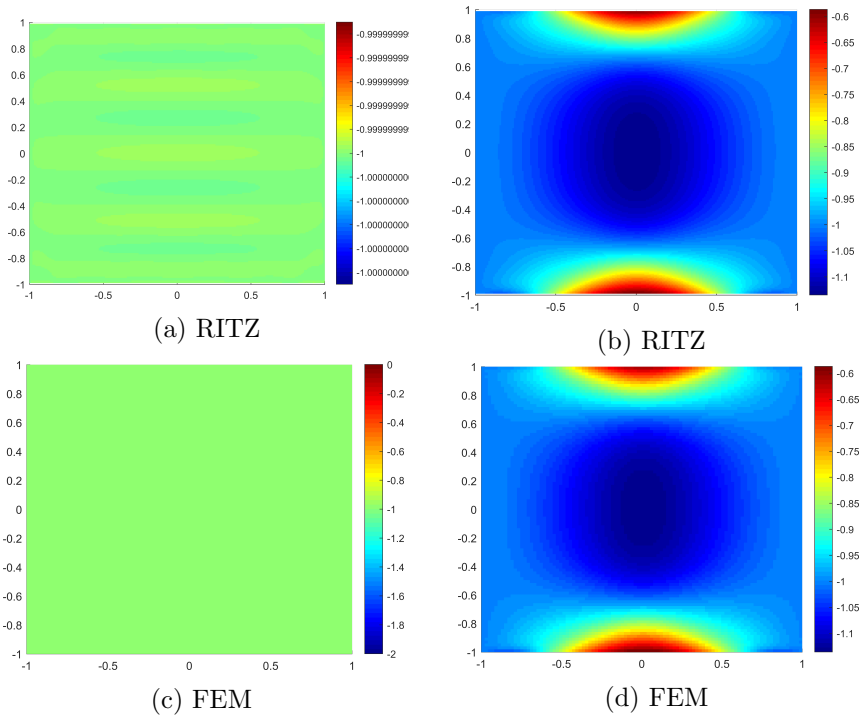

(a) RITZ (b) RITZ

(c) FEM (d) FEM

Figure 4.12: Stress distribution in the x-direction of a SSSS plate. (a,c): straight fibers (Layup 1) and (b,d) linear variation of fibers angles (Layup 2). Abaqus results are post-processed with Matlab.

P/M	0	2	4	6	8
0	2.4653	2.1734	2.1194	2.1049	2.0998
2	2.5132	2.2102	2.1518	2.1361	2.1306
4	2.4740	2.1785	2.1212	2.1057	2.1003
6	2.4715	2.1754	2.1177	2.1019	2.0963
8	2.4703	2.1741	2.1163	2.1003	2.0947
FEM	2.0883 [N/mm]				

Table 4.6: Convergence analysis for the buckling coefficient K_{cr} of a CCCC variable-stiffness panel with lamination sequence $[0 \pm \langle 45, 0 \rangle]_{3S}$.

P/M	0	2	4	6	8
0	1.1841	1.0757	1.0656	1.0649	1.0646
2	1.2265	1.1086	1.0972	1.0961	1.0957
4	1.2021	1.0877	1.0767	1.0756	1.0751
6	1.2021	1.0874	1.0765	1.0753	1.0748
8	1.2018	1.0871	1.0761	1.0749	1.0744
FEM	1.0736 [N/mm]				

Table 4.7: Convergence analysis for the buckling coefficient K_{cr} of a SCSC variable-stiffness panel with lamination sequence $[0 \pm \langle 45, 0 \rangle]_{3S}$.

4.12: it can be appreciated that for the straight fibers laminate the distribution is uniform, while it is non-uniform for Layup 2.

Example 4: Buckling analysis of variable-stiffness plates with different boundary conditions Up to now only panels with simply-supported boundary conditions have been considered. This example is introduced to demonstrate the ability of the present implementation of handling any kind of boundary condition. Clamped conditions are considered due to their relevance in typical aerospace structures: clamped edges are commonly assumed for modelling the effect of closed-section stringers on the edges of the skin.
The same plate of the Example 1 is considered: the analysis is performed for fully clamped conditions (CCCC) and mixed boundary conditions (SCSC).

The buckling load is reported for the case of fully clamped plate in Table 4.6: the results are in good agreement with the finite element ones, and they differ by 0.30%. In Table 4.7 the results, again in terms of buckling load, are reported for the SCSC case. The results obtained with Ritz differ from the result obtained with

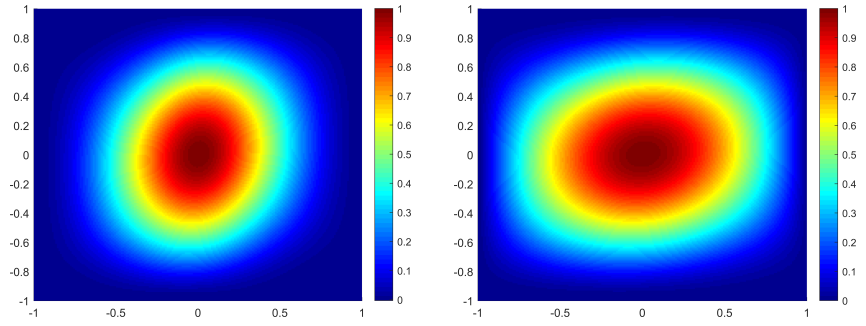

(a) CCCC (Ritz)

(b) SCSC (Ritz)

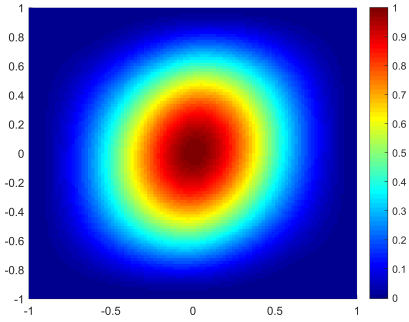

(c) CCCC (FEM)

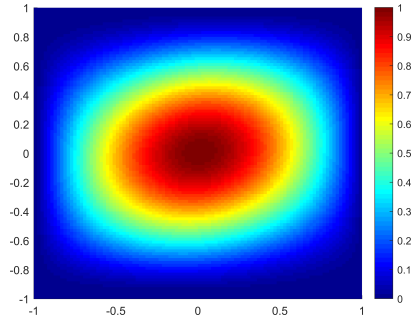

(d) SCSC (FEM)

Figure 4.13: Buckling shape of a variable stiffness plate ($[0 \pm \langle 45, 0 \rangle]_{3S}$) with various boundary conditions. Abaqus results are post-processed with Matlab.

Abaqus by 0.07%.
The buckling shape for the two set of boundary conditions are reported in Figure 4.13: the results obtained with Ritz are displayed in Figures 4.13a and 4.13b, while in 4.13c and 4.13d are displayed the ones obtained with Abaqus.

Example 5: Buckling analysis of a plate with non-linear fibers distribution The capabilities of the present tool to analyse plates with arbitrary fiber orientations is now investigated. In particular, the range of fiber angle distributions is now extended to the non-linear case.

Lagrangian polynomials are implemented to prescribe the fibers orientation angles. As shown in Eq. 2.53, the fiber path is expressed by means of the coefficients T_{mn}, that are the fibers angles at prescribed points in the panel domain.
Therefore, to define the non-linear path is necessary to build a grid of points where the angles are prescribed and then, by means of the Lagrangian polynomials, the path is interpolated. In the current analysis, 9 points are considered: four of them are located at the plate corners, four at the mid-points of the edges and one in the middle of the panel. A 3×3 matrix is used to represent the grid, as illustrated in

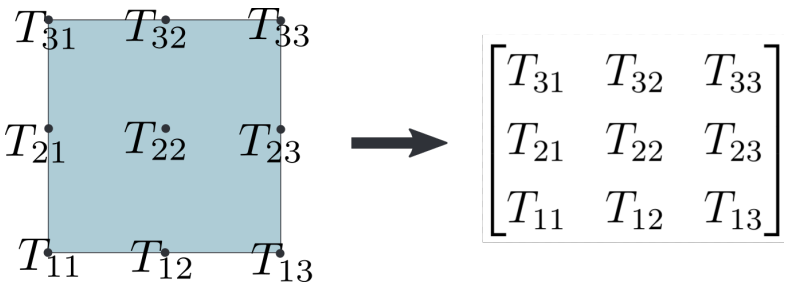

Figure 4.14: Grid points are used to specify the angle variation of fibers at certain position across the plate.

$^P/_M$	0	2	4	6	8
0	0.2766	0.2345	0.2337	0.2336	0.2336
2	0.2880	0.2438	0.2428	0.2427	0.2427
4	0.2858	0.2419	0.2409	0.2408	0.2408
6	0.2858	0.2419	0.2409	0.2408	0.2408
8	0.2858	0.2419	0.2409	0.2408	0.2408
FEM	0.240813 [N/mm]				

Table 4.8: Convergence analysis for the buckling coefficient K_{cr} of a simply-supported variable-stiffness panel with lamination sequence $[0 \pm \langle 45, 0\rangle]_{3S}$.

Figure 4.14. The orientation of each ply is thus specified by means of a matrix with nine entries:

$$T_\theta = \begin{bmatrix} T_{31} & T_{32} & T_{33} \\ T_{21} & T_{22} & T_{23} \\ T_{11} & T_{12} & T_{13} \end{bmatrix} \tag{4.137}$$

T_θ is specified for each layer.
As an example, a simply-supported square panel of dimensions $a = b = 1000\,\text{mm}$ is considered. The lamination sequence is defined as $[+T_\theta^1/-T_\theta^1]_{2S}$, where

$$T_\theta^1 = \begin{bmatrix} 0 & 45 & 0 \\ 0 & 45 & 0 \\ 0 & 45 & 0 \end{bmatrix} \tag{4.138}$$

The in-plane stress distribution is reported in Figure 4.15, where the results obtained with the Ritz method are compared against those available from Abaqus. In Figure 4.17 are reported the non-uniform stress resultants at $x = \pm a/2$ obtained with Ritz and Abaqus, and it can be noticed that the results are in good agreement. A convergence analysis has been performed in terms of buckling loads N_x^{cr}, and a

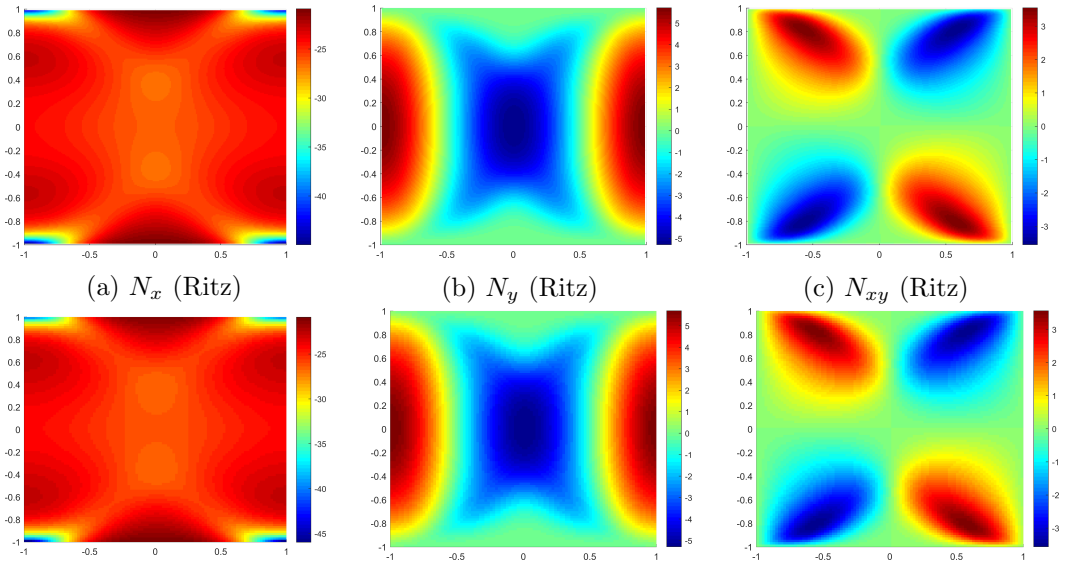

(a) N_x (Ritz) (b) N_y (Ritz) (c) N_{xy} (Ritz)

(d) N_x (FEM) (e) N_y (FEM) (f) N_{xy} (FEM)

Figure 4.15: In-plane stress distribution of an SSSS square plate with non-linear variation of fibers. Abaqus results are post-processed with Matlab.

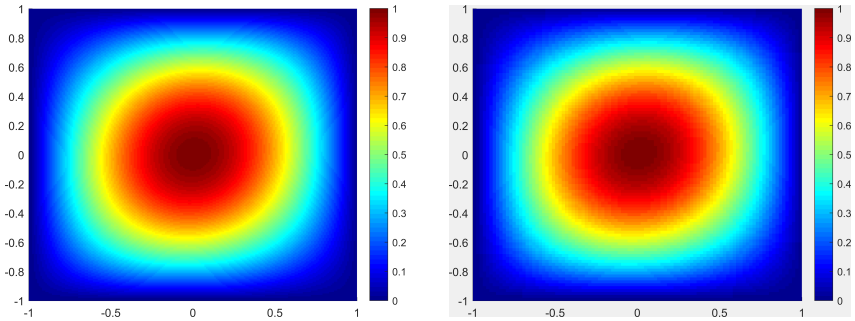

(a) (Ritz) (b) (FEM)

Figure 4.16: Buckling shape of an SSSS square plate with non-linear fibers distribution. .

good agreement has been found between the Ritz-type method and Abaqus. Results are reported in Table 4.8 for different numbers of terms in the series expansion.

The buckling shape obtained with Ritz and with Abaqus are reported in Figure 4.16.

Example 6: Buckling analysis of variable-stiffness shell panels In this example the buckling response of variable-stiffness shallow cylindrical shells is investigated.

Due to the assumption of linear membrane pre-buckling behaviour, the pre-buckling problem for shells is solved in the same way of plates: therefore, the pre-buckling procedure is formally identical, and the results are insensitive to the presence of a

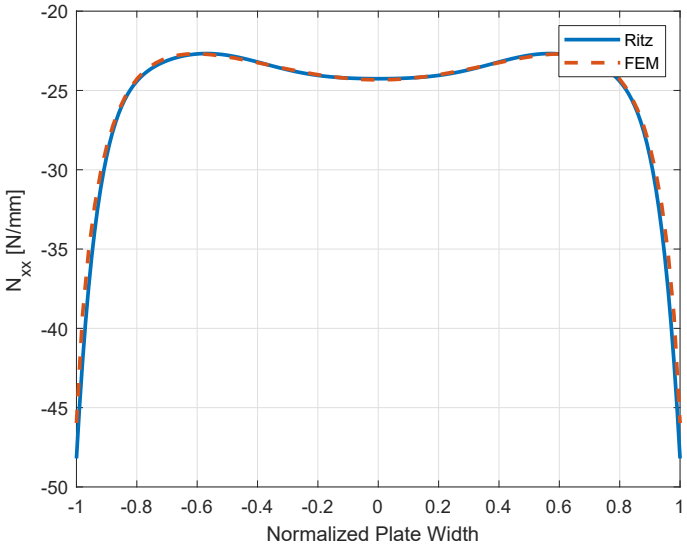

Figure 4.17: Non-uniform stress resultant of a simply-supported plate with non-linear distribution of fibers angles, evaluated at $x = \pm a/2$.

P/M	0	2	4	6	8	10
0	39.5072	33.5679	33.2224	32.8439	31.1068	30.1175
2	46.1588	41.7739	41.4752	39.8193	37.7841	36.7279
4	46.3208	42.2785	41.5052	41.0722	40.1442	39.4577
6	46.3112	42.3933	41.4027	40.8015	40.5572	40.4139
8	46.2782	42.3983	41.3294	40.6692	40.3923	40.2859
10	46.2574	42.3898	41.2945	40.6142	40.3260	40.2141
FEM	40.3923 [N/mm]					

Table 4.9: Convergence analysis for the buckling load N_x^{cr} of a simply-supported variable-stiffness shell, with lamination sequence $[0 \pm \langle 75, 15 \rangle]_{2S}$: displacement-control case.

P/M	0	2	4	6	8	10
0	27.8836	24.9492	24.9448	24.9447	24.9447	24.9447
2	28.2217	25.2777	25.2740	25.2740	25.2740	25.2740
4	28.2959	25.3503	25.3462	25.3462	25.3462	25.3462
6	28.3132	25.3678	25.3637	25.3637	25.3637	25.3637
8	28.3163	25.3709	25.3667	25.3667	25.3667	25.3667
10	28.3167	25.3713	25.3671	25.3671	25.3671	25.3671
FEM	25.3769 [N/mm]					

Table 4.10: Convergence analysis for the buckling load N_x^{cr} of a simply-supported shell, with lamination sequence $[0]_4$: displacement-control case.

P/M	0	2	4	6	8	10
0	39.5050	33.5653	33.2197	32.8411	31.1068	30.1174
2	40.2316	34.6862	34.5697	34.4515	34.3320	34.2313
4	40.4713	35.0688	35.0024	34.9730	34.9539	34.9293
6	40.5321	35.1794	35.1230	35.1168	35.1286	35.1319
8	40.5413	35.2060	35.1522	35.1533	35.1755	35.1889
10	40.5398	35.2104	35.1575	35.1612	35.1873	35.2048
FEM	35.1060 [N/mm]					

Table 4.11: Convergence analysis for the buckling load N_x^{cr} of a simply-supported variable-stiffness shell, with lamination sequence $[0 \pm \langle 75, 15 \rangle]_{2S}$: force-control case.

P/M	0	2	4	6	8	10
0	27.8836	24.9492	24.9447	24.9447	24.9447	24.9447
2	28.0737	25.1116	25.1084	25.1084	25.1084	25.1084
4	28.0842	25.1239	25.1206	25.1206	25.1206	25.1206
6	28.0853	25.1253	25.1220	25.1220	25.1220	25.1220
8	28.0856	25.1257	25.1224	25.1224	25.1224	25.1224
10	28.0857	25.1258	25.1225	25.1225	25.1225	25.1225
FEM	24.7260 [N/mm]					

Table 4.12: Convergence analysis for the buckling load N_x^{cr} of a simply-supported shell, with lamination sequence $[0]_4$: force-control case.

not null curvature.

To verify the reliability of the results, the buckling loads of two laminates have been computed for various numbers of terms of the expansions of ϕ and w. The two laminates are:

- Layup 1: $[0]_8$
- Layup 3: $[0 \pm \langle 75, 15 \rangle]_{2S}$

The shell considered is simply-supported, with $a = b = 100\,\text{mm}$ and curvature $R = 500\,\text{mm}$. The lamina properties are the one of *Material A*. Both the Layups have been analysed in either the displacement-control case and the force-control case.

The buckling load is displayed in terms of P and M for Layup 1 and Layup 3 in the case of a displacement-control loading condition in Tables 4.9 and 4.10. The buckling loads for the case of a force-control loading condition are reported in Tables 4.11 and 4.12.
It can be noticed that the results are quite in agreement with the finite element analyses. However, the convergence is not as good as for plates, and some differences do exists.
This discrepancy might be related to the assumption made for the pre-buckling state: for shells the assumption that the pre-buckling deformation is membrane is reasonable but not corrected, as there is coupling between the in-plane and the out-of-plane deformation.
As it can be appreciated in Figure 4.18, this behaviour is taken into consideration in the finite element analysis, and the pre-buckling solution of shells includes the out-of-plane displacement. This leads to a discrepancy in the stress distribution results, as it can be seen in Figure 4.19, where the in-plane stress distribution is reported for the Layup 3 (displacement-control strategy).

The coupling between in-plane and transverse deformation is due to the term related to the curvature, which is the matrix C_R defined in Eq. 4.58. The effect of the curvature on the convergence is investigated in Figure 4.20, where simply-supported variable-stiffness shells are analysed for different values of the angle T_1 and three values of the curvature R (0.5, 1 and 5 m), while the shell dimension are kept constant ($a = b = 100\,\text{mm}$). It can be noticed that as the curvature increase (and

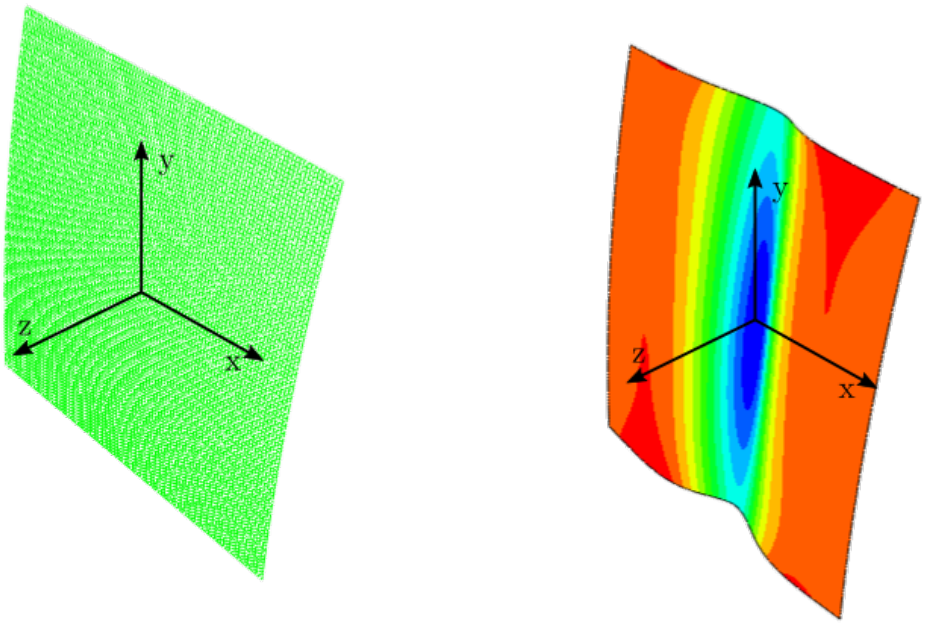

Figure 4.18: The in-plane and out-of-plane deformations of shells are coupled in the pre-buckling state: undeformed configuration (left) and deformed configuration (right) obtained with Abaqus. The transverse displacement is magnified by a factor of 100.

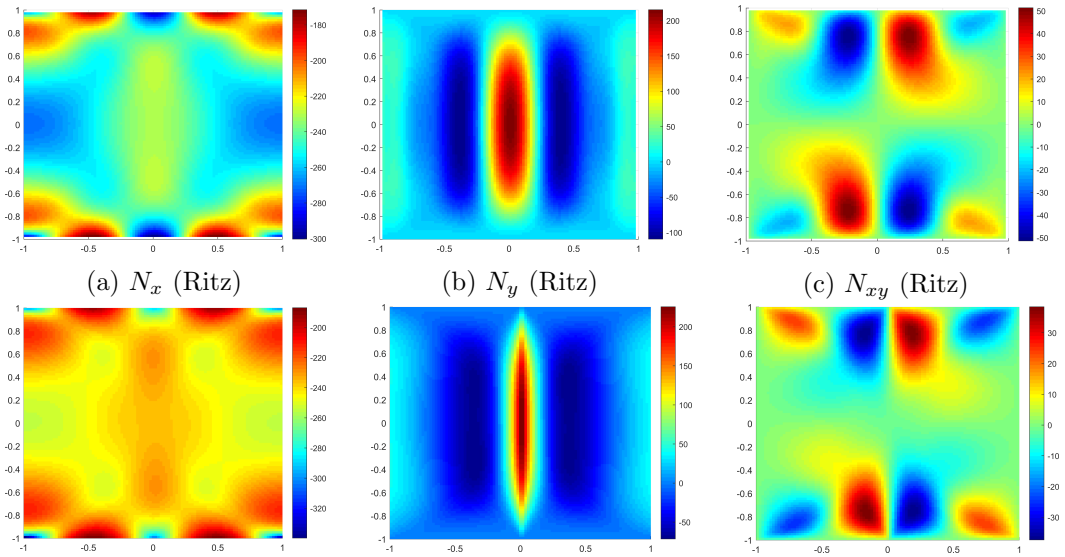

(a) N_x (Ritz) (b) N_y (Ritz) (c) N_{xy} (Ritz)

(d) N_x (FEM) (e) N_y (FEM) (f) N_{xy} (FEM)

Figure 4.19: In-plane stress distribution of an SSSS square shell panel with lamination sequence $[0 \pm \langle 75, 15 \rangle]_{2S}$. Abaqus results are post-processed with Matlab.

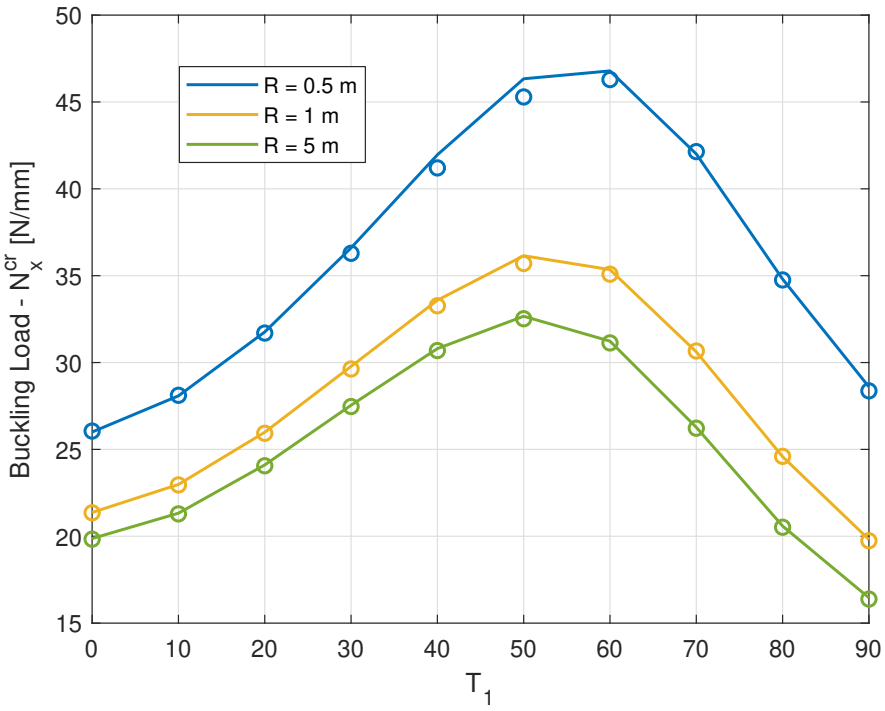

Figure 4.20: Buckling loads ([N/mm]) of a simply-supported shells for different curvature R with lamination sequence is $[\pm\langle 15, T_1\rangle]_{2S}$.

so the in-plane/out-of-plane coupling decrease), the discrepancy with the results obtained with Abaqus decrease.

This apparent inconsistency between the two models will be overcome in the post-buckling analysis, where the coupling between in-plane and out-of-plane deformation will be taken into account by solving a coupled non-linear system.

Example 7: Post-buckling analysis of a variable stiffness plate In this example, the post-buckling analysis capabilities of the Ritz approach are analysed. To this aim, a simply-supported variable-stiffness plate is considered. The dimensions are $a = b = 1000\,\text{mm}$, and the lamination sequence is $[0 \pm \langle 45, 0\rangle]_{3S}$. Material properties are the one of *Material A*, and a displacement-control strategy has been considered to introduce the loading condition. An initial imperfection with a shape equal to the first buckling mode is assumed. The amplitude is taken with a maximum non-dimensional displacement w/h equal to 10^{-3}.

The results obtained with Ritz are compared against the results obtained with Abaqus in Figure 4.21, where the normalized force-displacement curve is reported. The imposed displacement Δ is normalized against the critical edge displacement

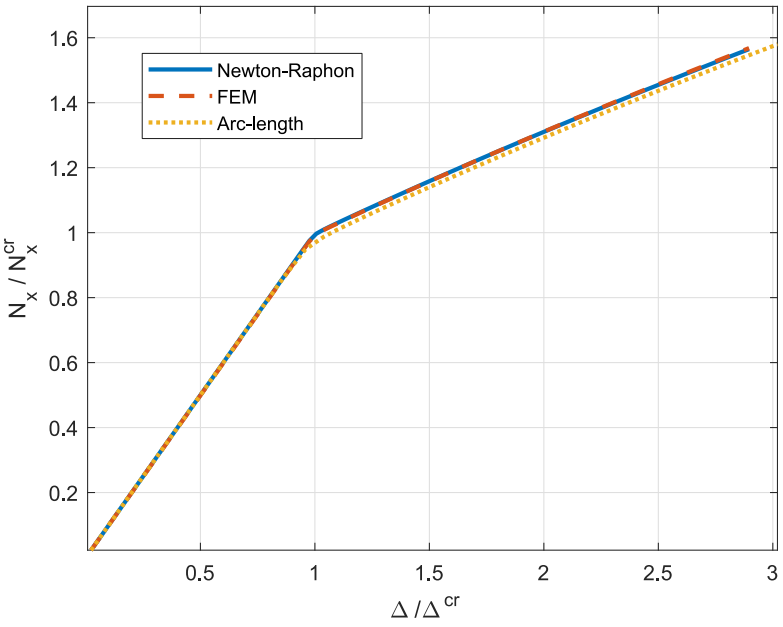

Figure 4.21: Normalized force-displacement curve obtained with different methods.

Δ_{cr}, while the average axial load N_x is normalized with respect to the critical buckling load N_x^{cr}.

The non-linear analysis is performed with both the Newton-Raphson method and the arc-length method, considering 7 terms in both the Airy stress function and the out-of-plane displacement series expansions. The methods provide solutions which are well in agreement with the results obtained with the finite element analysis.

In Table 4.13, the maximum transverse displacement of the plate in the post-buckling field is computed for different number of terms in the series expansion of ϕ and w. The displacement is evaluated for an imposed displacement which is twice

$^P/_M$	2	4	6	8	10
2	1.1790	1.1917	1.1953	1.1975	1.1988
4	1.1796	1.1929	1.1965	1.1987	1.2000
6	1.1804	1.1936	1.1972	1.1994	1.2008
8	1.1806	1.1939	1.1975	1.1997	1.2010
10	1.1807	1.1940	1.1976	1.1998	1.2012
FEM	1.2010 mm				

Table 4.13: Convergence analysis: maximum transverse displacement [mm] in the post-buckling field computed for an imposed displacement which is twice the critical one.

the critical one ($\Delta_{cr} = 0.0026\,\text{mm}$). For P=M=K=10 the Ritz results differ from the Abaqus results by 0.01%, thus the analysis are in good agreement. Nevertheless, for smaller values of P and Q the results obtained with Ritz are also close to the finite element ones, meaning that the analysis can be performed considering less terms in the series expansion, thus reducing the computational time. Moreover, in Table 4.13 it can be noticed that the convergence is faster when a high number of M is selected.

In Figure 4.22 the in-plane stress distribution along the x direction ($N_x(\xi, \eta)$) is reported for different steps: it can be noticed that prior to buckling (Figure 4.22a) the distribution is similar to the one obtained in Example 1 (see Figure 4.8a). After the first instability occurs, the stress distribution change shape: as the load increase, the distribution stretches in the loading direction, and the stresses are distributed near the unloaded edges. A good matching has been found between results obtained with Ritz and with Abaqus. On the other hand, in Figure 4.22 it can be noticed that there is a discrepancy in the in-plane distribution for imposed displacements far from the critical one: the Ritz method seems to fail in correctly considering the high in-plane anysotropy of the plate in the post-buckling field. However, as it can be noticed in Figure 4.21, this effect is less evident from the force-displacement curve. However, further investigations are needed to cover this aspect.

Example 8: Effect of imperfections on the post-buckling behaviour of a variable-stiffness plate In this example the effects that initial geometric imperfections have on the post-buckling behaviour are investigated.

To this aim, initial geometric imperfections of different magnitude have been considered. The shape of the imperfection is introduced as the first buckling mode shape, which has been normalized so that the maximum out-of-plane displacement is equal to one. A scaling factor S has been applied in order to modulate the imperfection's magnitude:

$$w_0(x, y) = S w_{cr}(x, y) \tag{4.139}$$

where w_{cr} is the first buckling mode and w_0 is the initial imperfection.
the analysis is performed for a simply-supported square plate $a = b = 1000\,\text{mm}$ with lamination sequence $[0 \pm \langle 45, 0\rangle]_{3S}$ subjected to an imposed displacement loading condition.

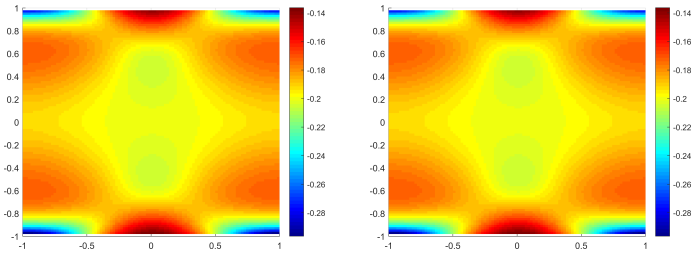

(a) Δ/Δ_{cr}=0.95

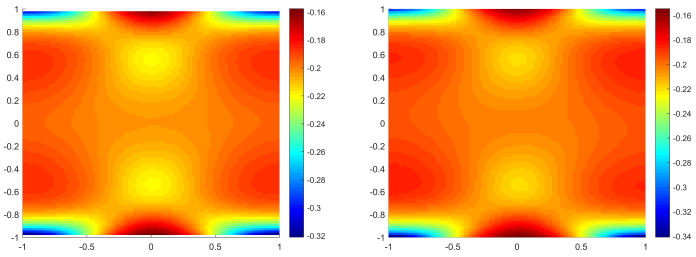

(b) Δ/Δ_{cr}=1.08

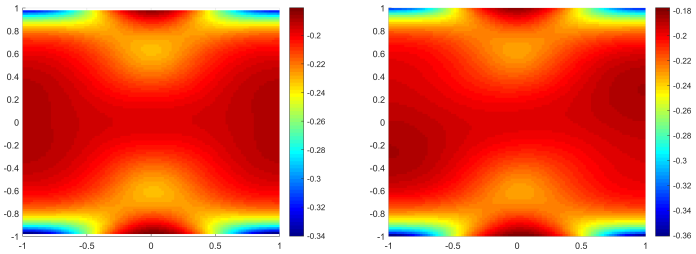

(c) Δ/Δ_{cr}=1.20

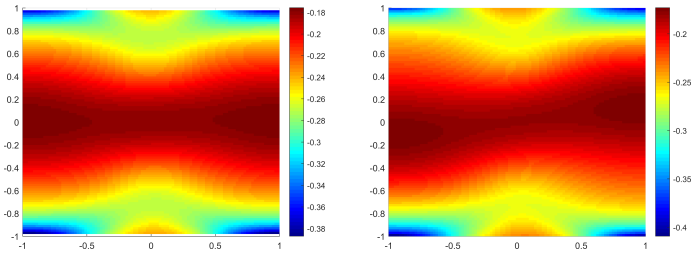

(d) Δ/Δ_{cr}=1.50

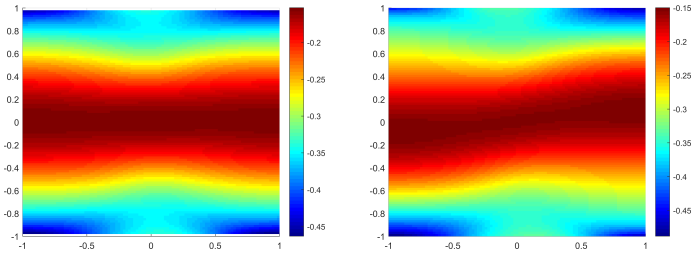

(e) Δ/Δ_{cr}=2.00

Figure 4.22: Non-linear analysis: stress distribution (x-direction) of a variable stiffness plate $[0 \pm \langle 45, 0\rangle]_{3S}$. Ritz results (left) and FEM results (right). Abaqus's results are post-processed with Matlab.

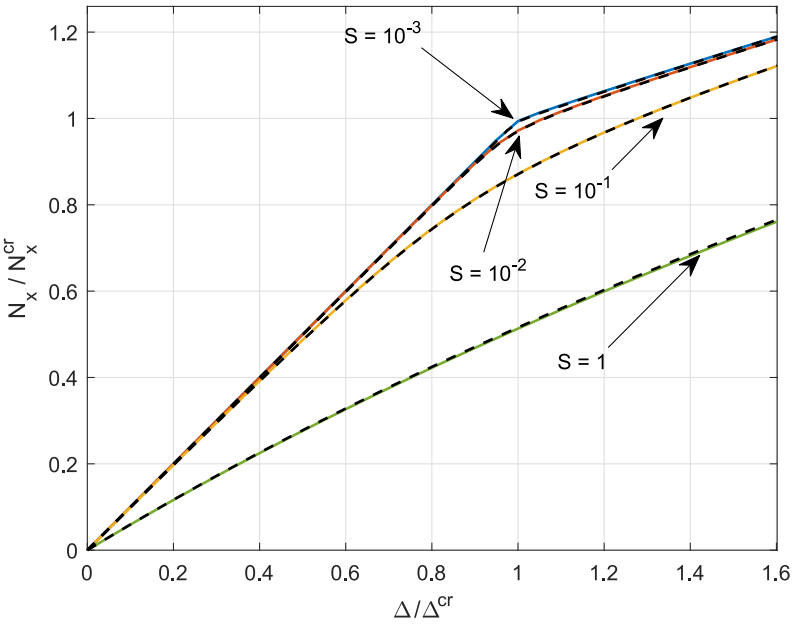

Figure 4.23: Normalized force-displacement curve: effects of an initial geometric imperfection. Dashed lines: FEM.

Including an imperfection in the analysis results in a smoother transition between the pre-buckling state and the post-buckling state. The normalized force-displacement curve is reported in Figure 4.23 for four different scaling factors. It can be noticed that the greater the imperfection's magnitude, the smoother the transition.
Moreover, the Ritz results are in agreement with results obtained with the finite element analysis. The analyses have been performed with $P = M = 8$, and the non-linear system has been solved with the Newton-Raphson method.

Example 9: Effect of fibers orientation on the post-buckling behaviour Variable-stiffness plates allow for higher buckling loads with respect to classical straight fibers laminates. Moreover, the non-constant orientation of the fibers affect the post-buckling behaviour: by properly tailoring the lamination sequence, structures which exhibit an high post-buckling strength can be obtained.

In this example, the post-buckling behaviour of variable-stiffness plates with different lamination sequence is investigated.
To this aim, simple-supported square plates with dimensions $a = b = 1000\,\text{mm}$ are considered. The lamination sequence is characterized by 8 plies, and the lamina properties are the one of *Material A*. The following lamination sequences have been

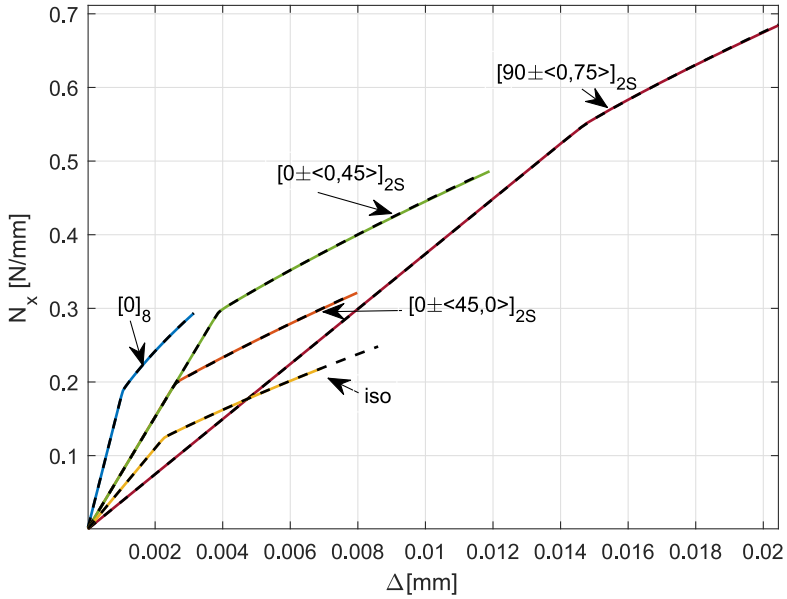

Figure 4.24: Force-displacment curve of plates. Dashed lines: FEM.

considered:

- $[0]_8$
- $[0 \pm \langle 45, 0 \rangle]_{2S}$
- $[0 \pm \langle 0, 45 \rangle]_{2S}$
- $[90 \pm \langle 0, 75 \rangle]_{2S}$

For comparison purposes, an isotropic plate has also been considered.

The results obtained in terms of force-displacement curve are reported in Figure 4.24: it can be observed that, as discussed in Example 2, the first instability occurs for load levels that can be higher when variable-stiffness laminates are employed. Moreover, it can be noticed that for some lamination sequences the slope of the post-buckling branch is steeper than others: a more inclined curve indicates less reduction of axial stiffness after the first instability. This trend is more visible in Figure 4.25, where the results are reported in the normalized force-displacement curve: the laminate with lamination sequence $[90 \pm \langle 0, 75 \rangle]_{2S}$ has the most inclined curve, while the straight fiber laminate posses the lowest one.

The maximum out-of-plane displacement, normalized with respect to the plate's thickness, is plotted against the imposed displacement, normalized with respect to

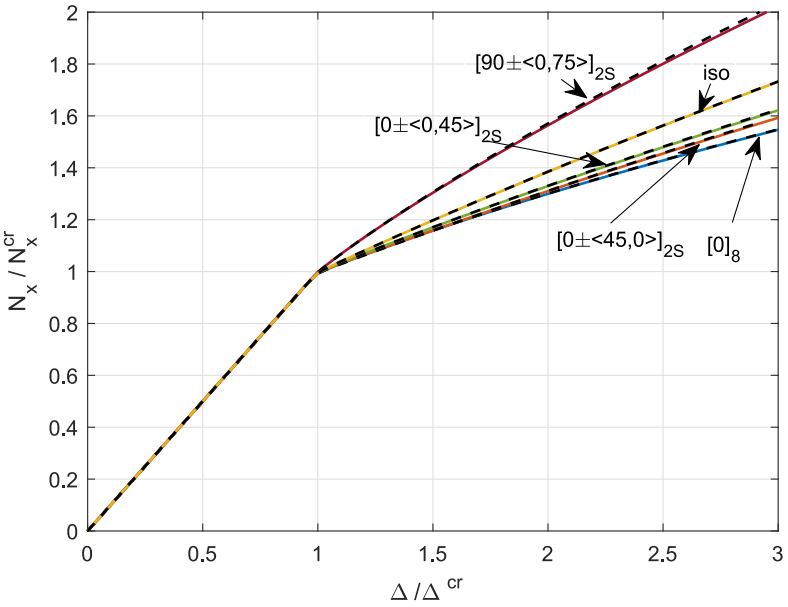

Figure 4.25: Normalized force-displacment curve of different plates. Dashed lines: FEM.

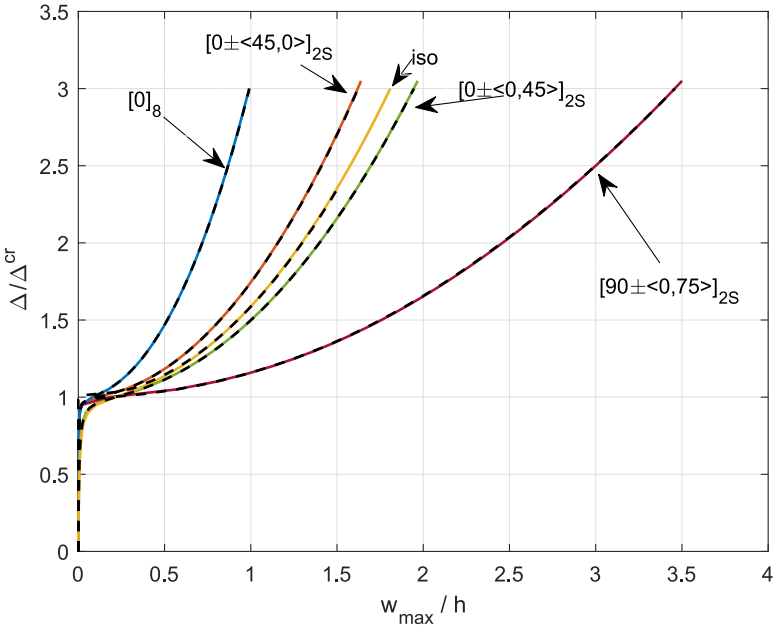

Figure 4.26: Normalized transverse displacement out-of-plane displacement curve. Dashed lines: FEM.

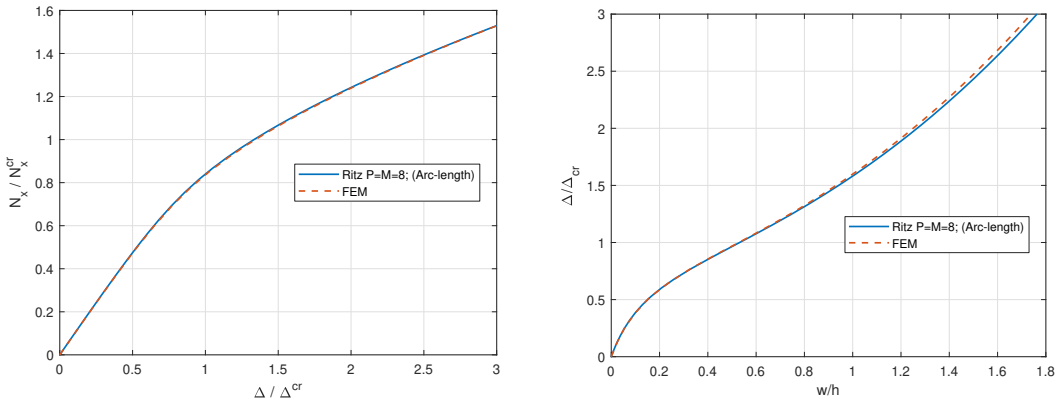

(a) (b)

Figure 4.27: Shell post-buckling analysis ($[0 \pm \langle 45, 0\rangle]_{2S}$)

the critical axial displacement Δ_{cr} in Figure 4.26. In the Figure, it can be appreciated that the transverse displacement is null until the critical edge compression is imposed. However, a small deviation exists in the proximity of the bifurcation point: this is related to the small initial imperfection that was included.
It can be noticed that the out-of-plane displacement of the laminate $[90 \pm \langle 0, 75\rangle]_{2S}$ after the bifurcation increase faster with respect to the other laminates.

Example 10: Post-buckling analysis of variable-stiffness shells In this example the post-buckling analysis of variable-stiffness shells is addressed.
Two variable stiffness shell panels have been considered. The dimensions are $a = b = 100\,\text{mm}$ and the curvature is $R = 500$ mm. The lamination sequences are:

- $[0 \pm \langle 45, 0\rangle]_{2S}$
- $[0 \pm \langle 75, 15\rangle]_{2S}$

The lamina properties are the ones of *Material A*. In the analyses, a small initial imperfection of 10^{-3} mm has been considered. The two laminates exhibit a quite different post-buckling behaviour: the normalized force-displacement curves are reported for the layup $[0 \pm \langle 45, 0\rangle]_{2S}$ and $[0 \pm \langle 75, 15\rangle]_{2S}$ in Figures 4.27 and 4.28, respectively, together with the corresponding transverse displacement - out-of-plane displacement graphs. In the first case the transition from the pre-buckling state to the post-buckling state is very smooth even for a very small imperfection value, and the out-of-plane displacement is different from zero even for very low load levels.
In the second case, the pre-buckling behaviour is more similar to the one of a plate,

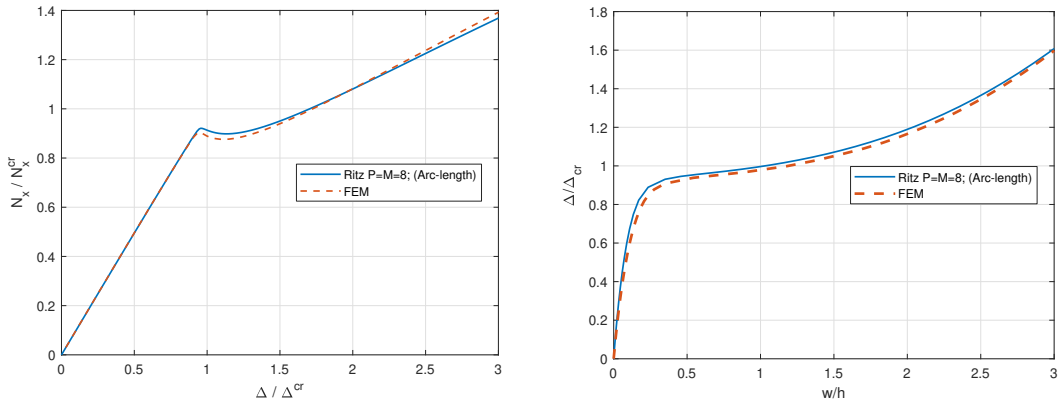

(a) (b)

Figure 4.28: Shell post-buckling analysis ($[0 \pm \langle 75, 15 \rangle]_{2S}$)

but in the neighbourhood of the critical point the behaviour is unstable, resulting in a reduction of the capability of carrying loads. This behaviour is clearly visible in the in-plane stress distribution, reported in Figure 4.29. In the pre-buckling state the stresses are concentrated in the boundary regions, and the central part is relatively unloaded. When the imposed displacement value is close to the buckling load, the stresses are redistributed, and the shell's corners carries the majority of the stresses. As the load increases, the central part is more and more unloaded, and the stress are concentrated at the unloaded edges.

The analyses have been performed by employing the arc-length method. In Figures 4.27, 4.28 and 4.29 it can be noticed that the results are in agreement with the finite element analysis. However, it can be noticed that in the case of unstable behaviour the solutions appear to diverge, and a small difference in the normalized force-displacement curve is visible nearby the critical point.

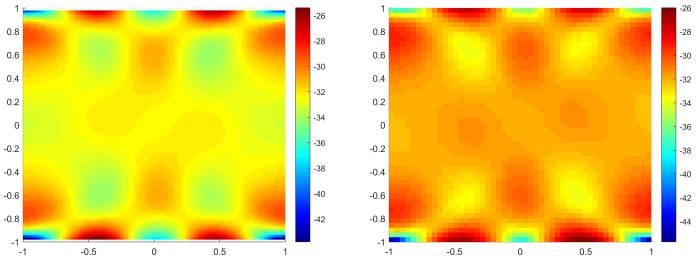

(a) $\Delta/\Delta_{cr} \approx 0.80$

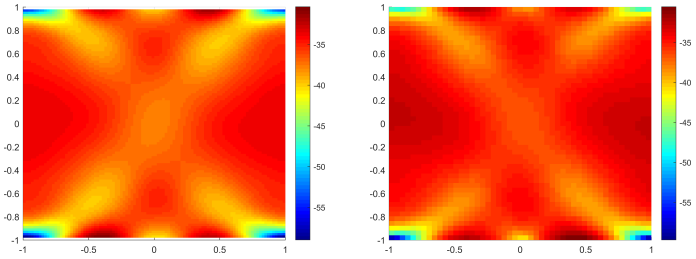

(b) $\Delta/\Delta_{cr} \approx 0.90$

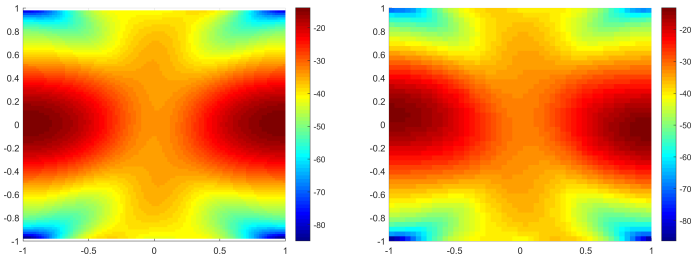

(c) $\Delta/\Delta_{cr} \approx 1.10$

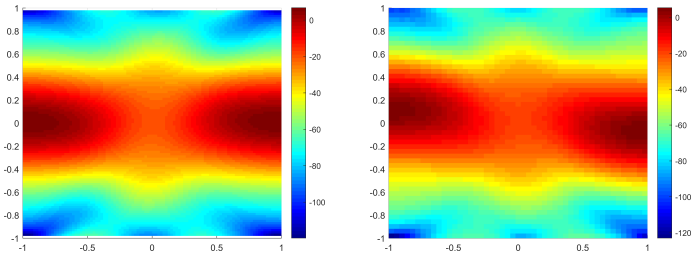

(d) $\Delta/\Delta_{cr} \approx 2.00$

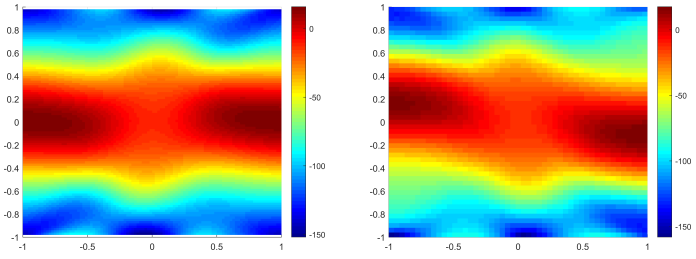

(e) $\Delta/\Delta_{cr} \approx 3.00$

Figure 4.29: Non-linear analysis: stress distribution (x-direction) of a variable stiffness shell $[0 \pm \langle 75, 15 \rangle]_{3S}$. Ritz results (left) and FEM results (right). Abaqus's results are post-processed with Matlab.

Chapter 5

Koiter Approach

In this chapter a perturbation method based on Koiter's approach is discussed for variable-stiffness plates. The problem is formulated with an energy-based approach, consistent with the Ritz formulation presented in the previous chapter, starting from the energy functional derived in Chapter 3.
The analyses are performed for plates subjected to compressive loads. The formulation is developed such that force-control and displacement-control can be considered.

Firstly, a brief introduction of the method is provided, then the relevant equations for the "displacement-control case" are derived. The equations for the same problems specialized for the prescribed load case are available in the Appendix A.
The results are reported for an extensive set of variable-stiffness configurations. The comparison is presented against results from literature and finite element simulations.

5.1 The Perturbation Method

The perturbation method has been introduced by WT Koiter in his work "The Stability of Elastic Equilibrium" [33], where the author investigated the behaviour of buckled structures in the neighbourhood of the bifurcation point. This monumental work allowed the buckling community to understand why some structures are able to carry loads above the buckling point and why others experience a buckling load which is drastically different from the one obtained through a linear buckling analysis. Many researchers applied the perturbation method to investigate the post-buckling behaviour of imperfection sensitive elastic structures; also, the

Koiter-type analysis has been employed to justify the discrepancy between the predicted post-buckling behaviour and the actual experimental results of compressed cylindrical shells. In particular, the Koiter analysis allows to understand the reasons why the behaviour of shells corresponds to imperfection sensitivity.
This method provides a very useful tool for the analysis of the post-buckling behaviour of lightweight structures: instead of solving a non-linear problem, as it is usually done in a classical post-buckling analysis, the Koiter theory allows to reduce the problem to the solution of an additional set of linear equations (besides the pre-buckling and buckling ones) to approximate the initial post-buckling behaviour. Therefore, informations about the response of the structure after the critical point are quickly gained, with a significant reduction of the computational effort. This feature makes the Koiter's approach appropriate for the fast analysis of the post-buckling response of thin plates and shells, including the case of variable-stiffness panels. The method offers the advantage of requiring a relatively small computational effort, which can be particularly useful when performing preliminary computations. The possibility of easily realizing sensitivity and parametric studies can thus be exploited for gathering insight into the behaviour of variable-stiffness panels.

The underlying idea of the Koiter approach is to apply a perturbation expansion to the load parameter around the bifurcation point, that is the point corresponding to the first instability of the structure.
Consider, for instance, a generic function $A(x, y, z, \lambda)$ that depends on the coordinates x, y, z and on the generic load parameter λ. The function can be, for instance, the displacement field or the stress field. The expansion is performed by introducing the following perturbation series

$$A(x, y, z, \lambda) = A^{(0)}(x, y, z, \lambda) + \xi A^{(1)}(x, y, z) + \xi^2 A^{(2)}(x, y, z) + \cdots \tag{5.1}$$

where ξ is a general perturbation parameter. Often ξ is assumed as the out-of-plane displacement, properly normalized. For instance, in the case of thin panels, ξ can be normalised with respect to the wall thickness, or:

$$\xi = \frac{w(x, y)}{h} \tag{5.2}$$

The expansion of $A(x, y, z, \lambda)$ around the buckling point is usually limited to the second order of ξ, and is then composed of three terms. According to the notation

in Eq. 5.1, the zeroth order term is denoted with $(.)^{(0)}$ and corresponds to the pre-buckling part. The first-order term, denoted with $(.)^{(1)}$, is the buckling part, while the second order contribution are denoted with $(.)^{(2)}$ and correspond to the so called second-order solution. This last term can be interpreted as a *correction* that is applied to the zero and first order contributions.
The solution of the initial post-buckling problem implies the evaluation of the three unknowns field in Eq. 5.1. Once the solution is available it is possible to compute specific quantities, such as the b-factor, that give a direct indication on the initial post-buckling behaviour of the structure.

It is important to remark that the perturbation approach is suitable for analysing the post-buckling behaviour in the proximity of the first instability, i.e. in the initial post-buckling region. Indeed, the perturbation is performed after linearising around the bifurcation point. Depending on the case at hand, the loading condition might be either an imposed displacement or an imposed load. Without loss of generality, the load is identified here with the general parameter λ, this representation holding both for the case of load-control and displacement control.
In the case of a structure without clustered buckling modes[1], the load parameter can be expanded around the critical point by means of an asymptotic expansion

$$\lambda = \lambda_{cr} + a\xi\lambda_{cr} + b\xi^2\lambda_{cr} + \cdots \tag{5.3}$$

where λ_{cr} corresponds to the critical load parameter, i.e. the critical load. The coefficients a and b are the so called first and second post-buckling factor. The evaluation of these two non-dimensional factors allows to describe the influence of the perturbation parameter ξ on load factor λ, and so to provide an approximation of the post-buckling behaviour.

A graphical representation can be useful in understanding how the post-buckling parameters describe the structure's behaviour: in Figure 5.1 the imposed load λ is plotted against ξ for three general kind of bifurcation shapes, along with the corresponding force-displacement curve N_x-Δ. The non-linear equilibirum path of both perfect (solid line) and non-perfect structures characterized by an initial shape imperfection $\overline{\xi}$ (dashed line) is represented in the Figure. The behaviour of imperfect structures is discussed in a dedicated section.

[1]In some cases a structure might be characterized by simultaneous or nearly simultaneous buckling loads. If this is the case, the modal interaction should be considered to account for its degrading effect on the load-carrying capability.

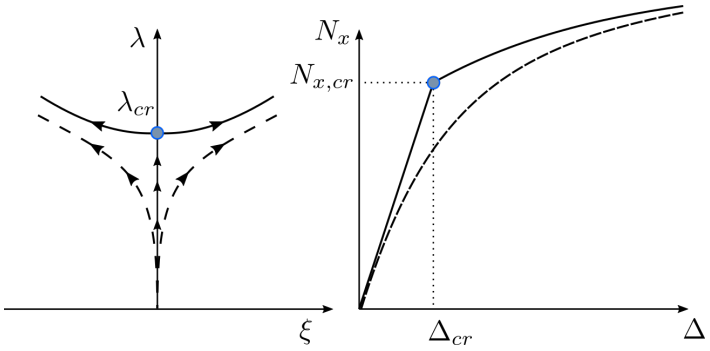

(a) Stable Case ($a = 0$, $b > 0$)

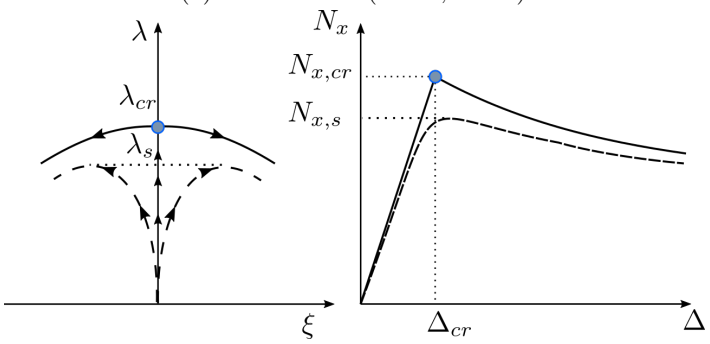

(b) Unstable Case ($a = 0$, $b < 0$)

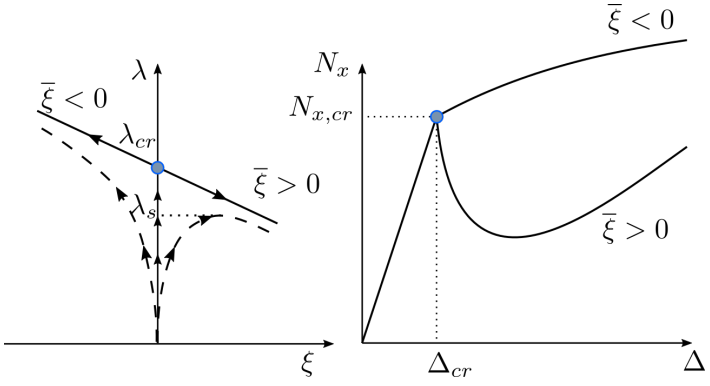

(c) General Case ($a \neq 0$, $b \neq 0$)

Figure 5.1: Symmetric and asymmetric bifurcation path.

For a perfect structure, the out-of-plane displacement ξ, which is normalized with respect to the wall thickness, is zero, as long as the load is below the critical load λ_{cr}. After the bifurcation load λ_{cr} the structure can follow, in principle, any of the three equilibirum branches departing from the bifurcation. One of them is associated with the undeflected configuration, and corresponds to an unstable configuration. The two other branches can be either stable or not, and are associated with a deflected pattern. The structural response beyond the buckling load is strictly related to the panel properties, and it is possible to identify three main cases according to the shape of the curve $\lambda - \xi$. If $a = 0$ (Figures 5.1a and 5.1b) the bifurcation is symmetric, and the behaviour of the structure is dominated by the b-factor. When $b > 0$ the structure can develop post-buckling strength and it can keep operating after buckling occurs, thus resulting in a stable response. In the load-displacement plot this corresponds to a positive slope of the post-buckling branch. On the other hand, in the case $b < 0$ the structure will lose stiffness, and the post-buckling equilibirum path is unstable. This response may promote the collapse of the structure once the load is further increased. In the force-displacement curve this corresponds to a negative inclination of the post-buckling branch. In the case of $a \neq 0$ (Figure 5.1c), the path is asymmetric and the structure will exhibit an unstable post-buckling behaviour. Moreover, as explained later, for $a \neq 0$ the response is strictly dependent on the imperfection shape. From a graphical stand point, a is the post-buckling slope and b is the post-buckling curvature. Therefore the response of a perfect structure in the post-buckled state can be captured once the parameters a and b are available.

The perturbation method can be presented as a sequence of steps.
The first one consists in writing an equation (or a set of equations) describing the problem under investigation, i.e. the behaviour of a compressed structure. With this regard, different formulations are available in the literature: the set of equations can be sought starting, for instance, from the governing differential equations (e.g. Donnell-type equations [36]), the principle of virtual work [46] or the principle of stationary potential energy [45].
The second step of the approach consists in expanding the unknown functions around the critical point. By recalling the general expression of Eq. 5.1, and considering now, instead of a function A, the stresses, strains and displacements, it

is possible to write:

$$\begin{cases} \sigma = \sigma^{(0)}(\lambda_{cr}) + \xi\sigma^{(1)} + \xi^2\sigma^{(2)} + \cdots \\ \epsilon = \epsilon^{(0)}(\lambda_{cr}) + \xi\epsilon^{(1)} + \xi^2\epsilon^{(2)} + \cdots \\ u = u^{(0)}(\lambda_{cr}) + \xi u^{(1)} + \xi^2 u^{(2)} + \cdots \end{cases} \tag{5.4}$$

where the notation introduced by Budiansky and Hutchinson [40] has been adopted. The expansion is performed around the critical point, given by $\lambda = \lambda_{cr}$. An assumption that is commonly introduced consists in considering the pre-buckling field as linear. In this case, the zeroth order terms can be written as constant terms (the general pre-buckling solution for any imposed load) multiplied by the critical load factor λ_{cr}

$$\begin{aligned} \sigma^{(0)}(\lambda_{cr}) &= \lambda_{cr}\sigma^{(0)} \\ \epsilon^{(0)}(\lambda_{cr}) &= \lambda_{cr}\epsilon^{(0)} \\ u^{(0)}(\lambda_{cr}) &= \lambda_{cr}u^{(0)} \end{aligned} \tag{5.5}$$

and, according to Eq. 5.5, the expression of Eq. 5.4 can be re-written as:

$$\begin{cases} \sigma = \lambda_{cr}\sigma^{(0)} + \xi\sigma^{(1)} + \xi^2\sigma^{(2)} + \cdots \\ \epsilon = \lambda_{cr}\epsilon^{(0)} + \xi\epsilon^{(1)} + \xi^2\epsilon^{(2)} + \cdots \\ u = \lambda_{cr}u^{(0)} + \xi u^{(1)} + \xi^2 u^{(2)} + \cdots \end{cases} \tag{5.6}$$

The expression of Eq. 5.6 can be substituted back into the relevant functional and the terms multiplied by the same powers of ξ are collected. Every power of ξ multiplies a different set of equations: for instance, if the Donnell-type equations are employed, the pre-buckling equations are retrieved as those multiplied by ξ^0; the buckling ones are multiplied by ξ, whilst the equations of the second-order problem are those multiplied by ξ^2.

If the governing equations are sought by means of an energetic formulation, the power of ξ to be retained are the even ones. The resulting set of equations –which correspond to the pre-buckling, buckling and second-order problems– are obtained in the form of partial differential equations, whose solution can be obtained referring to well known numerical techniques. In each problem, the constant term is the result of a lower order problem, and it represent the forcing term of the current state. For this reason, the set of equations are solved in subsequent order: firstly

the pre-buckling problem, secondly the buckling problem, and finally the second order one.
The expansion of Eq. 5.5 can be extended to account for higher-order contributions: by doing so, the accuracy of the approximation would increase. However, an expansion up to the second-order is, in most cases, enough to gain insights into the initial post-buckling behaviour.
Once the solutions of the different levels are obtained, it is possible to compute the post-buckling factors and obtain informations about the post-buckling behaviour. By looking at a and b, it is possible to qualitatively predict whether the post-buckling path is going to be stable or unstable.
Moreover, by imposing a load λ and substituting a and b in Eq. 5.3, it is possible to retrieve ξ, and therefore σ, ϵ and u can be computed according to Eq. 5.6.
However, a and b are properties of the perfect structure and thus they are not sufficient to describe the behaviour of an imperfect plate or an imperfect shell. In the next section it will be shown how the perturbation method is used for evaluating the initial post-buckling behaviour of imperfect structures.

5.1.1 Imperfections

A real structure is always affected by deviations from the nominal configuration, both in terms of geometry, material, loading and boundary conditions. In a panel, geometric imperfections are in the form of deviation from the ideal shape, and are mainly due to the manufacturing process. The effects of imperfections on the behaviour of a structure have been the subject of several investigations in the past: experiments and theoretical studies showed that there is no general rule, and the way imperfections affect the response of a structure is related to many different factors, such as the way the load is prescribed, the geometry of the structure, the boundary conditions and the magnitude of imperfections. The sensitivity of the response due to imperfections is particularly relevant in the case of cylindrical shells loaded in compression, as investigated by Arbocz [36], Jansen [68] and Koth [35]. As a matter of fact, the buckling load of the perfect structure is never reached when imperfections, such as those encountered in real-life applications, are accounted for. This aspect is illustrated in the sketches in Figure 5.1, where the dashed lines represent the equilibrium path of an imperfect structure. As observed, the out-of-plane displacement is different from zero in the pre-buckling branch. This is a consequence of the initial imperfection, whose amplitude is denoted as $\overline{\xi}$. In the

case of symmetric unstable bifurcation (Figure 5.1b), the structure is not able to reach the theoretical buckling load and can only withstand loads up to the limit load λ_s. If the post-buckling response is stable (Figure 5.1a), the structure can carry loads above the critical point.
In the case of an imperfection sensitive structure, a deviation from the ideal shape can severely affect the post-buckling response. As can be seen in Figure 5.1c, if the imperfection's magnitude is positive ($\overline{\xi} > 0$), the structure loses stiffness and its ability to further carry loads. If the imperfection's magnitude is negative ($\overline{\xi} < 0$), the structure will still be able to carry loads and operate.
The previous observations highlight the importance of accounting for the presence of initial imperfections. With this regard, Koiter's theory can be modified to account for these effects. Assuming a small, stress-free initial imperfection, Eq. 5.3 can be rewritten as

$$(\lambda - \lambda_{cr})\xi = +a\xi^2\lambda_{cr} + b\xi^3\lambda_{cr} + \cdots - \alpha\lambda_{cr}\bar{\xi} - \beta(\lambda - \lambda_{cr})\bar{\xi} + \cdots \tag{5.7}$$

where α and β are the first and second imperfection form factors. These parameters were firstly introduced by Cohen [69].

If linear pre-buckling is assumed, then α=β [69]. Furthermore, if the imperfections are taken in the form of the first buckling mode, $\overline{\xi} = w^{(1)}$, then $\alpha = \beta = 1$, and 5.7 becomes

$$(1 - \frac{\lambda}{\lambda_{cr}})\xi + a\xi^2 + b\xi^3 + \cdots = \frac{\lambda}{\lambda_{cr}}\bar{\xi} \tag{5.8}$$

The coefficients a and b in Eq. 5.8 are properties of the perfect structure. For this reason, the formulation for the three level problems is derived for a perfect, imperfection free structure. In a subsequent phase, the α and β factors are computed by means of the shape of the imperfection and the second-order solution.
Thus, as investigated by Garcea et al. [38], it is possible to run sensitivity analysis by including *a posteriori* the effect of geometric imperfections: the real behaviour of a structure can be initially studied by considering the properties of a perfect structure by computing the coefficients a and b. Subsequently, it is possible to account for the presence of initial imperfections $\overline{\xi}$ by evaluating the imperfections form factors α and β.

5.2 Ritz-Koiter Formulation for Plates

In the present work the equations that serve as basis for the perturbation method are obtained by means of the unitary functional introduced in Section 3.3. The discrete equations are derived by employing the same Ritz approach adopted for the linear and non-linear buckling analysis and, for this reason, the formulation can be seen as a unified Ritz-Koiter approach. All the observations made about the method in Chapter 4 and the selected admissible functions remain unchanged. Also, the coordinates are normalized according to Eq. 4.11.
To the best of the author's knowledge, no previous attempt can be found in literature to develop a similar approach.

In the following sections the equations related to the three level of expansion are obtained for a plate subjected to displacement-control loading conditions. The equations for the force-control case are reported in Appendix A.
Secondly, the general expression of the post-buckling and imperfection form factors is given. Finally, an expression of the post-buckling stiffness based on the perturbation analysis results is derived to asses the behaviour of variable-stiffness panels after buckling.

The three levels of linear equations (pre-buckling, buckling and second order) are obtained from the unitary functional adopted in Chapter 4. The function has already been presented in Eq. 3.26, however it is reported here for convenience:

$$\begin{aligned}\Pi_F = &-\frac{1}{2}\int_S [a_{11}(x,y)\phi_{/yy}^2 + 2a_{12}(x,y)\phi_{/xx}\phi_{/yy} + a_{22}(x,y)\phi_{/xx}^2 + \\ &+ a_{66}(x,y)\phi_{/xy}^2 - 2a_{16}(x,y)\phi_{/yy}\phi_{/xy} - 2a_{26}(x,y)\phi_{/xx}\phi_{/xy}]dS + \\ &+ \frac{1}{2}\int_S [D_{11}(x,y)w_{/xx}^2 + 2D_{12}(x,y)w_{/xx}w_{/yy} + D_{22}(x,y)w_{/yy}^2 + \\ &+ 4D_{66}(x,y)w_{/xy}^2 + 4D_{16}(x,y)w_{/xx}w_{/xy} + 4D_{26}(x,y)w_{/xy}w_{/yy}]dS + \\ &+ \frac{1}{2}\int_S [\phi_{/yy}w_{/x}^2 + \phi_{/xx}w_{/y}^2 - 2\phi_{/xy}w_{/x}w_{/y}]dS + \\ &+ \int_{S_2} [u_0 N_{xv} + v_0 N_{yv}]dy\end{aligned} \tag{5.9}$$

Note that the unitary functional is reported without the imperfection-related contribution since, as outlined in Section 5.1.1, the behaviour of the imperfect structure in the post-buckling regime can be initially investigated by considering

the structure as perfect.

There are two possibilities for obtaining the set of equations from this functional. The first is to expand directly the Airy stress function ϕ and the out-of-plane displacement w, substitute their expression in Eq. 5.9, collect the power of ξ, and use the Ritz approach and minimize each collected term.
The second possibility consists in approximating the functional with a Ritz-like approach, and perform the perturbation in a subsequent step, at discrete equation level. In this work the second option has been chosen, which is believed more straightforward. Either way, the resulting linear systems will be the same.
It should be noted that the powers of ξ to collect in the energy expression are the even ones up to the fourth order (0 for pre-buckling, 2 for buckling and 4 for the second order problem), even if the expansions for the displacement and stress fields are carried out only up to the second order.
The Airy stress function and the out-of-plane displacement are assumed to have the following series-form

$$\phi(\xi,\eta) = \phi_0(\xi,\eta) + \phi_1(\xi,\eta) = \phi_0(\xi,\eta) + \sum_{p=0}^{P}\sum_{q=0}^{Q} X_p(\xi)Y_q(\eta)\Phi_{pq} \tag{5.10}$$

$$w(\xi,\eta) = \sum_{m=0}^{M}\sum_{n=0}^{N} \overline{X}_m(\xi)\overline{Y}_n(\eta)W_{mn} \tag{5.11}$$

where Φ_{pq},W_{mn},c_k are the unknown coefficients of the series and $X_p, Y_q, \overline{X}_m, \overline{Y}_n, \psi_k$ are the admissible functions, assumed as

$$\begin{aligned} X_p(\xi) &= (1-\xi^2)^2 L_p(\xi) \\ Y_q(\eta) &= (1-\eta^2)^2 L_q(\eta) \\ \overline{X}_m(\xi) &= (1-\xi)^{i_1}(1+\xi)^{i_2} L_m(\xi) \\ \overline{Y}_n(\eta) &= (1-\eta)^{j_1}(1+\eta)^{j_2} L_n(\eta) \end{aligned} \tag{5.12}$$

and

$$\phi_{0/\eta\eta} = \sum_{k=0}^{K} \psi_k(\eta)c_k \tag{5.13}$$

For a detailed description the reader is referred to Section 4.3.

The resulting functional is obtained by substituting Eqs. 5.10 and 5.11 into 5.9,

and is obtained as:

$$\begin{aligned}\Pi_F = &- \frac{2b}{a^3}\sum_{pq\overline{pq}=0}^{PQPQ} U_{pq\overline{pq}}\Phi_{pq}\Phi_{\overline{pq}} - \frac{4b}{a^3}\sum_{pqk=0}^{PQK} U_{C,pqk}\Phi_{pq}c_k - \\ &- \frac{2b}{a^3}\sum_{k\overline{k}=0}^{KK} C_{k\overline{k}}c_k c_{\overline{k}} + \frac{2b}{a^3}\sum_{mn\overline{mn}=0}^{MNMN} K_{mn\overline{mn}}W_{mn}W_{\overline{mn}} + \\ &+ \frac{2}{ab}\sum_{pqmn\overline{mn}=0}^{PQMNMN} L_{1,pqmn\overline{mn}}\phi_{pq}W_{mn}W_{\overline{mn}} + \\ &+ \frac{2}{ab}\sum_{kmn\overline{mn}=0}^{KMNMN} L_{2,kmn\overline{mn}}c_k W_{mn}W_{\overline{mn}} + \\ &- \lambda\frac{2}{b}\sum_{k=0}^{K} P_k c_k\end{aligned} \tag{5.14}$$

where the compact notation of Eq. 4.39 is adopted. For further details on the terms in Eq. 5.14 see Sections 4.5 and 4.6.

The unknowns of the problem are the amplitudes Φ_{pq}, W_{mn} and c_k. Assuming linear pre-buckling behaviour, the perturbation expansion around the critical point λ_{cr} is

$$\begin{cases}\Phi_{pq} = \lambda_{cr}\Phi_{pq}^{(0)} + \xi\Phi_{pq}^{(1)} + \xi^2\Phi_{pq}^{(2)} + \cdots \\ W_{mn} = \lambda_{cr}W_{mn}^{(0)} + \xi W_{mn}^{(1)} + \xi^2 W_{mn}^{(2)} + \cdots \\ c_k = \lambda_{cr}c_k^{(0)} + \xi c_k^{(1)} + \xi^2 c_k^{(2)} + \cdots\end{cases} \tag{5.15}$$

The expansions of Eq. 5.15 can be then substituted in the discrete counterpart of the functional given by Eq. 5.14, and the resulting series is truncated at the fourth order.

It can be noticed that amplitudes Φ_{pq}, W_{mn} and c_k are either multiplied by themselves (quadratic terms $A \times A$), multiplied by another series of amplitudes (mixed quadratic terms $A \times B$) or multiplied by another quadratic term (third order terms $A \times B^2$), where A and B are generic amplitudes. So, in order to improve the readability of the procedure followed to obtain the three set of equations, the products are not shown here, but are performed for generic quantities A and B in Appendix C. Due to the adoption of the unitary functional, the power of interest of ξ are only 0, 2 and 4: only the terms multiplying these powers of the perturbation parameter will be retained. It can be easily verified that the expressions multiplied by the odd-powers of ξ are null [70].

The expanded terms products are substituted into Eq. 5.14, maintaining only the terms multiplied by either ξ^0, ξ^2 or ξ^4. Each member of Eq. 5.14 will be treated separately to facilitate the reading of the document.

$$U_{pq\overline{pq}}\Phi_{pq}\Phi_{\overline{pq}} = U_{pq\overline{pq}}(\lambda_{cr}^2\Phi_{pq}^{(0)}\Phi_{\overline{pq}}^{(0)} + \xi^2\lambda_{cr}\Phi_{pq}^{(0)}\Phi_{\overline{pq}}^{(2)} + \xi^2\Phi_{pq}^{(1)}\Phi_{\overline{pq}}^{(1)} + \\ + \xi^2\lambda_{cr}\Phi_{pq}^{(2)}\Phi_{\overline{pq}}^{(0)} + \xi^4\Phi_{pq}^{(2)}\Phi_{\overline{pq}}^{(2)}) \quad (5.16)$$

$$U_{c,pqk}\Phi_{pq}c_k = U_{c,pqk}(\lambda_{cr}^2\Phi_{pq}^{(0)}c_k^{(0)} + \xi^2\lambda_{cr}\Phi_{pq}^{(0)}c_k^{(2)} + \xi^2\Phi_{pq}^{(1)}c_k^{(1)} + \\ + \xi^2\lambda_{cr}\Phi_{pq}^{(2)}c_k^{(0)} + \xi^4\Phi_{pq}^{(2)}c_k^{(2)}) \quad (5.17)$$

$$C_{k\overline{k}}c_k c_{\overline{k}} = C_{k\overline{k}}(\lambda_{cr}^2 c_k^{(0)}c_{\overline{k}}^{(0)} + \xi^2\lambda_{cr}c_k^{(0)}c_{\overline{k}}^{(2)} + \xi^2 c_k^{(1)}c_{\overline{k}}^{(1)} + \\ + \xi^2\lambda_{cr}c_k^{(2)}c_{\overline{k}}^{(0)} + \xi^4 c_k^{(2)}c_{\overline{k}}^{(2)}) \quad (5.18)$$

$$K_{mn\overline{mn}}W_{mn}W_{\overline{mn}} = K_{mn\overline{mn}}(\lambda_{cr}^2 W_{mn}^{(0)}W_{\overline{mn}}^{(0)} + \xi^2\lambda_{cr}W_{mn}^{(0)}W_{\overline{mn}}^{(2)} + \xi^2 W_{mn}^{(1)}W_{\overline{mn}}^{(1)} + \\ + \xi^2\lambda_{cr}W_{mn}^{(2)}W_{\overline{mn}}^{(0)} + \xi^4 W_{mn}^{(2)}W_{\overline{mn}}^{(2)}) \quad (5.19)$$

$$\begin{aligned} L_{1,pqmn\overline{mn}}W_{mn}W_{\overline{mn}}\Phi_{pq} =& L_{1,pq\overline{mn}mn}(\lambda_{cr}^2\Phi_{pq}^{(0)}W_{mn}^{(0),2} + \xi^2\lambda_{cr}\Phi_{pq}^{(0)}W_{mn}^{(1),2} + \\ &+ \xi^4\lambda_{cr}\Phi_{pq}^{(0)}W_{mn}^{(2),2} + 2\xi^2\Phi_{pq}^{(1)}W_{mn}^{(0)}W_{mn}^{(1)} + \\ &+ 2\xi^4\Phi_{pq}^{(1)}W_{mn}^{(1)}W_{mn}^{(2)} + \xi^2\lambda_{cr}^2\Phi_{pq}^{(2)}W_{mn}^{(0),2} + \\ &+ 2\xi^4\lambda_{cr}\Phi_{pq}^{(2)}W_{mn}^{(0)}W_{mn}^{(2)} + \\ &+ \xi^4\Phi_{pq}^{(2)}W_{mn}^{(1),2}) \end{aligned} \quad (5.20)$$

$$\begin{aligned} L_{2,kmn\overline{mn}}W_{mn}W_{\overline{mn}} =& L_{2,k\overline{mn}mn}(\lambda_{cr}^2 c_k^{(0)}W_{mn}^{(0),2} + \xi^2\lambda_{cr}c_k^{(0)}W_{mn}^{(1),2} + \\ &+ \xi^4\lambda_{cr}c_k^{(0)W_{mn}^{(2),2}} + 2\xi^2 c_k^{(1)}W_{mn}^{(0)}W_{\overline{mn}}^{(1)} + \\ &+ 2\xi^4 c_k^{(1)}W_{mn}^{(1)}W_{\overline{mn}}^{(2)} + \xi^2\lambda_{cr}^2 c_k^{(2)}W_{mn}^{(0),2} + \\ &+ 2\xi^4 c_k^{(2)}W_{mn}^{(0)}W_{\overline{mn}}^{(2)} + \xi^4 c_k^{(2)}W_{mn}^{(1),2}) \end{aligned} \quad (5.21)$$

$$\begin{aligned} \lambda\Delta P_k c_k =& (\lambda_{cr} + \xi a\lambda_{cr} + \xi^2 b\lambda_{cr})\Delta P_k(\lambda_{cr}c_k^{(0)} + \xi c_k^{(1)} + \xi^2 c_k^{(2)}) = \\ =& \Delta P_k[\lambda_{cr}^2 c_k^{(0)} + \xi^2(b\lambda_{cr}^2 c_k^{(0)} + a\lambda_{cr}c_k^{(1)} + b\lambda_{cr}c_k^{(2)}) + \\ &+ \xi^4 b\lambda_{cr}c_k^{(2)}] \end{aligned} \quad (5.22)$$

The contributions are collected according to the power of ξ such that

$$\begin{aligned} \xi^0 &\rightarrow \Pi_F^{(0)} \rightarrow \text{Zeroth Order Problem} \\ \xi^2 &\rightarrow \Pi_F^{(1)} \rightarrow \text{First Order Problem} \\ \xi^4 &\rightarrow \Pi_F^{(2)} \rightarrow \text{Second Order Problem} \end{aligned} \tag{5.23}$$

The zeroth order problem is obtained by minimizing $\Pi_F^{(0)}$, whose expression is

$$\begin{aligned} \Pi_F^{(0)} =& \xi^0 \lambda_{cr}^2 (-\frac{2b}{a^3} U_{pq\overline{pq}} \Phi_{pq}^{(0)} \Phi_{\overline{pq}}^{(0)} - \frac{4b}{a^3} U_{c,pqk} \Phi_{pq}^{(0)} c_k^{(0)} - \frac{2b}{a^3} C_{k\bar{k}} c_k^{(0)} c_{\bar{k}}^{(0)} + \\ &+ \frac{2b}{a^3} K_{mn\overline{mn}} W_{mn}^{(0)} W_{\overline{mn}}^{(0)} + \frac{2}{ab} L_{1,pq\overline{mn}mn} \Phi_{pq}^{(0)} W_{\overline{mn}}^{(0)} W_{mn}^{(0)} + \\ &+ \frac{2}{ab} L_{2,k\overline{mn}mn} c_k^{(0)} W_{\overline{mn}}^{(0)} W_{mn}^{(0)} - \Delta P_k c_k^{(0)}) \end{aligned} \tag{5.24}$$

with respect to $\Phi_{pq}^{(0)}$, $c_k^{(0)}$ and $W_{mn}^{(0)}$:

$$\begin{aligned} \frac{\partial \Pi_F^{(0)}}{\partial \Phi_{pq}^{(0)}} =& \quad \boldsymbol{U} \boldsymbol{\Phi}_{\overline{pq}}^{(0)} + \boldsymbol{U_C} \boldsymbol{c}_k^{(0)} + \boldsymbol{L_1}^{pq} \boldsymbol{W}_{\overline{mn}}^{(0)} \boldsymbol{W}_{mn}^{(0)} = 0 \\ \frac{\partial \Pi_F^{(0)}}{\partial c_k^{(0)}} =& \quad \boldsymbol{U_C} \boldsymbol{\Phi}_{pq}^{(0)} + \boldsymbol{C} \boldsymbol{c}_k^{(0)} + \boldsymbol{L_2}^{k} \boldsymbol{W}_{\overline{mn}}^{(0)} \boldsymbol{W}_{mn}^{(0)} = \boldsymbol{P} \\ \frac{\partial \Pi_F^{(0)}}{\partial W_{mn}^{(0)}} =& \quad \boldsymbol{K} \boldsymbol{W}_{\overline{mn}}^{(0)} + \boldsymbol{L_1}^{mn} \boldsymbol{\Phi}_{pq}^{(0)} \boldsymbol{W}_{\overline{mn}}^{(0)} + \boldsymbol{L_2} \boldsymbol{c}_k^{(0)} \boldsymbol{W}_{\overline{mn}}^{(0)} = 0 \end{aligned} \tag{5.25}$$

which is the pre-buckling problem. In Eq. 5.24 summatory is implied over the repeated indexes. The matrix terms in Eq. 5.25 are the same employed in Section 4.6. The unknown coefficients $W_{mn}^{(0)}$, $\Phi_{pq}^{(0)}$ and $c_k^{(0)}$ have been collected in the vectors $\boldsymbol{W}_{mn}^{(0)}$, $\boldsymbol{\Phi}_{pq}^{(0)}$ and $\boldsymbol{c}_k^{(0)}$,

Since linear pre-buckling is assumed, the out-of-plane displacement, in this phase, is null, meaning that $W_{mn}^{(0)} = 0$. The system is then

$$\begin{aligned} \boldsymbol{U} \boldsymbol{\Phi}_{\overline{pq}}^{(0)} + \boldsymbol{U_C} \boldsymbol{c}_k^{(0)} &= 0 \\ \boldsymbol{U_C} \boldsymbol{\Phi}_{pq}^{(0)} + \boldsymbol{C} \boldsymbol{c}_k^{(0)} &= \boldsymbol{P} \end{aligned} \tag{5.26}$$

which is the same linear system obtained in Eq. 4.45, whose unknown are now given by the coefficients of the zero order terms.

The first order problem is obtained by minimizing $\Pi_F^{(1)}$, which is:

$$\begin{aligned}\Pi_F^{(1)} =&\xi^2(-\frac{2b}{a^3}U_{pq\overline{pq}}(\lambda_{cr}\Phi_{pq}^{(0)}\Phi_{\overline{pq}}^{(2)}+\Phi_{pq}^{(1)}\Phi_{\overline{pq}}^{(1)}+\lambda_{cr}\Phi_{pq}^{(2)}\Phi_{\overline{pq}}^{(0)})+\\
&-\frac{2b}{a^3}U_{c,pqk}(\lambda_{cr}\Phi_{pq}^{(0)}c_k^{(2)}+\Phi_{pq}^{(1)}c_k^{(1)}+\lambda_{cr}\Phi_{pq}^{(2)}c_k^{(0)})+\\
&-\frac{2b}{a^3}C_{k\bar{k}}(\lambda_{cr}c_k^{(0)}c_{\bar{k}}^{(2)}+c_k^{(1)}c_{\bar{k}}^{(1)}+\lambda_{cr}c_k^{(2)}c_{\bar{k}}^{(0)})+\\
&+\frac{2b}{a^3}K_{mn\overline{mn}}(\lambda_{cr}W_{mn}^{(0)}W_{\overline{mn}}^{(2)}+W_{mn}^{(1)}W_{\overline{mn}}^{(1)}+\lambda_{cr}W_{mn}^{(2)}W_{\overline{mn}}^{(0)})+\\
&+\frac{2}{ab}L_{1,pq\overline{mn}mn}(\lambda_{cr}\Phi_{pq}^{(0)}W_{\overline{mn}}^{(1)}W_{mn}^{(1)}+2\lambda_{cr}\Phi_{pq}^{(1)}W_{mn}^{(0)}W_{\overline{mn}}^{(1)}+\lambda_{cr}^2\Phi_{pq}^{(2)}W_{mn}^{(0)}W_{\overline{mn}}^{(0)})+\\
&+\frac{2}{ab}L_{2,k\overline{mn}mn}(\lambda_{cr}c_k^{(0)}W_{mn}^{(1)}W_{\overline{mn}}^{(1)}+2\lambda_{cr}\xi^2c_k^{(1)}W_{mn}^{(0)}W_{\overline{mn}}^{(1)}+\lambda_{cr}^2c_k^{(2)}W_{mn}^{(0)}W_{\overline{mn}}^{(0)}))\end{aligned} \tag{5.27}$$

The minimization is carried out with respect to $\Phi_{pq}^{(1)}$, $c_k^{(1)}$ and $W_{mn}^{(1)}$, and the following linear system is obtained

$$\begin{aligned}\frac{\partial\Pi_F^{(1)}}{\partial\Phi_{pq}^{(1)}} =&\quad \boldsymbol{U}\boldsymbol{\Phi}_{\overline{pq}}^{(1)}+\boldsymbol{U_C}\boldsymbol{c}_k^{(1)}+2\boldsymbol{L_1}^{pq}\boldsymbol{W}_{\overline{mn}}^{(0)}\boldsymbol{W}_{mn}^{(1)}=0\\
\frac{\partial\Pi_F^{(1)}}{\partial c_k^{(1)}} =&\quad \boldsymbol{U_C}\boldsymbol{\Phi}_{pq}^{(1)}+\boldsymbol{C}\boldsymbol{c}_k^{(1)}+2\boldsymbol{L_2}^{k}\boldsymbol{W}_{\overline{mn}}^{(0)}\boldsymbol{W}_{mn}^{(1)}=0\\
\frac{\partial\Pi_F^{(1)}}{\partial W_{mn}^{(1)}} =&\quad \boldsymbol{K}\boldsymbol{W}_{\overline{mn}}^{(1)}+\lambda_{cr}[\boldsymbol{L_1}^{mn}(\boldsymbol{\Phi}_{pq}^{(0)}\boldsymbol{W}_{\overline{mn}}^{(1)}+2\boldsymbol{\Phi}_{pq}^{(1)}\boldsymbol{W}_{\overline{mn}}^{(0)})+\boldsymbol{L_2}^{mn}(\boldsymbol{c}_k^{(0)}\boldsymbol{W}_{\overline{mn}}^{(1)}+2\boldsymbol{c}_k^{(1)}\boldsymbol{W}_{\overline{mn}}^{(0)})]=0\end{aligned} \tag{5.28}$$

after observing that, due to the linear pre-buckling assumptions, $W_{mn}^{(0)}=0$, it can be noted that the first two equations in 5.28 are identically satisfied by $\Phi_{pq}^{(1)}=0$ and $c_k^{(1)}=0$. The third equation provides the same eigenvalue problem obtained in Section 4.5, which represents the buckling problem. In particular it is:

$$[\boldsymbol{K}+\lambda_{cr}(\boldsymbol{L_1}^{mn}\boldsymbol{\Phi}_{pq}^{(0)}+\boldsymbol{L_2}^{mn}\boldsymbol{c}_k^{(0)})]\boldsymbol{W}_{\overline{mn}}^{(1)}=0 \tag{5.29}$$

where $\boldsymbol{W}_{mn}^{(1)}$ and λ_{cr} are the eigenvector and the eigenvalue, respectively. Due to the not uniqueness nature of eigenvectors, the amplitude of $\boldsymbol{W}_{mn}^{(1)}$ can be arbitrary, and therefore it must be properly normalized. In the present work $\boldsymbol{W}_{mn}^{(1)}$ has been normalized such that the amplitude of the first buckling mode correspond to the wall thickness.

The second order problem is obtained by minimizing the functional $\Pi_F^{(2)}$, which is:

$$\begin{aligned}\Pi_F^{(2)} =&\xi^4[-\frac{2b}{a^3}U_{pq\overline{pq}}\Phi_{pq}^{(2)}\Phi_{\overline{pq}}^{(2)} - \frac{2b}{a^3}U_{c,pqk}\Phi_{pq}^{(2)}c_k^{(2)} - \frac{2b}{a^3}C_{k\bar{k}}c_k^{(2)}c_{\bar{k}}^{(2)} + \\ &+ \frac{2b}{a^3}K_{mn\overline{mn}}W_{mn}^{(2)}W_{\overline{mn}}^{(2)} + \frac{2}{ab}L_{1,pq\overline{mn}mn}(\lambda_{cr}\Phi_{pq}^{(0)}W_{mn}^{(2)}W_{\overline{mn}}^{(2)} + 2\Phi_{pq}^{(1)}W_{mn}^{(1)}W_{\overline{mn}}^{(2)} + \\ &+ 2\Phi_{pq}^{(2)}W_{mn}^{(0)}W_{\overline{mn}}^{(2)} + \Phi_{pq}^{(2)}W_{mn}^{(1)}W_{\overline{mn}}^{(1)}) + \frac{2}{ab}L_{2,k\overline{mn}mn}(\lambda_{cr}c_k^{(0)}W_{mn}^{(2)}W_{\overline{mn}}^{(2)} + \\ &+ 2c_k^{(1)}W_{mn}^{(1)}W_{\overline{mn}}^{(2)} + 2c_k^{(2)}W_{mn}^{(0)}W_{\overline{mn}}^{(2)} + c_k^{(2)}W_{mn}^{(1)}W_{\overline{mn}}^{(1)})]\end{aligned} \tag{5.30}$$

The minimization is now carried out with respect to the coefficients $\Phi_{pq}^{(2)}$, $c_k^{(2)}$ and $W_{mn}^{(2)}$ in order to obtain the second order problem

$$\begin{aligned}\frac{\partial\Pi_F^{(2)}}{\partial\Phi_{pq}^{(2)}} =& \quad \boldsymbol{U}\boldsymbol{\Phi}_{\overline{pq}}^{(2)} + \boldsymbol{U_C}\boldsymbol{c}_k^{(2)} + \boldsymbol{L_1}^{pq}\boldsymbol{W}_{\overline{mn}}^{(1)}\boldsymbol{W}_{mn}^{(1)} = 0 \\ \frac{\partial\Pi_F^{(2)}}{\partial c_k^{(2)}} =& \quad \boldsymbol{U_C}\boldsymbol{\Phi}_{pq}^{(2)} + \boldsymbol{C}\boldsymbol{c}_k^{(2)} + \boldsymbol{L_2}^{k}\boldsymbol{W}_{\overline{mn}}^{(1)}\boldsymbol{W}_{mn}^{(1)} = 0 \\ \frac{\partial\Pi_F^{(2)}}{\partial W_{mn}^{(2)}} =& \quad \boldsymbol{K}\boldsymbol{W}_{\overline{mn}}^{(2)} + 2\lambda_{cr}\boldsymbol{L_1}^{mn}\boldsymbol{\Phi}_{pq}^{(0)}\boldsymbol{W}_{\overline{mn}}^{(2)} + 2\lambda_{cr}\boldsymbol{L_2}^{mn}\boldsymbol{c}_k^{(0)}\boldsymbol{W}_{\overline{mn}}^{(2)} = 0\end{aligned} \tag{5.31}$$

It is straightforward to notice that the solution of the third equation is $\boldsymbol{W}_{mn}^{(2)} = 0$. This aspect is due to the expansion of the solution around the critical point: the second-order solution is only related to the in-plane stress distribution due to the instability.

For the reason mentioned above, the second order problem reduces to the solution of the first two equations of the system in Eq. 5.31, as:

$$\begin{aligned}\boldsymbol{U}\boldsymbol{\Phi}_{\overline{pq}}^{(2)} + \boldsymbol{U_C}\boldsymbol{c}_k^{(2)} &= -\boldsymbol{L_1}^{pq}\boldsymbol{W}_{\overline{mn}}^{(1)}\boldsymbol{W}_{mn}^{(1)} \\ \boldsymbol{U_C}\boldsymbol{\Phi}_{pq}^{(2)} + \boldsymbol{C}\boldsymbol{c}_k^{(2)} &= -\boldsymbol{L_2}^{k}\boldsymbol{W}_{\overline{mn}}^{(1)}\boldsymbol{W}_{mn}^{(1)}\end{aligned} \tag{5.32}$$

which is, as expected, a linear system that can be solved for $\boldsymbol{\Phi}_{pq}^{(2)}$ and $\boldsymbol{c}_k^{(2)}$. The terms on the right side are "forcing terms" that depend on the first order solution. The solution of the eigenvalue problem in Eq. 5.29 requires the knowledge of the pre-buckling solution, thus it is evident how it is necessary to solve first the pre-buckling and buckling problems in order to obtain the second order solution.

5.3 Post-buckling Factors

The series expansion of the load parameter in Eq. 5.3 is indeed helpful in describing the initial post-buckling behaviour of a panel under compression, and it is written by means of the post-buckling factors a and b. As explained, the parameters a and b provide a quick estimate regarding the stability of the structure after the bifurcation point.
The expression of the first and second post-buckling factors is

$$a = -\frac{3}{2}\frac{\Phi^{(1)} \cdot (w^{(1)}, w^{(1)})}{\lambda_{cr}\hat{\Delta}} \tag{5.33}$$

$$b = -\frac{2\Phi^{(1)} \cdot (w^{(1)}, w^{(2)}) + \Phi^{(2)} \cdot (w^{(1)}, w^{(1)})}{\lambda_{cr}\hat{\Delta}} \tag{5.34}$$

where

$$\hat{\Delta} = \mathring{\Phi}^{(0)}(\lambda_{cr}) \cdot (w^{(1)}, w^{(1)}) \tag{5.35}$$

and $\mathring{A}(\lambda_{cr})$ means that the quantity A is evaluated in the critical point and derived with respect to λ_{cr}

$$\mathring{A}(\lambda_{cr}) = \frac{\partial A(\lambda_{cr})}{\partial \lambda_{cr}} \tag{5.36}$$

In Eq. 5.33-5.35 the notation $A \cdot (B, C)$ is adopted, where:

$$A \cdot (B, C) = \int_{-l_x/2}^{+l_x/2} \int_{-l_y/2}^{+l_y/2} [A_{/xx} B_{/y} C_{/y} + A_{/yy} B_{/x} C_{/x} - A_{/xy}(B_{/x} C_{/y} + B_{/y} C_{/x})] dy dx \tag{5.37}$$

The expressions of these two factors are of general validity: in order to derive them, the asymptotic expansion of the load parameter in Eq. 5.3 is substituted in Eqs. 5.16 - 5.22. The procedure is reported in several works available in literature (see, for instance, the works of Cohen [69] and Byskov [71]).
For an axisymmetric structure without clustered buckling modes when subjected to axisymmetric load (such as the cases under consideration), the first post-buckling coefficient is zero [69]. Since $a = 0$, the post-buckling behaviour is characterized by a symmetric bifurcation.
This is confirmed by the expression of the a-factor in Eq. 5.33 where, as seen, the numerator depend upon the first order solution for the Airy stress function $\Phi^{(1)}$. In the case of plates the membrane stress solution of the first-order problem is null,

and thus $a = 0$.

For the same reason the expression of the b-factor reduces to

$$b = -\frac{\Phi^{(2)} \cdot (w^{(1)}, w^{(1)})}{\lambda_{cr}\hat{\Delta}} \tag{5.38}$$

As expected, the expression is function of the results of the first- and second-order solutions. The evaluation of the b-factor, which is a post-buckling-related quantity, is then performed in a post-processing phase, when the solution of the relevant governing equations is available.

It is important to recall that the b-factor refers to the nominally perfect configuration. To recover the effect of initial imperfections – that have a drastic impact on the characteristics of the panel response –, it is necessary to evaluate the parameters α and β, already introduced in the context of the expansion of Eq. 5.7. The expression of the parameters α and β is not derived here for the sake of conciseness but could be obtained, following a procedure similar to the one leading to the a and b factors, as [69]:

$$\alpha = \frac{\Phi^{(0)}(\lambda_{cr}) \cdot (\hat{W}, W^{(1)})}{\lambda_{cr}\hat{\Delta}} \tag{5.39}$$

$$\beta = \frac{\mathring{\Phi}^{(0)}(\lambda_{cr}) \cdot (\hat{W}, W^{(1)})}{\hat{\Delta}} \tag{5.40}$$

where the imperfection w_0 is expressed as $w_0 = \overline{\xi}\hat{W}$. Under the assumptions of linear pre-buckling, the term $\mathring{\Phi}^{(0)}$ is derived as:

$$\mathring{\Phi}^{(0)}(\lambda_{cr}) = \frac{\partial \Phi^{(0)}(\lambda_{cr})}{\partial \lambda_{cr}} = \frac{\partial \lambda_{cr}\Phi^{(0)}}{\partial \lambda_{cr}} = \Phi^{(0)} \tag{5.41}$$

and therefore Equations 5.39 and 5.40 become

$$\alpha = \frac{\Phi^{(0)(\lambda_{cr})} \cdot (\hat{W}, W^{(1)})}{\lambda_{cr}\mathring{\Phi}^{(0)}(\lambda_{cr}) \cdot (w^{(1)}, w^{(1)})} = \frac{\lambda_{cr}\Phi^{(0)} \cdot (\hat{W}, W^{(1)})}{\lambda_{cr}\dfrac{\partial \lambda_{cr}\Phi^{(0)}}{\partial \lambda_{cr}} \cdot (w^{(1)}, w^{(1)})} = \frac{\Phi^{(0)} \cdot (\hat{W}, W^{(1)})}{\Phi^{(0)} \cdot (W^{(1)}, W^{(1)})} \tag{5.42}$$

$$\beta = \frac{\mathring{\Phi}^{(0)}(\lambda_{cr}) \cdot (\hat{W}, W^{(1)})}{\mathring{\Phi}^{(0)}(\lambda_{cr}) \cdot (w^{(1)}, w^{(1)})} = \frac{\Phi^{(0)} \cdot (\hat{W}, W^{(1)})}{\Phi^{(0)} \cdot (W^{(1)}, W^{(1)})} \tag{5.43}$$

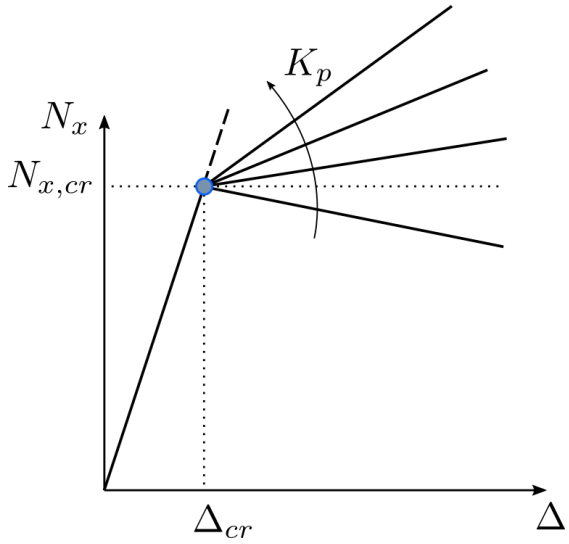

Figure 5.2: The slope of the post-buckling branch is related to the post-buckling stiffness K_p. The higher the slope of the post-buckling path, the stiffer is the structure.

which means that $\alpha = \beta$. The analysis is further simplified by assuming the shape of the initial imperfection as equal to the first buckling mode:

$$w_0 = \overline{\xi} \sum_{m=0}^{M} \sum_{n=0}^{N} W_{mn}^{(1)} \overline{X}_m \overline{Y}_n = \overline{\xi} W^{(1)} \tag{5.44}$$

which leads to $\alpha = \beta = 1$. Therefore the imperfection sensitivity of a panel, whenever the pre-buckling can be assumed linear and the imperfection modelled as the first buckling shape, can be assessed using Eq. 5.7 once the magnitude and sign of the imperfection are available.

5.4 Post-buckling Stiffness

The perturbation method can be applied to quickly establish the post-buckling behaviour nearby the critical point. In particular, the a and b factors were found to be meaningful parameters for understanding the quality of the post-buckling equilibrium. Another useful parameter is given by the post-buckling stiffness, a scalar parameter that quantifies the loss of stability due to the onset of buckling. In terms of the typical force-displacement plot, the post-buckling stiffness parameters defines the slope of curve just after the bifurcation. In this graph a positive slope ($b > 0$) corresponds to a stable post-buckling behaviour, while a negative slope ($b < 0$) to an unstable one, (see Figure 5.1c). Moreover, the higher the

post-buckling stiffness, the higher the slope of the post-buckling branch, and the smaller the loss of stiffness associated with the instability phenomenon. In the limit case, the structure could experience a null reduction of stiffness, meaning that the post-buckling stiffness equals the pre-buckling one.
The evaluation of the post-buckling stiffness is therefore extremely helpful in interpreting the behaviour in the non-linear regime. In this regard, the Koiter's approach is a straightforward strategy to gather insightful design information. In the following sections the expression of the post-buckling stiffness for the case of imposed displacement is derived within the present theoretical framework.

When the load is applied in the form of a prescribed displacement, the control parameter is $\lambda\Delta$, where Δ defines the shape of the displacement, in this case constant along the edge. The resulting average edge load N_x is expanded as

$$\begin{aligned} N_x &= \lambda N_x^{(0)} + \xi N_x^{(1)} + \xi^2 N_x^{(2)} + \cdots \\ &= \lambda_{cr} N_x^{(0)} + (\lambda - \lambda_{cr}) N_x^{(1)} + \xi N_x^{(1)} + \xi^2 N_x^{(2)} + \cdots \end{aligned} \tag{5.45}$$

where λ_{cr} is the critical multiplier corresponding to the critical end-shortening $\Delta_{cr} = \lambda_{cr}\Delta$.
The load-parameter is expanded as function of the perturbation parameter ξ as:

$$\lambda = \lambda_{cr} + \lambda_{cr}\xi a + \lambda_{cr}\xi^2 b + \cdots \tag{5.46}$$

and, recalling that for plates $a = 0$, the expression of Eq. 5.46 is rearranged as:

$$\frac{\lambda}{\lambda_{cr}} = 1 + \xi^2 b \tag{5.47}$$

from which:

$$\xi^2 = \left(\frac{\lambda}{\lambda_{cr}} - 1\right)\frac{1}{b} \tag{5.48}$$

Substituting now Eq. 5.48 into Eq. 5.45 leads to:

$$N_x - N_x^{cr} = (\lambda - \lambda_{cr}) N_x^{(0)} + \left(\frac{\lambda}{\lambda_{cr}} - 1\right)\frac{1}{b} N_x^{(2)} \tag{5.49}$$

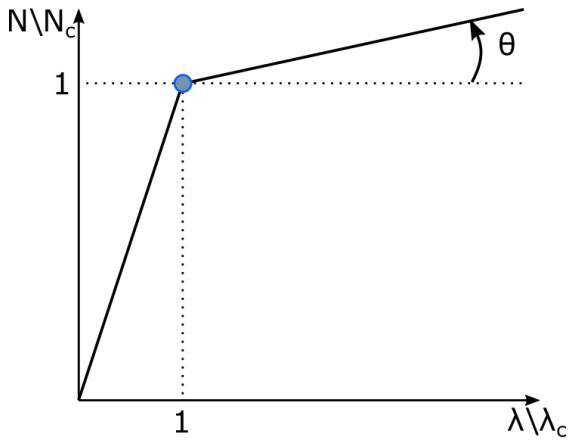

Figure 5.3: General normalized load vs normalized displacement graph for an imposed edge displacement Δ.

And finally, dividing both sides of the equation by $\lambda - \lambda_{cr}$ and properly rearranging the terms, it is possible to obtain:

$$\frac{(N_x - N_x^{cr})}{(\lambda - \lambda_{cr})} = N_x^{(0)} + \frac{N_x^{(2)}}{\lambda_{cr} b} = \frac{N_x^{(0)} \lambda_{cr} b + N_x^{(2)}}{\lambda_{cr} b} \tag{5.50}$$

In the normalized edge load vs normalized displacement graph in Figure 5.3, the slope m of the curve is

$$m = \left(\frac{N_x - N_x^{cr}}{\lambda \Delta - \lambda_{cr} \Delta} \right) \frac{\lambda_{cr} \Delta}{N^{cr}} \tag{5.51}$$

and so the expression of the post-buckling path slope is:

$$K_P = \frac{N_x^{cr} b + N_x^{(2)}}{N_x^{cr} b} \tag{5.52}$$

which is the so-called relative post-buckling stiffness, i.e. the ratio between the post-buckling stiffness and the pre-buckling stiffness.
If needed, the angle between the post-buckling branch and the horizontal axis can be obtained as:

$$\theta = \arctan(K_p) \tag{5.53}$$

The expression of Eq. 5.52 requires the evaluation of $N_x^{(2)}$, which is obtained starting from the expression of the edge load, which is:

$$N_x = \frac{1}{l_y} \int_{-l_y/2}^{+l_y/2} \sum_k^K \psi(y) c_k \lambda \Delta dy \tag{5.54}$$

Note that l_i is used here to denote the plate length along the direction i. This is intended to avoid ambiguity with the symbols a and b, denoting, in the present formulation, the post-buckling factors.
The perturbation expansion of c_k defined in Eq. 5.15 is substituted in the edge load expression

$$N_x = \frac{1}{l_y}\int_{-l_y/2}^{+l_y/2}\sum_{k}^{K}\psi(y)(\lambda c_k^{(0)} + \xi c_k^{(1)} + \xi^2 c_k^{(2)})\lambda\Delta dy \tag{5.55}$$

and, regrouping the different terms according to the order of the perturbation parameter ξ, the expression of $N_x^{(2)}$ is available as:

$$N_x^{(2)} = \frac{1}{l_y}\int_{-l_y/2}^{+l_y/2}\sum_{k}^{K}\psi(y)c_k^{(2)}\lambda\Delta dy \tag{5.56}$$

5.5 Summary of the Procedure

For clarity, a brief summary of the perturbation method is reported in this section. The procedure to derive the governing equations can be summarized in the following steps:

1. Definition of the formulation, either in the form of governing partial differential equations or variational principle (this latter is the strategy puresed in the present approach) to describe the pre- and post-buckling behaviour.

2. Expansion of the solution around the critical (buckling) point.

3. Substitution of the expanded solution in the governing equation.

4. Collection of the terms according to the powers of ξ.

5. Derivation of the zero-, first- and second-order equations as those pre-multiplied by the first three even power of ξ.

6. Approximation of the set of governing equations by means of a Ritz expansion of the unknowns.

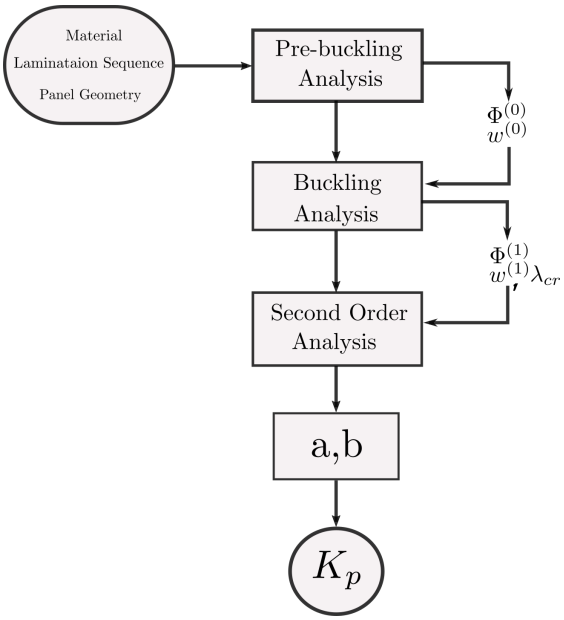

Figure 5.4: Perturbation Analysis: script flow.

5.6 Results

In this Section the model developed within the framework of the Koiter's perturbation theory is used to investigate the post-buckling behaviour of variable-stiffness panels. The validity of the results is compared against results from literature and finite element analysis. To this purpose, the finite element analysis solver DIANA [72] was used. Only plates have been considered in the analysis: for this particular case, the a-factor is identically null, therefore the results are reported only in terms of b-factor.

Implementation Aspects The perturbation analysis is implemented in a Matlab program, whose logical work-flow of the script is schematically represented in Figure 5.4. The inputs are the geometry of the panel, the material characteristics, the lamination sequence, the boundary and loading conditions.
The three problems –pre-buckling, buckling, and second-order– are solved sequentially, using the result of the lower-order problem to build the right-hand side of the higher-order problem.
Once the solution is available, the results can be post-processed to determine the post-buckling factors (in this case just b, as a=0) and the post-buckling stiffness K_p.
Additionally, the user can request as output the shape of the solution of the three

Case	Normalized Buckling Load			b-factor		
	Lanzo [73]	Rahman [74]	Present	Lanzo [73]	Rahman [74]	Present
(SSSS)	4.0026	4.0905	4.0000	0.1824	0.1867	0.1826
(SCSC)	7.7134	7.6528	7.6913	0.1957	0.1962	0.1955

Table 5.1: Comparison of normalized buckling loads and b-factor for a simply supported isotropic plate.

problems, the $\lambda - \xi$ curve, the stress and the out-of-plane field in the post-buckling state.

Comparison against reference results

A preliminary set of analyses is carried out to check the correctness of the present implementation. In particular, the comparison is presented against reference results in terms of b-factors. Due to the scarcity of results in the literature for variable-stiffness plates, the comparison is initially performed for plates with uniform stiffness distribution. In particular, isotropic plates are analysed first, while the case of straight-fiber laminates is investigated next.

Isotropic Plate The first test case is taken from the work of Lanzo [73] and Rahman [74]. In particular, a square plate is considered with dimension equal to 1000 mm. The thickness is 10 mm, thus the width-to-thickness ratio is 100, meaning that the assumption of thin plate is actually reasonable. Two different set of boundary conditions are assumed: simply-supported (SSSS) and simply-supported along two edges and clamped along the two remaining edges (SCSC). The compressive load is introduced in the form of a prescribed force per unit length along the plate transverse edges. A homogeneous and isotropic material is assumed, with Young's modulus of 21 MPa and Poisson's ratio 0.25.

The results are summarized in Table 5.1, where the b-factor and the nondimensional buckling load are reported for the reference results and the present Koiter-Ritz approach.

$$\overline{N}_1 = \lambda_{cr} \left(\frac{\pi^2}{l_y^2} \frac{Eh^3}{12(1-\nu^2)} \right)^{-1} \tag{5.57}$$

$^P/_M$	2	4	6	8
2	0.1797	0.1822	0.1822	0.1822
4	0.1800	0.1825	0.1825	0.1825
6	0.1800	0.1826	0.1826	0.1826
8	0.1800	0.1826	0.1826	0.1826
Lanzo [73]		0.1824		
Rahman[74]		0.1867		

Table 5.2: Convergence analysis for the b-factor of a simply supported isotropic plate.

It can be noticed that the results are in agreement with literature: the b-factor for the simply supported plate differs by 0.10% from the result obtained by Lanzo with the finite element method, and by 2.25% from the same value obtained by Rahman, who also employed a finite element analysis.

It is interesting to investigate the convergence of the solution with respect to the number of terms used for expanding the Airy stress function and the out-of-plane displacement. To this aim, the b-factors of the same simply-supported panel analysed above are summarized in Table 5.2 for variable number of Ritz functions. Note that the same number of trial functions are assumed along the x and y directions, meaning that P=Q=K and M=N. The good convergence properties of the method are clearly visible from the results of Table 5.2. Convergence up to the third digit is reached by taking P=4 and M=4, corresponding to a reduced number of total degrees of freedom.

Laminate Plate: force-control case This second set of results deals with the case of composite materials. In particular, straight fiber laminated plates subjected to prescribed edge load are considered. The material properties of each ply are:

$$E_1 = 21\,\text{MPa}; \quad E_2 = \frac{E_1}{C}; \quad \frac{G_{12}}{E_2} = 0.6; \quad \nu_{12} = 0.25$$

where C is a constant expressing the orthotropy ratio, i.e. the ratio between the longitudinal and transverse elastic moduli. The thickness of each ply is 2.5 mm. The plate is simply-supported along the four edges (SSSS), and a cross-ply lamination sequence is assumed $[0/90/90/0]_S$.

The results are compared against the buckling loads and the b-factors obtained by

C	Normalized Buckling Load ($\overline{N}_2$)			b coefficient		
	Lanzo [73]	Rahman [74]	Present	Lanzo [73]	Rahman [74]	Present
3	5.7561	5.6976	5.7538	0.1986	0.1999	0.1987
20	19.7148	19.601	19.7124	0.1260	0.1263	0.1259

Table 5.3: Comparison of normalized buckling loads and b coefficients: force-control case.

Lanzo and Rahman. The buckling loads are normalized as

$$\overline{N}_2 = \lambda_{cr} \left(\frac{E_2 h^3}{l_y^2} \right)^{-1} \tag{5.58}$$

The comparison in presented in Table 5.3 for different values of the orthotropy ratio. Also in this case the results are in good agreement, and the b-factors obtained with the current Koiter-Ritz approach are closer to the values obtained by Lanzo than the ones obtained by Rahman.

Laminated Plate: displacement-control case In this example, simply supported plates are considered subjected to a compression by means of an uniform edge displacement, (displacement-control case in Section 4.2). Two plates with dimensions $l_x = l_y = 1000\,\text{mm}$ have been analysed: a laminate with a four-ply layup $[\pm 45]_S$ and lamina properties of the *Material A* (Section 4.9), and a quasi-isotropic (QI) plate with material properties:

$$E_{iso} = U_1(1 - \nu_{iso}^2), \qquad \nu_{\text{iso}} = \frac{U_4}{U_1}, \qquad D_{\text{iso}} = \frac{E_{\text{iso}} h^3}{12(1 - \nu_{\text{iso}}^2)} \tag{5.59}$$

where $U_{1,4}$ are computed by means of Eq. 2.28 and considering the *Material A*. For comparison purposes, the analyses have been also performed with the finite element code DIANA. The mesh is realized by means of triangular three-node flat shell elements with six degrees of freedom per node [74], and a mesh density of 20×20×2 is used: with this notation, the plate is made of 400 square sections, each of which is divided in two triangular elements, for a total of 800 elements.

The buckling loads and the b-factors are reported in Table 5.4, and it can be noticed that the results obtained with the Koiter-Ritz method are in good agreement with the finite element analysis: the b-factors of the quasi-isotropic plate differs by 1.44%, while in the laminate case the error is 0.36%.

Case	Buckling Load [N/mm]		b-factor	
	DIANA	Present	DIANA	Present
QI	0.7861×10^{-2}	0.7861×10^{-2}	0.5727	0.5808
$[\pm 45]_S$	0.9375×10^{-2}	0.9375×10^{-2}	0.1901	0.1908

Table 5.4: Comparison of buckling loads [N/mm] and b coefficients: displacement-control case.

Case	b-factor	K_P
isotropic	0.5767	0.4083
$[0]_8$	1.8166	0.3404
$[0 \pm \langle 45, 0 \rangle]_{2S}$	0.7329	0.3243
$[0 \pm \langle 0, 45 \rangle]_{2S}$	0.4858	0.3696
$[90 \pm \langle 0, 75 \rangle]_{2S}$	0.1608	0.7032

Table 5.5: b coefficients and post-buckling relative stiffness for different lamination sequences: displacement-control case.

Variable-Stiffness Panels

Following the validation against reference results, the analysis is now extended to the case of variable-stiffness plates. The results presented in this section are believed of special importance, especially in light of the lack of available results in the literature.

To this purpose, the panels studied in the Example 9 of Chapter 4 are considered. The load is introduced in the form of either a prescribed displacement or a prescribed force.

The results are reported in terms of b-factors and post-buckling stiffness in Tables

Case	b-factor	K_P
isotropic	0.1772	0.1749
$[0]_8$	0.0624	0.3404
$[0 \pm \langle 45, 0 \rangle]_{2S}$	0.0946	0.0888
$[0 \pm \langle 0, 45 \rangle]_{2S}$	0.0707	0.0721
$[90 \pm \langle 0, 75 \rangle]_{2S}$	0.1063	0.0375

Table 5.6: b coefficients and post-buckling relative stiffness for different lamination sequences: force-control case.

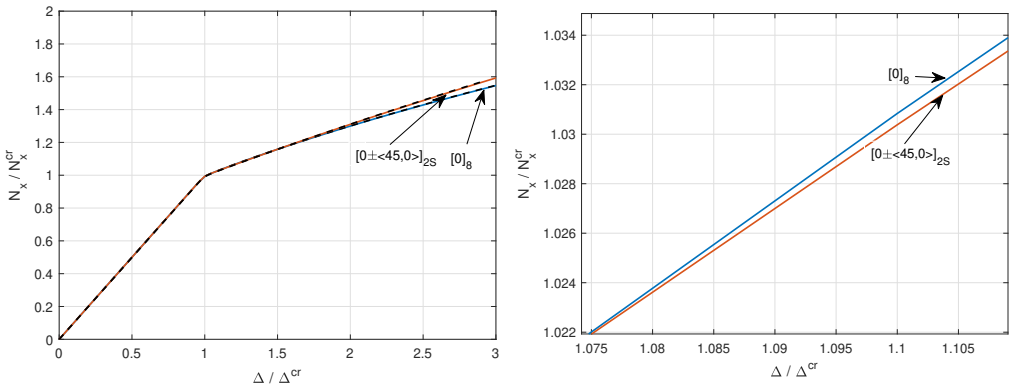

(a) (b)

Figure 5.5: Initial post-buckling behaviour of two laminated plates: 5.5a global curve, 5.5b zoom close to the buckling load.

5.5 and 5.6 for the displacement-control and force-control cases, respectively.
Concerning the displacement-control case, it can be observed that the plate with layup $[90\pm < 0, 75 >]_{2S}$ is the one exhibiting the smallest drop of stiffness after buckling, whilst the plate with layup $[0\pm < 45, 0 >]_{2S}$ is the one undergoing the highest drop. As expected, these results are in agreement with the non-linear force-displacement curves obtained with the Ritz formulation. In this regard, the reader is referred to Figures 4.25-4.26.
The Koiter results of Table 5.5 clearly demonstrate that the layup $[0]_8$ determines a higher non-dimensional post-buckling stiffness with respect to the variable-stiffness configuration $[0 \pm \langle 45, 0\rangle]_{2S}$. On the contrary, the Ritz results of Section 4.9, reported here for convenience in Figure 4.25, do not provide such a clear response over the superiority of one configuration with respect to the other. To this aim, a zoom is performed in the force-displacement curve, in correspondence of the buckling condition, as reported in Figure 5.5b. As seen, the Ritz results, even for this case, agree with those obtained using the Koiter approach.

The results provided in Table 5.5 can be interpreted by considering the second-order solution. In the case of the isotropic plate, the pre-buckling stress distribution is uniform (Figure 5.6a): this is expected, since the stiffness properties are constant. However, the second order solution shows that after the critical point the stresses concentrates in the boundary regions, and the central part is less loaded (Figure 5.6b), resulting in a reduction of the post-buckling stiffness.
A similar result is obtained for the plate with lamination sequence $[0 \pm \langle 45, 0\rangle]_{2S}$. Due to the stiffness variability, the stress distribution in the pre-buckling state is

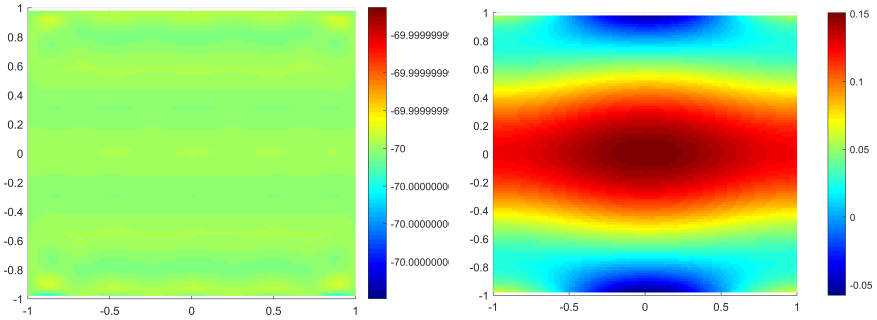

(a) Zero Order (b) Second Order

Figure 5.6: Stress resultants distribution (isotropic plate)

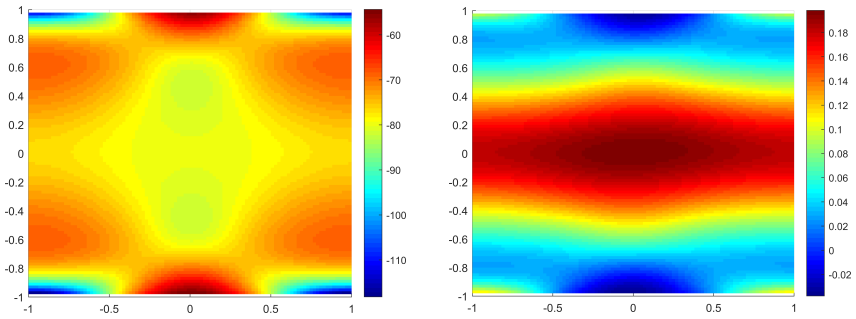

(a) Zero Order (b) Second Order

Figure 5.7: Stress resultants distribution ($[0 \pm \langle 45, 0 \rangle]_{2S}$)

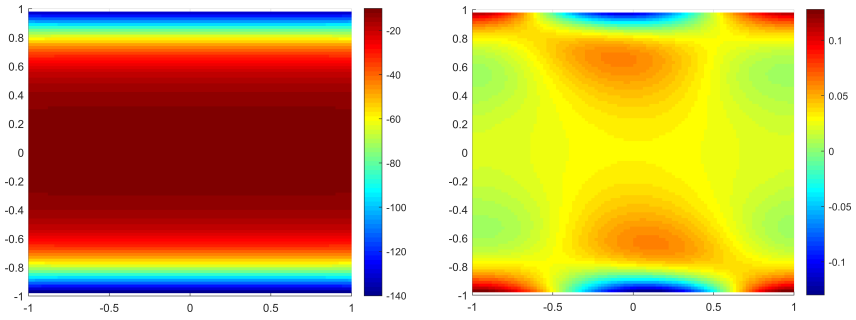

(a) Zero Order (b) Second Order

Figure 5.8: Stress resultants distribution ($[90 \pm \langle 0, 75 \rangle]_{2S}$)

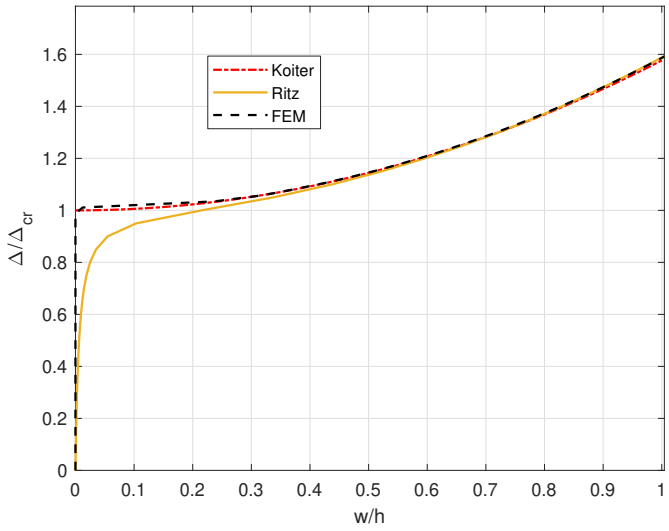

Figure 5.9: Normalized transverse displacement-imposed displacement curve: isotropic plate.

not uniform, and the stresses are concentrated at the unloaded edges (Figure 5.7a), meaning that the central part is weaker then the edges; this behaviour results in an higher buckling load. Furthermore, the second order solution shows that in the post-buckled state the central part is still less loaded (Figure 5.7b) and, as in the case of the isotropic plate, the result is a decrease of the post-buckling stiffness. However, in this case the reduction is more accentuated because, as mentioned above, the central part is weaker. This observation are in agreement with the values of relative post-buckling stiffness reported in Table 5.5.
Finally, in the case of a plate with lamination sequence $[90 \pm \langle 0, 75 \rangle]_{2S}$ it can be noticed that in the pre-buckling state the stresses are also concentrated at the unloaded edges leaving the central part only slightly loaded (Figure 5.8a). This distribution results in a even more high buckling load. The second order solution results in a stress-distribution where the weaker, central part is loaded, but most of the in-plane loads are still carried by the surrounding, stronger edges (Figure 5.8b). This behaviour mitigate the reduction in post-buckling stiffness, as confirmed by the perturbation analysis.

The agreement of the Ritz and the Koiter approaches is checked by comparison of the λ-ξ curve. Recalling Eq. 5.2, the perturbation parameter ξ is the maximum-out-of-plane displacement normalized with respect to the wall thickness. Therefore, the λ-ξ curve actually corresponds to the normalized displacement-transverse displacement curve reported in Figure 4.26.

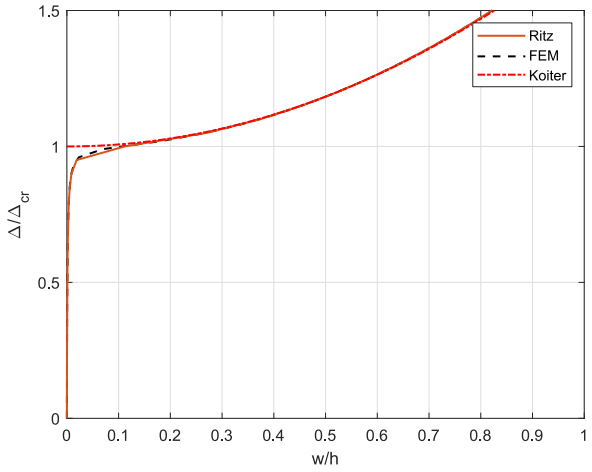

Figure 5.10: Normalized transverse displacement-imposed displacement curve: variable-stiffness plate $[0 \pm \langle 45, 0 \rangle]_{2S}$.

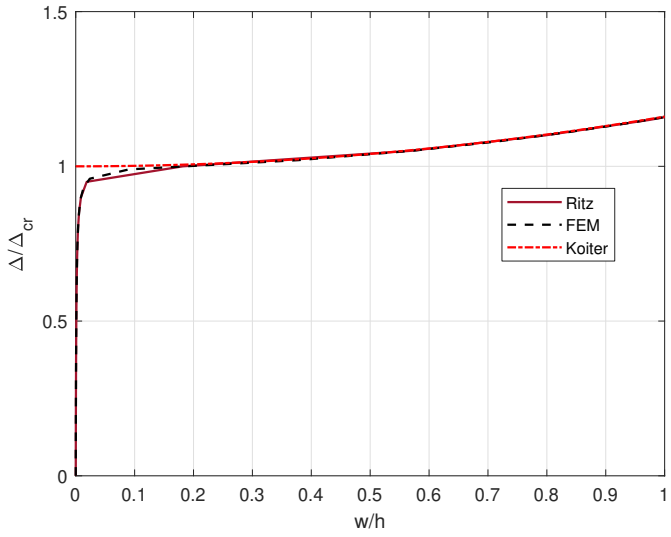

Figure 5.11: Normalized transverse displacement-imposed displacement curve: variable-stiffness plate $[90 \pm \langle 0, 75 \rangle]_{2S}$.

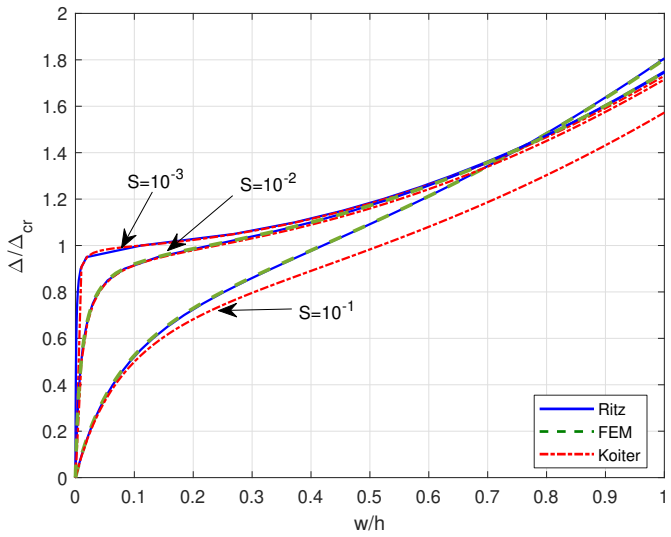

Figure 5.12: Effect of imperfections in terms of normalized transverse displacement-imposed displacement curve: variable-stiffness plate $[0 \pm \langle 45, 0 \rangle]_{2S}$. Imperfection effects.

Three relevant case are investigated: the normalized edge displacement versus out-of-plane deflection curves are reported in Figures 5.9-5.11 for the case of an isotropic plate, and plates with lamination sequence $[0 \pm \langle 45, 0 \rangle]_{2S}$ and $[0 \pm \langle 45, 0 \rangle]_{2S}$, respectively. The curves are computed with the Koiter method, the Ritz method and the finite element method. It can be noticed that the results of the three approaches are in close agreement.

Effect of imperfections in variable-stiffness plates The capability of the developed Koiter-Ritz formulation to take into account the presence of initial imperfections is tested.

To this aim, a simply-supported square plate of planar dimensions equal to 1000 mm is considered. The plate is made of the *Material A* reported in Table 4.2 and the stacking sequence is taken as $[0 \pm \langle 45, 0 \rangle]_{2S}$. The non-linear response of this laminate has already been studied in the framework of the Ritz method (Chapter 4, Example 8). In the current Koiter approach, initial imperfections are introduced according to the procedure outlined in Section 5.1.1. Firstly, the a and b factors are computed for the perfect structure, then Eq. 5.8 is solved for λ.

The response is reported in terms of normalized Δ-transverse displacement curve in Figure 5.12 for different magnitude of the imperfection value. The amplitude S, introduced in Eq. 4.139, is taken equal to 10^{-3}, 10^{-2} and 10^{-1}.

A first check deals with the effect of increasing the magnitude of imperfection. As expected, larger imperfections determine smoother transitions between the pre- and the post-buckling region. This behaviour is correctly captured by the formulation, as seen from Figure 5.12. Furthermore, one can notice the substantial agreement between Ritz and Koiter predictions. As seen from Figure 5.12, the results obtained with the two methods are similar as long as the imperfection's magnitude is small: for an imperfection magnitude equal to 10% of the plate thickness (S=0.1) the Koiter method leads to results which are drastically away from the Ritz and the finite element ones. This is due to the assumption of linear pre-buckling that has been adopted while developing the perturbation approach.
This restriction due to the linear pre-buckling assumption is well known, and has been investigated by Cohen [69], leading to similar conclusions. Improved quality of the description can be achieved by accounting for the non-linearities associated with the pre-buckling field. Thus, further developments in the current formulation should be considered to take into account these effects.

Chapter 6

Conclusions and Future Developments

In this thesis two semi-analytical tools for the study of variable-stiffness panels have been developed.

The first part of the work has been focused on the development of a model for the linear and non-linear analysis within the context of the Ritz method. A variational approach has been employed to derive the pre-, buckling and post-buckling problems. The formulation has been developed for variable-stiffness plates and shallow cylindrical shells.
The second part of the work covered the application of Koiter's approach for the initial post-buckling analysis of variable-stiffness plates. The perturbation method has been applied referring to a variational approach, and the different order problems have been obtained by minimizing the resulting contributions by applying the Ritz method. For this reason this approach can be seen as a unified Ritz-Koiter strategy.
The formulation has been derived only in the case of variable-stiffness plates.

Concerning the Ritz method, the results showed that the adopted approach is capable of correctly capturing the in-plane stress resultants, which are highly non-uniform in the case of variable-stiffness panels.
A good accuracy has been found in the buckling loads computed with the current method. In the case of plates, the results differ from the ones available in literature by a maximum of 0.10%, while they differ by less than 0.20% from the ones obtained with Abaqus. In the case of shells the error is slightly higher, as a maximum error

of 1.4% has been found with respect to the results obtained with finite element analyses, suggesting that the membrane-bending coupling should be considered in the formulation.
The influence of the number of terms used to approximate the unknown of the problem has been studied: employing an high number of terms for the Airy stress function results in a stiffer system, whilst employing an high number of terms of the out-of-plane displacement results in a more flexible system.
The developed Ritz model also provides good accuracy in terms of post-buckling response. The developed method is capable of capturing the post-buckling behaviour either with the Newton-Raphson method and the arc-length solution strategy: the maximum out-of-plane displacement has been computed for a load level which is twice the critical one, and the results computed with Ritz differ from the one obtained with Abaqus by 0.01%. This result has been obtained by adopting 10 terms per function in each direction. However, using only 6 terms provides an error of 0.30%: this result is a good compromise between accurate predictions and low computational effort. On the other hand, some discrepancies have been noted in the in-plane stress distribution in the deep post-buckling field, thus further investigations are required.
Nevertheless, the proposed approach represent a good choice to investigate the behaviour of variable-stiffness panels: it allows to keep the size of the problem small, resulting in a code that do not require too much computational effort to reproduce finite element results.

The validity of the results obtained with the perturbation approach have been checked by comparisons against results available in literature and obtained with finite element computations. To this aim, only classical straight-fiber laminates have been analysed: it resulted that the proposed Ritz-Koiter model is able to reproduce results available in literature, as a maximum error of 2.20% has been found in terms of b-factor. However, comparisons with other resources showed that the error can be even lower.
The code has been used to compute the b-factors of variable-stiffness plates to analyse the initial post-buckling behaviour of these kind of laminates. The results of this approach have been found to be consistent with the results obtained with Ritz and with Abaqus, thus they could be used, in the future, as a reference.
The Koiter's method allowed to develop a model that requires even less computational efforts than the Ritz method. Thus, this model can be used to quickly gain

insights on the initial post-buckling behaviour of variable-stiffness plates.

With the developed semi-analytical tools it has been possible to confirm that enhanced performances should be expected from variable-stiffness panels with respect to classical straight fibers laminates: the results showed that the buckling load can be increased by properly tailoring the lamination sequence, and the same holds for the post-buckling behaviour: variable-stiffness panels, if properly designed, experience a reduced loss of post-buckling stiffness.
The developed tools represent a valid alternative to the finite element method, which is quite expensive both in terms of computational power and time: the Ritz method is less expensive, but still take some time and computational resources to perform the post-buckling analysis. Instead, the Koiter approach provides the results in few seconds by employing very few terms of the trial functions, hence confirming the advantages that this method provides. Nevertheless, this model is suitable for correctly predict the initial post-buckling behaviour, and there is no guarantee that the approximation is valid for higher load levels: for the study of the deep post-buckling response the Ritz method shall be used instead.

Indeed, the presented formulation allows to develop tools that are quite cheap in terms of computational effort and time. However, one of the main difficulties encountered in the implementation of the approach was the development of an efficient framework to integrate the matrix terms: due to the variable-stiffness nature of the structures considered, this aspect is of primary importance in order to keep the computational effort at low levels.

The analyses have been developed only considering symmetrical laminates: future developments should extend the formulation to non-symmetrical panels, thus expanding the investigation to a greater number of lamination sequences. With this regard, it would be interesting to implement the developed models in an optimization routine.
The Ritz-Koiter formulation should also be developed for variable-stiffness shells: this aspect is very interesting, since is has been proved that an highly non-linear post-buckling behaviour can be expected from curved panels.
Another interesting development would be the inclusion in the model of full-cylindrical shells, in order to extend the analysis capabilities to more realistic space launcher-type constructions.

Appendix A

Force-control equations

The in-plane boundary conditions in the force-control case are:

$$\begin{aligned} x = \pm\frac{a}{2}: \qquad & N_{y0} = \mp\overline{N}_x \qquad & N_{xy0} = 0 \\ y = \pm\frac{b}{2}: \qquad & N_{y0} = 0 \qquad & N_{xy0} = 0 \end{aligned} \tag{6.1}$$

The panel is compressed at $x = \pm a/2$ by a uniform load $\overline{N}_x$, and the Airy stress function is approximated as:

$$\phi(\xi,\eta) = \phi_0(\xi) + \phi_1(\xi,\eta) = \frac{b^2}{4}\frac{\overline{N}_x\eta}{2} + \sum_{p=0}^{P}\sum_{q=0}^{Q} X_p(\xi)Y_q(\eta)\Phi_{pq} \tag{6.2}$$

Hereafter are reported the set of equations describing the pre-, buckling and post-buckling problems.

Pre-buckling equations The pre-buckling problem equations are a set of are obtained

$$\boldsymbol{U}\boldsymbol{\Phi}_{pq} + \boldsymbol{u_C}\overline{N}_x\frac{b^2}{4} = 0 \tag{6.3}$$

which is a set of PQ×PQ algebraic linear equations- The matrix $\boldsymbol{U}$ is the same matrix defined in Eq. 4.46 and the U_C is a P×Q vector defined as

$$\begin{aligned} \boldsymbol{u_C}(pq) = \sum_{\overline{pq}=0}^{PQ} U_{C,pq} = \int_{-1}^{+1}\int_{-1}^{+1} [a_{11}\mu^4 X_p Y_q'' + a_{12}\mu^2 X_p'' Y_q - \\ - a_{16}\mu^3 X_p' Y_q'] d\xi d\eta \end{aligned} \tag{6.4}$$

Buckling equations The buckling problem is:

$$[\boldsymbol{K} + \lambda(\boldsymbol{L_1} + \boldsymbol{L_N})]\boldsymbol{\delta W}_{mn} = 0 \tag{6.5}$$

that is an eigenvalue problem of dimensions MN×MN. The vector $\boldsymbol{L_N}$ is

$$\boldsymbol{L_N} = \sum_{mn\overline{mn}=0}^{MNMN} \int_{-1}^{+1}\int_{-1}^{+1} [\overline{X}'_m \overline{Y}_n \overline{X}'_{\overline{m}} \overline{Y}_{\overline{n}}] d\xi d\eta \tag{6.6}$$

Post-buckling equations The non-linear system to be solved for the post-buckling analysis is:

$$\begin{cases} \boldsymbol{U\Phi}_{pq} + \boldsymbol{u_C}\overline{N}_x + \boldsymbol{L_1}^{pq}\boldsymbol{W}_{mn}\boldsymbol{W}_{\overline{mn}} + \boldsymbol{L_{01}}^{pq}\boldsymbol{W}_{mn}\boldsymbol{W}_{tu} + \boldsymbol{C_R}^T\boldsymbol{W}_{mn} = 0 \\ \boldsymbol{K W}_{\overline{mn}} + \boldsymbol{L_1}^{mn}\boldsymbol{\Phi}_{pq}\boldsymbol{W}_{\overline{mn}} + \boldsymbol{L_{01}}^{mn}\boldsymbol{\Phi}_{pq}\boldsymbol{W}_{tu} + \boldsymbol{C_R}\boldsymbol{\Phi}_{pq} + \boldsymbol{L_N}^{mn}\boldsymbol{W}_{\overline{mn}}\overline{N}_x + \boldsymbol{L_{0N}}^{mn}\overline{N}_x = 0 \end{cases} \tag{6.7}$$

Where the matrix terms are the same adopted in the Imposed Load Case, with the exception of $\boldsymbol{u_C}$, which is defined as in Eq. 6.4 and the terms $\boldsymbol{L^N}$ and $\boldsymbol{L_{N0}}$, which are defined as

$$\boldsymbol{L_N} = \frac{2}{ab}\int_{-1}^{+1}\int_{-1}^{+1} [\overline{X}'_m \overline{Y}_n \overline{X}'_m \overline{Y}_n] d\xi d\eta \tag{6.8}$$

and

$$\boldsymbol{L_{N0}} = \frac{2}{ab}\sum_{tu=0}^{TU} W_{tu}\int_{-1}^{+1}\int_{-1}^{+1} [\overline{X}'_m \overline{Y}_n X_{0m} Y_{0n}] d\xi d\eta \tag{6.9}$$

Perturbation analysis The zero and first problems corresponds to the pre-buckling and buckling problems respectively. The second order problem is given by the following set of linear equations:

$$\begin{aligned} \frac{\partial \Pi_F^{(2)}}{\partial \Phi_{pq}^{(2)}} &= \boldsymbol{U\Phi}_{pq}^{(2)} + \boldsymbol{L_1}^{pq}\boldsymbol{W}_{\overline{mn}}^{(1)}\boldsymbol{W}_{mn}^{(1)} = 0 \\ \frac{\partial \Pi_F^{(2)}}{\partial W_{mn}^{(2)}} &= \boldsymbol{K W}_{\overline{mn}}^{(2)} + 2\lambda_{cr}\boldsymbol{L_1}^{mn}\boldsymbol{\Phi}_{pq}^{(0)}\boldsymbol{W}_{\overline{mn}}^{(2)} + 2\lambda_{cr}\overline{N}\lambda_{cr}\boldsymbol{L_1}^{mn}\boldsymbol{W}_{\overline{mn}}^{(2)} = 0 \end{aligned} \tag{6.10}$$

It can be observed that the second set of equations gives $W_{mn}^{(2)} = 0$, so the second order problem can be solved by solving the following set of equations

$$\boldsymbol{U\Phi_{pq}}^{(2)} = -\boldsymbol{L_1}^{pq}\boldsymbol{W}_{\overline{mn}}^{(1)}\boldsymbol{W}_{mn}^{(1)} \tag{6.11}$$

The slope of the post-buckling branch is:

$$m = \left(\frac{\lambda - \lambda_{cr}}{\Delta - \Delta_{cr}} \right) \frac{\Delta_{cr}}{\lambda_{cr}} \tag{6.12}$$

that can be compared with the expression that exploits the results of the perturbation analysis

$$K_P = \frac{b\Delta_{cr}}{b\Delta_{cr} + \Delta^{(2)}} \tag{6.13}$$

The second-order edge displacement $\Delta^{(2)}$ is computed as:

$$\Delta^{(2)} = \frac{1}{l_y} \int_{-l_y/2}^{+l_y/2} \int_{-l_x/2}^{+l_x/2} [\epsilon_x^{(2)} - \frac{1}{2}(w_{/x}^{(1),2} + 2\lambda w_{/x}^{(0)} w_{/x}^{(2)})] dxdy \tag{6.14}$$

Appendix B

Gauss Quadrature integration method

The Gaussian quadrature is a numerical integration rule that allows to approximate the definite integral of a function.

If $f(\xi)$ is a function, the definite integral over the domain [-1,+1] can be approximated as:

$$\int_{-1}^{+1} f(\xi)d\xi \approx \sum_{i=1}^{I} \omega_i f(\xi_i) \tag{6.15}$$

where ξ_i are a set of points evaluated as zeros of the Legendre polynomial L_i and ω_i are the *weights*, computed as:

$$\omega_i = \frac{2}{(1-\xi_i^2)L_i'(\xi_i)^2} \tag{6.16}$$

The approximation of Eq. 6.15 is exact only if $f(\xi)$ is a polynomial of degree $2I-1$ or less.
If the function is integrated above the 2D domain, the Gaussian quadrature rule reads:

$$\int_{-1}^{+1}\int_{-1}^{+1} f(\xi,\eta)d\xi d\eta \approx \sum_{i=1}^{I}\sum_{j=1}^{J} \omega_i\omega_j f(\xi_i,\eta_j) \tag{6.17}$$

where the weight and the points are evaluated as in Eq. 6.16. In the following, an example on how the Gaussian quadrature rule can be used to integrate the matrices presented in the thesis will be given.

The matrix $\boldsymbol{A}$ is defined as:

$$\boldsymbol{A} = \sum_{pqmn=0}^{\mathrm{PQMN}} \int_{-1}^{+1}\int_{-1}^{+1} X_p(\xi)Y_q(\eta)X_m(\xi)Y_n(\eta)d\xi d\eta \tag{6.18}$$

where $X_p(\xi), Y_q(\eta), X_m(\xi), Y_n(\eta)$ are general polynomials functions of order p, q, m, n. The matrix is in the form:

$$\boldsymbol{A} = \begin{bmatrix} X_0Y_0X_0Y_0 & X_0Y_0X_0Y_1 & \cdots & X_0Y_0X_0Y_N & X_0Y_0X_1Y_1 & \cdots & X_0Y_0X_1Y_N & \cdots & X_0Y_0X_MY_N \\ X_0Y_1X_0Y_0 & X_0Y_1X_0Y_1 & \cdots & X_0Y_1X_0Y_N & X_0Y_1X_1Y_1 & \cdots & X_0Y_1X_1Y_N & \cdots & X_0Y_1X_MY_N \\ \vdots & \vdots & & \vdots & \vdots & & \vdots & & \vdots \\ X_0Y_QX_0Y_0 & X_0Y_QX_0Y_1 & \cdots & X_0Y_QX_0Y_N & X_0Y_QX_1Y_1 & \cdots & X_0Y_QX_1Y_N & \cdots & X_0Y_QX_MY_N \\ X_1Y_0X_0Y_0 & X_1Y_0X_0Y_1 & \cdots & X_1Y_0X_0Y_N & X_1Y_0X_1Y_1 & \cdots & X_1Y_0X_1Y_N & \cdots & X_1Y_0X_MY_N \\ \vdots & \vdots & & \vdots & \vdots & & \vdots & & \vdots \\ X_PY_QX_0Y_0 & X_PY_QX_0Y_1 & \cdots & X_PY_QX_0Y_N & X_PY_QX_1Y_1 & \cdots & X_PY_QX_1Y_N & \cdots & X_PY_QX_MY_N \end{bmatrix} \tag{6.19}$$

where every term of the matrix is:

$$\boldsymbol{A}(pq, mn) = \int_{-1}^{+1}\int_{-1}^{+1} X_p(\xi)Y_q(\eta)X_m(\xi)Y_n(\eta)d\xi d\eta \tag{6.20}$$

The integral in Eq. 6.20 can be approximated as:

$$\boldsymbol{A}(pq, mn) \approx \sum_{i=1}^{I}\sum_{j=1}^{J} \omega_i\omega_j X_p(\xi_i)Y_q(\eta_j)X_m(\xi_i)Y_n(\eta_j) \tag{6.21}$$

or, separating the terms that depends on ξ from the one that depends on η:

$$\boldsymbol{A}(pq, mn) \approx \sum_{i=1}^{I}[\omega_i X_p(\xi_i)X_m(\xi_i)\sum_{j=1}^{J}\omega_j Y_q(\eta_j)Y_n(\eta_j)] \tag{6.22}$$

Appendix C

Jacobian Matrices

The Jacobian matrix of the non-linear system in Eq. 4.99 is:

$$\boldsymbol{J} = \begin{bmatrix} \frac{\partial \boldsymbol{R}_i^1}{\partial \Phi_{pq}} & \frac{\partial \boldsymbol{R}_i^1}{\partial c_k} & \frac{\partial \boldsymbol{R}_i^1}{\partial W_{mn}} \\ \frac{\partial \boldsymbol{R}_i^2}{\partial \Phi_{pq}} & \frac{\partial \boldsymbol{R}_i^2}{\partial c_k} & \frac{\partial \boldsymbol{R}_i^2}{\partial W_{mn}} \\ \frac{\partial \boldsymbol{R}_i^3}{\partial \Phi_{pq}} & \frac{\partial \boldsymbol{R}_i^3}{\partial c_k} & \frac{\partial \boldsymbol{R}_i^3}{\partial W_{mn}} \end{bmatrix} =$$

$$= \begin{bmatrix} \boldsymbol{U} & \boldsymbol{U_C} & (\boldsymbol{L_1}^{pq,J} + \boldsymbol{L_{01}}^{pq,J} + \boldsymbol{C_R}^T) \\ \boldsymbol{U_C} & \boldsymbol{C} & (\boldsymbol{L_2}^{k,J} + \boldsymbol{L_{02}}^{k,J}) \\ (\boldsymbol{L_1}^{mn,J} + \boldsymbol{L_{01}}^{mn,J} + \boldsymbol{C_R}^T) & (\boldsymbol{L_2}^{mn,J} + \boldsymbol{L_{02}}^{mn,J}) & \boldsymbol{K} + \boldsymbol{L_{12}}^{mn,J} \end{bmatrix} \tag{6.23}$$

which is a matrix of size (PQ+K+MN)×(PQ+K+MN).
The matrix components are computed as:

$$\begin{aligned} \boldsymbol{L_1}^{pq,J} = +\frac{4}{ab} \int_{-1}^{+1} \int_{-1}^{+1} [X_p Y_q'' X'_{\overline{m}} Y_{\overline{n}} \sum_{\overline{mn}=0}^{MN} X'_m Y_n W_{mn} + \\ + X_p'' Y_q X_{\overline{m}} Y'_{\overline{n}} \sum_{mn=0}^{MN} X_m Y'_n W_{mn} - \\ - (X'_p Y'_q X_{\overline{m}} Y'_{\overline{n}} \sum_{mn=0}^{MN} X'_m Y_n W_{mn} + X'_p Y'_q X'_{\overline{m}} Y_{\overline{n}} \sum_{mn=0}^{MN} X_m Y'_n W_{mn})] d\xi d\eta \end{aligned} \tag{6.24}$$

$$\boldsymbol{L_2}^{k,J} = +2\frac{2}{ab} \int_{-1}^{+1} \int_{-1}^{+1} [\psi_k X'_{\overline{m}} Y_{\overline{n}} \sum_{mn=0}^{MN} X'_m Y_n W_{mn}] d\xi d\eta \tag{6.25}$$

$$\begin{aligned}\boldsymbol{L^1}^{mn,J} = +\frac{2}{ab}2\int_{-1}^{+1}\int_{-1}^{+1}[X_pY_q''X_m'Y_n\sum_{\overline{mn}=0}^{MN}X_{\overline{m}}'Y_{\overline{n}}W_{\overline{mn}}+\\ +X_p''Y_qX_mY_n'\sum_{\overline{mn}=0}^{MN}X_{\overline{m}}Y_{\overline{n}}'W_{\overline{mn}}-\\ -(X_p'Y_q'X_m'Y_n\sum_{\overline{mn}=0}^{MN}X_{\overline{m}}Y_{\overline{n}}'W_{\overline{mn}}+\\ +X_p'Y_q'X_mY_n'\sum_{\overline{mn}=0}^{MN}X_{\overline{m}}'Y_{\overline{n}}W_{\overline{mn}})]d\xi d\eta\end{aligned} \tag{6.26}$$

$$\boldsymbol{L_1}^{mn,J} = +\frac{2}{ab}2\int_{-1}^{+1}\int_{-1}^{+1}[\psi_kX_m'Y_n\sum_{\overline{mn}=0}^{MN}X_{\overline{m}}'Y_{\overline{n}}W_{\overline{mn}}]d\xi d\eta \tag{6.27}$$

$$\begin{aligned}\boldsymbol{L_{12}^J} = \boldsymbol{L_1}^{mn,J}+\boldsymbol{L_2}^{mn,J} = +\frac{2}{ab}2\int_{-1}^{+1}\int_{-1}^{+1}[X_m'Y_nX_{\overline{m}}'Y_{\overline{n}}\sum_{k=0}^{K}\psi_kc_k]d\xi d\eta+\\ +\frac{2}{ab}2\int_{-1}^{+1}\int_{-1}^{+1}[X_m'Y_nX_{\overline{m}}'Y_{\overline{n}}\sum_{pq=0}^{PQ}X_pY_q''\Phi_{pq}+\\ +X_mY_n'X_{\overline{m}}Y_{\overline{n}}'\sum_{pq=0}^{PQ}X_p''Y_q\Phi_{pq}-\\ -(X_m'Y_nX_{\overline{m}}Y_{\overline{n}}'\sum_{pq=0}^{PQ}X_p'Y_q'\Phi_{pq}+\\ +X_mY_n'X_{\overline{m}}'Y_{\overline{n}}\sum_{pq=0}^{PQ}X_p'Y_q'\Phi_{pq})]d\xi d\eta\end{aligned} \tag{6.28}$$

$$\begin{aligned}\boldsymbol{L_{01}}^{pq,J} = -\frac{4}{ab}\int_{-1}^{+1}\int_{-1}^{+1}[X_pY_q''X_m''Y_n\sum_{tu=0}^{TU}X_{0t}Y_{0u}W_{0tu}+\\ +X_p''Y_qX_mY_n''\sum_{tu=0}^{TU}X_{0t}Y_{0u}W_{0tu}-\\ -2X_p'Y_q'X_m'Y_n'\sum_{tu=0}^{TU}X_{0t}Y_{0u}W_{0tu}]d\xi d\eta\end{aligned} \tag{6.29}$$

$$\boldsymbol{L_{02}}^{k,J} = -\frac{4}{ab}\int_{-1}^{+1}\int_{-1}^{+1}[\psi_kX_m''Y_n\sum_{tu=0}^{TU}X_{0t}Y_{0u}W_{0tu}]d\xi d\eta \tag{6.30}$$

$$\begin{aligned}\boldsymbol{L_{01}}^{mn,J} = -\frac{4}{ab}\int_{-1}^{+1}\int_{-1}^{+1}[X''_m Y_n X_p Y''_q \sum_{tu=0}^{TU} X_{0t}Y_{0u}W_{0tu}+ \\ + X_m Y''_n X''_p Y_q \sum_{tu=0}^{TU} X_{0t}Y_{0u}W_{0tu}- \\ - 2X'_m Y'_n X'_p Y'_q \sum_{tu=0}^{TU} X_{0t}Y_{0u}W_{0tu}]d\xi d\eta\end{aligned} \tag{6.31}$$

$$\boldsymbol{L_{02}}^{mn,J} = -\frac{4}{ab}\int_{-1}^{+1}\int_{-1}^{+1}[X''_m Y_n \psi_k \sum_{tu=0}^{TU} X_{0t}Y_{0u}W_{0tu}]d\xi d\eta \tag{6.32}$$

A×B products

The identities used Section 5.2 to substitute the expanded solution in the unitary functional reported here.

$$\begin{aligned}A \times A =&(\lambda_{cr}A^{(0)} + \xi A^{(1)} + \xi^2 A^{(2)})^2 = \\ =&+ \lambda_{cr}^2 A^{(0),2} + \xi^2 A^{(1),2} + \xi^4 A^{(2),2} + 2\xi\lambda_{cr}A^{(0)}A^{(1)}+ \\ &+ 2\xi^2\lambda_{cr}A^{(0)}A^{(2)} + 2\xi^3 A^{(1)}A^{(2)}\end{aligned} \tag{6.33}$$

$$\begin{aligned}A \times B =&(\lambda_{cr}A^{(0)} + \xi A^{(1)} + \xi^2 A^{(2)}) \times (\lambda_{cr}B^{(0)} + \xi B^{(1)} + \xi^2 B^{(2)}) = \\ =&+ \lambda_{cr}^2 A^{(0)}B^{(0)} + \xi\lambda_{cr}A^{(0)}B^{(1)} + \xi^2\lambda_{cr}A^{(0)}B^{(2)}+ \\ &+ \xi\lambda_{cr}A^{(1)}B^{(0)} + \xi^2 A^{(1)}B^{(1)} + \xi^3 A^{(1)}B^{(2)}+ \\ &+ \xi^2\lambda_{cr}A^{(2)}B^{(0)} + \xi^3 A^{(2)}B^{(1)} + \xi^4 A^{(2)}B^{(2)}\end{aligned} \tag{6.34}$$

$$\begin{aligned}A \times B^2 =&(\lambda_{cr}A^{(0)} + \xi A^{(1)} + \xi^2 A^{(2)}) \times (\lambda_{cr}B^{(0)} + \xi B^{(1)} + \xi^2 B^{(2)})^2 = \\ =&(\lambda_{cr}A^{(0)} + \xi A^{(1)} + \xi^2 A^{(2)}) \times (\lambda_{cr}^2 B^{(0),2} + \xi^2 B^{(1),2} + \xi^4 B^{(2),2}+ \\ &+ 2\xi\lambda_{cr}B^{(0)}B^{(1)} + 2\xi^2\lambda_{cr}B^{(0)}B^{(2)} + 2\xi^3 B^{(1)}B^{(2)}) = \\ =&+ \lambda_{cr}^2 A^{(0)}B^{(0),2} + \xi^2\lambda_{cr}A^{(0)}B^{(1),2} + \xi^4\lambda_{cr}A^{(0)}B^{(2),2} + 2\xi\lambda_{cr}A^{(0)}B^{(0)}B^{(1)}+ \\ &+ 2\xi^3\lambda_{cr}A^{(0)}B^{(0)}B^{(2)} + 2\xi^3 A^{(0)}B^{(1)}B^{(2)} + \xi\lambda_{cr}^2 A^{(1)}B^{(0),2} + \xi^3 A^{(1)}B^{(1),2}+ \\ &+ \xi^5 A^{(1)}B^{(2),2} + 2\xi^2 A^{(1)}B^{(0)}B^{(1)} + 2\xi^3 A^{(1)}B^{(0)}B^{(2)} + 2\xi^4 A^{(1)}B^{(1)}B^{(2)}+ \\ &+ \xi^2\lambda_{cr}^2 A^{(2)}B^{(0),2} + \xi^4 A^{(2)}B^{(1),2} + \xi^6 A^{(2)}B^{(2),2}+ \\ &+ 2\xi^3\lambda_{cr}A^{(2)}B^{(0)}B^{(1)} + 2\xi^4 A^{(2)}B^{(0)}B^{(2)}+ \\ &+ 2\xi^5 A^{(2)}B^{(1)}B^{(2)}\end{aligned} \tag{6.35}$$

Bibliography

[1] AW Leissa and AF Martin. "Vibration and buckling of rectangular composite plates with variable fiber spacing". *Composite Structures* 14.4 (1990), pp. 339–357.

[2] MW Hyer and HH Lee. "The use of curvilinear fiber format to improve buckling resistance of composite plates with central circular holes". *Composite Structures* 18.3 (1991), pp. 239–261.

[3] Z Gurdal and R Olmedo. "Composite laminates with spatially varying fiber orientations-'Variable stiffness panel concept'". In: *33rd Structures, Structural Dynamics and Materials Conference*. 1992, p. 2472.

[4] E Senocak and H Tanriover. "Analysis of composite plates with variable stiffness using Galerkin method". *The Aeronautical Journal* 111.1118 (2007), pp. 247–255.

[5] S Setoodeh, MM Abdalla, ST IJsselmuiden, and Z Gurdal. "Design of variable-stiffness composite panels for maximum buckling load". *Composite Structures* 87.1 (2009), pp. 109–117.

[6] JM Curry and JH Tarnes. "Effect of dropped plies on the strength of graphite-epoxy laminates". *AIAA Journal* 30.2 (1992), pp. 449–456.

[7] B Paluch, M Grediac, and A Faye. "Combining a finite element programme and a genetic algorithm to optimize composite structures with variable thickness". *Composite Structures* 83.3 (2008), pp. 284–294.

[8] JR Barth. "Fabrication of complex composite structures using advanced fiber placement technology". In: *International SAMPE Symposium and Exhibition, 35 th, Anaheim, CA*. 1990, pp. 710–720.

[9] C Waldhart, Z Gurdal, and C Ribbens. "Analysis of tow placed, parallel fiber, variable stiffness laminates". In: *37th Structure, Structural Dynamics and Materials Conference*. 1996, p. 1569.

[10] Z Gurdal, BF Tatting, and CK Wu. "Variable stiffness composite panels: effects of stiffness variation on the in-plane and buckling response". *Composites Part A: Applied Science and Manufacturing* 39.5 (2008), pp. 911–922.

[11] BF Tatting, Z Gurdal, and D Jegley. "Design and manufacture of elastically tailored tow placed plates" (2002).

[12] P Ribeiro, H Akhavan, A Teter, and J Warmiński. "A review on the mechanical behaviour of curvilinear fibre composite laminated panels". *Journal of Composite Materials* 48.22 (2014), pp. 2761–2777.

[13] A Alhajahmad, MM Abdalla, and Z Gurdal. "Design tailoring for pressure pillowing using tow-placed steered fibers". *Journal of Aircraft* 45.2 (2008), pp. 630–640.

[14] H Akhavan and P Ribeiro. "Natural modes of vibration of variable stiffness composite laminates with curvilinear fibers". *Composite Structures* 93.11 (2011), pp. 3040–3047.

[15] PT Langley. "Finite Element Modeling of Tow-placed Variable-Stiffness Composite Laminates". PhD thesis. Virginia Tech, 1999.

[16] MT DiNardo and PA Lagace. "Buckling and postbuckling of laminated composite plates with ply dropoffs". *AIAA Journal* 27.10 (1989), pp. 1392–1398.

[17] Z Wu, PM Weaver, G Raju, and BC Kim. "Buckling analysis and optimisation of variable angle tow composite plates". *Thin-Walled Structures* 60 (2012), pp. 163–172.

[18] G Raju, Z Wu, BC Kim, and PM Weaver. "Prebuckling and buckling analysis of variable angle tow plates with general boundary conditions". *Composite Structures* 94.9 (2012), pp. 2961–2970.

[19] A Haldar, E Jansen, R Rolfes, and PM Weaver. "Tailoring Snap-through Loads in Variable Stiffness Composites". In: *2018 AIAA/ASCE/AHS/ASC Structures, Structural Dynamics, and Materials Conference*. 2018, p. 2245.

[20] G Harris. "Buckling and post-buckling of orthotropic laminated plates". In: *16th Structural Dynamics, and Materials Conference*. 1975, p. 813.

[21] GB Chai. "Large deflections of laminated composite plates". *Composites Science and Technology* 42.4 (1991), pp. 349–360.

[22] R Vescovini and C Bisagni. "Single-mode Solution for Post-buckling Analysis of Composite Panels with Elastic Restraints Loaded in Compression". *Composites Part B: Engineering* 43.3 (2012), pp. 1258–1274.

[23] K Marguerre. "The apparent width of the plate in compression" (1937).

[24] S Levy. *Bending of Rectangular Plates with Large Deflections*. Tech. rep. National Bureau Of Standards Gathersburg MD, 1942.

[25] MK Prabhakara and CY Chia. "Post-buckling behaviour of rectangular orthotropic plates". *Journal of Mechanical Engineering Science* 15.1 (1973), pp. 25–33.

[26] R Vescovini and C Bisagni. "Two-step Procedure for Fast Post-buckling Analysis of Composite Stiffened Panels". *Computers & Structures* 128 (2013), pp. 38–47.

[27] C Bisagni and R Vescovini. "Analytical formulation for local buckling and post-buckling analysis of stiffened laminated panels". *Thin-Walled Structures* 47.3 (2009), pp. 318–334.

[28] V Giavotto. "Variational theory of thin shells and panels". *Meccanica* 1.3-4 (1966), pp. 98–107.

[29] A Milazzo and V Oliveri. "Buckling and postbuckling of stiffened composite panels with cracks and delaminations by Ritz approach". *AIAA Journal* 55.3 (2016), pp. 965–980.

[30] V Oliveri, A Milazzo, and PM Weaver. "Thermo-mechanical post-buckling analysis of variable angle tow composite plate assemblies". *Composite Structures* 183 (2018), pp. 620–635.

[31] Z Wu, G Raju, and PM Weaver. "Postbuckling analysis of variable angle tow composite plates". *International Journal of Solids and Structures* 50.10 (2013), pp. 1770–1780.

[32] SC White and PM Weaver. "Towards imperfection insensitive buckling response of shell structures-shells with plate-like post-buckled responses". *The Aeronautical Journal* 120.1224 (2016), pp. 233–253.

[33] WT Koiter. *The Stability of Elastic Equilibrium*. Tech. rep. Standford Univ CA Dept Of Aeronautics and Astronautics, 1970.

[34] E Jansen, J Wijker, and J Arbocz. "A hierarchical approach for the buckling analysisof the VEGA 1/2 interstage". In: *Proceedings of the 10th European Conference on Spacecraft Structures, Materials, and Mechanical Testing, DLR, Berlin, Paper No. CEAS-2007-311*. 2007.

[35] NS Khot. *On the influence of initial geometric imperfections on the buckling and postbuckling behavior of fiber-reinforced cylindrical shells under uniform axial compression*. Tech. rep. Air Force Flight Dynamics Lab Wright-Patterson AFB OH, 1968.

[36] J Arbocz. "The effect of initial imperfections on shell stability". *Thin-shell Structures: Theory, Experiment, and Design* (1974), pp. 205–245.

[37] NS Khot and VB Venkayya. *Effect of fiber orientation on initial postbuckling behavior and imperfection sensitivity of composite cylindrical shells*. Tech. rep. Air Force Flight Dynamics Lab Wright-Patterson AFB OH, 1970.

[38] G Garcea, FS Liguori, L Leonetti, D Magisano, and A Madeo. "Accurate and efficient a posteriori account of geometrical imperfections in Koiter finite element analysis". *International Journal for Numerical Methods in Engineering* 112.9 (2017), pp. 1154–1174.

[39] E Jansen. "The effect of geometric imperfections on the vibrations of anisotropic cylindrical shells". *Thin-Walled Structures* 45.3 (2007), pp. 274–282.

[40] B Budiansky and JW Hutchinson. "Dynamic buckling of imperfection-sensitive structures". In: *Applied Mechanics*. Springer, 1966, pp. 636–651.

[41] E Byskov and JW Hutchinson. "Mode interaction in axially stiffened cylindrical shells". *AIAA Journal* 15.7 (1977), pp. 941–948.

[42] T Rahman and E Jansen. "Finite element based coupled mode initial post-buckling analysis of a composite cylindrical shell". *Thin-Walled Structures* 48.1 (2010), pp. 25–32.

[43] JF Olesen and E Byskov. "Accurate determination of asymptotic postbuckling stresses by the finite element method". *Computers & Structures* 15.2 (1982), pp. 157–163.

[44] T Rahman, ST Ijsselmuiden, MM Abdalla, and E Jansen. "Postbuckling analysis of variable stiffness composite plates using a finite element-based perturbation method". *International Journal of Structural Stability and Dynamics* 11.04 (2011), pp. 735–753.

[45] SC White, G Raju, and PM Weaver. "Initial post-buckling of variable-stiffness curved panels". *Journal of the Mechanics and Physics of Solids* 71 (2014), pp. 132–155.

[46] SR Henrichsen, PM Weaver, E Lindgaard, and E Lund. "Post-buckling optimization of composite structures using Koiter's method". *International Journal for Numerical Methods in Engineering* 108.8 (2016), pp. 902–940.

[47] A Madeo, RMJ Groh, G Zucco, PM Weaver, G Zagari, and R Zinno. "Post-buckling analysis of variable-angle tow composite plates using Koiter's approach and the finite element method". *Thin-Walled Structures* 110 (2017), pp. 1–13.

[48] RM Jones. *Mechanics of Composite Materials*. CRC press, 2014.

[49] L Cedolin and ZP BazĬant. *Stability of Structures: Elastic, Inelastic, Fracture and Damage Theories*. World Scientific, 2010.

[50] MW Hyer. *Stress Analysis of Fiber-reinforced Composite Materials*. DEStech Publications, Inc, 2009.

[51] K Washizu. *Variational Methods in Elasticity and Plasticity*. Pergamon press, 1975.

[52] MM Abdalla, S Setoodeh, and Z Gurdal. "Design of variable stiffness composite panels for maximum fundamental frequency using lamination parameters". *Composite Structures* 81.2 (2007), pp. 283–291.

[53] ST IJsselmuiden, MM Abdalla, and Z Gurdal. "Optimization of variable-stiffness panels for maximum buckling load using lamination parameters". *AIAA Journal* 48.1 (2010), pp. 134–143.

[54] JE Ashton and JM Whitney. *Theory of Laminated Plates*. Vol. 4. CRC Press, 1970.

[55] W Ritz. "Uber eine neue Methode zur Lösung gewisser Variationsprobleme der mathematischen Physik." *Journal Fuer die Eeine und Angewandte Mathematik* 135 (1909), pp. 1–61.

[56] R Vescovini and L Dozio. "A variable-kinematic model for variable stiffness plates: Vibration and buckling analysis". *Composite Structures* 142 (2016), pp. 15–26.

[57] V Oliveri and A Milazzo. "A Rayleigh-Ritz approach for postbuckling analysis of variable angle tow composite stiffened panels". *Computers & Structures* 196 (2018), pp. 263–276.

[58] G Raju, Z Wu, and PM Weaver. "Postbuckling analysis of variable angle tow plates using differential quadrature method". *Composite Structures* 106 (2013), pp. 74–84.

[59] JN Reddy. *Energy Principles and Variational Methods in Applied Mechanics*. John Wiley & Sons, 2017.

[60] R Vescovini, L Dozio, M D'Ottavio, and O Polit. "On the application of the Ritz method to free vibration and buckling analysis of highly anisotropic plates". *Composite Structures* 192 (2018), pp. 460–474.

[61] M Abramowitz and IA Stegun. *Handbook of Mathematical Functions: with Formulas, Graphs, and Mathematical Tables*. Vol. 55. Courier Corporation, 1964.

[62] CV Verhoosel, JJC Remmers, and MA Gutiérrez. "A dissipation-based arc-length method for robust simulation of brittle and ductile failure". *International Journal for Numerical Methods in Engineering* 77.9 (2009), pp. 1290–1321.

[63] D Bellora and R Vescovini. "Hybrid geometric-dissipative arc-length methods for the quasi-static analysis of delamination problems". *Computers & Structures* 175 (2016), pp. 123–133.

[64] M Fafard and B Massicotte. "Geometrical interpretation of the arc-length method". *Computers & Structures* 46.4 (1993), pp. 603–615.

[65] MA Crisfield. "An arc-length method including line searches and accelerations". *International Journal for Numerical Methods in Engineering* 19.9 (1983), pp. 1269–1289.

[66] User's Guide Matlab. "The mathworks". *Inc., Natick, MA* 1992 (1760).

[67] DS Simulia. "ABAQUS 6.13 User's manual". *Dassault Systems, Providence, RI* (2013).

[68] E Jansen. "A perturbation method for nonlinear vibrations of imperfect structures: application to cylindrical shell vibrations". *International Journal of Solids and Structures* 45.3-4 (2008), pp. 1124–1145.

[69] GA Cohen. "Effect of a nonlinear prebuckling state on the postbuckling behaviorand imperfect on sensitivity of elastic structures." *AIAA Journal* 6.8 (1968), pp. 1616–1619.

[70] JMT Thompson and GW Hunt. *A General Theory of Elastic Stability*. J. Wiley London, 1973.

[71] E Byskov. *Elementary Continuum Mechanics for Everyone: with Applications to Structural Mechanics*. Vol. 194. Springer Science & Business Media, 2013.

[72] FEA DIANA. *Diana User's Manual, Release 10.1*. 2017.

[73] AD Lanzo, G Garcea, and R Casciaro. "Asymptotic post-buckling analysis of rectangular plates by HC finite elements". *International Journal for Numerical Methods in Engineering* 38.14 (1995), pp. 2325–2345.

[74] T Rahman. "A perturbation approach for geometrically nonlinear structural analysis using a general purpose finite element code" ().

[75] MD Maisel. *The History of the XV-15 Tilt Rotor Research Aircraft: From Concept to Flight*. Monographs in aerospace history. National Aeronautics, Space Administration, Office of Policy, and Plans, NASA History Division, 2000.

[76] AF Martin and AW Leissa. "Application of the Ritz method to plane elasticity problems for composite sheets with variable fibre spacing". *International Journal for Numerical Methods in Engineering* 28.8 (1989), pp. 1813–1825.

[77] S Murugan and MI Friswell. "Morphing wing flexible skins with curvilinear fiber composites". *Composite Structures* 99 (2013), pp. 69–75.

[78] B Tatting and Z Gurdal. "Analysis and design of tow-steered variable stiffness composite laminates". In: *American Helicopter Society Hampton Roads Chapter, Structure Specialists' Meeting, Williamsburg, VA*. 2001.

[79] V Giavotto. "Sulla meccanica dei pannelli anisotropi ed eterogenei". *Memorie dell'Ist. lombardo-Accad. di scienze e lettere, Classe di scienze mat. e naturali* (1969).

[80] P Vannucci, B Cochelin, Ne Damil, and M Potier-Ferry. "An asymptotic-numerical method to compute bifurcating branches". *International Journal for Numerical Methods in Engineering* 41.8 (1998), pp. 1365–1389.

[81] B Budiansky. "Dynamic buckling of elastic structures: criteria and estimates". In: *Dynamic stability of structures*. Elsevier, 1967, pp. 83–106.

[82] C Bisagni and R Vescovini. “Fast Tool for Buckling Analysis and Optimization of Stiffened Panels”. *Journal of Aircraft* 46.6 (2009), pp. 2041–2053.